TU Delft

Modelling the changes in waveform in combined wave-current flow

Tolga Cömert

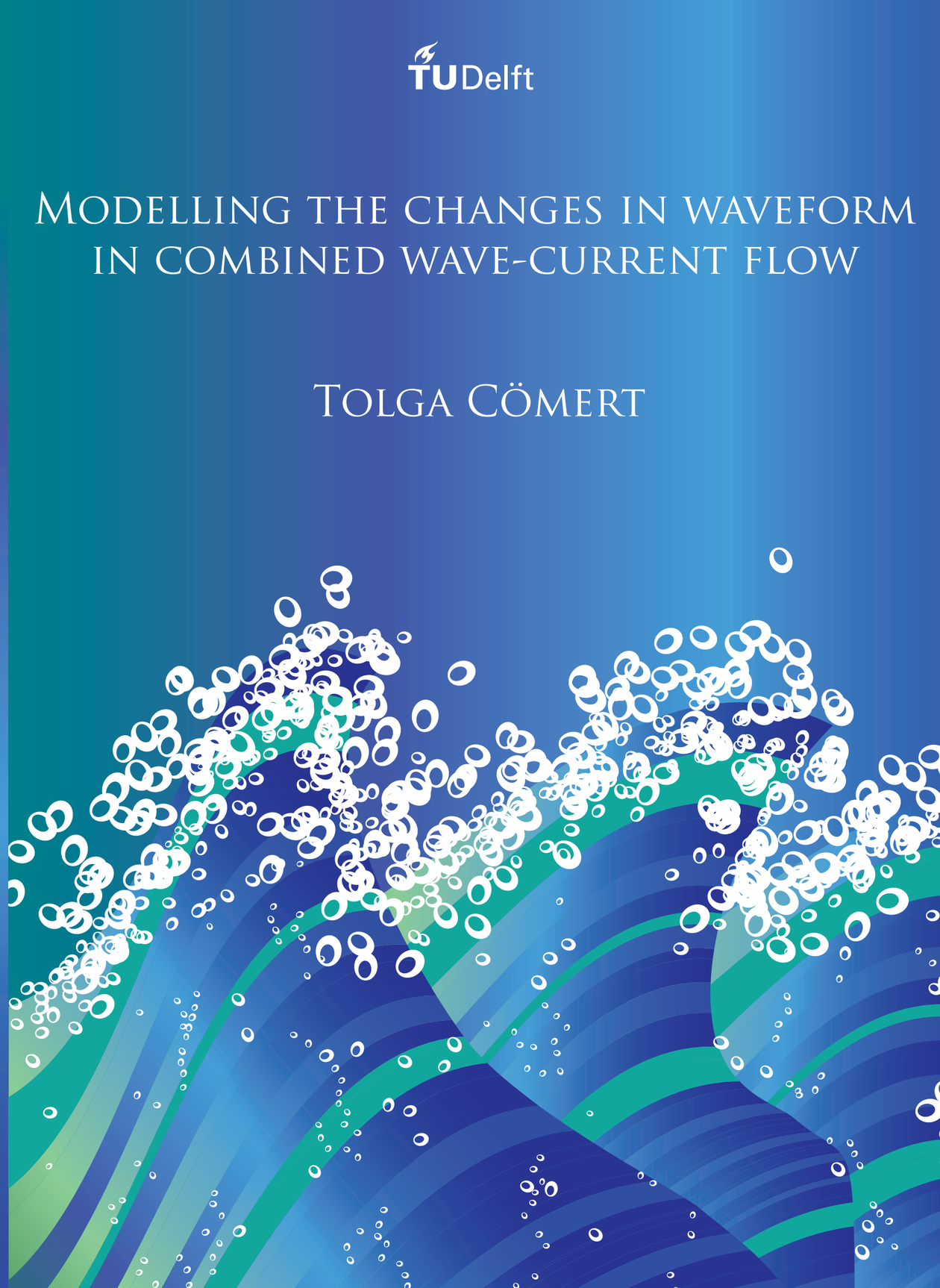

Modelling the changes in waveform in combined wave-current flow

Tolga Cömert

TU Delft

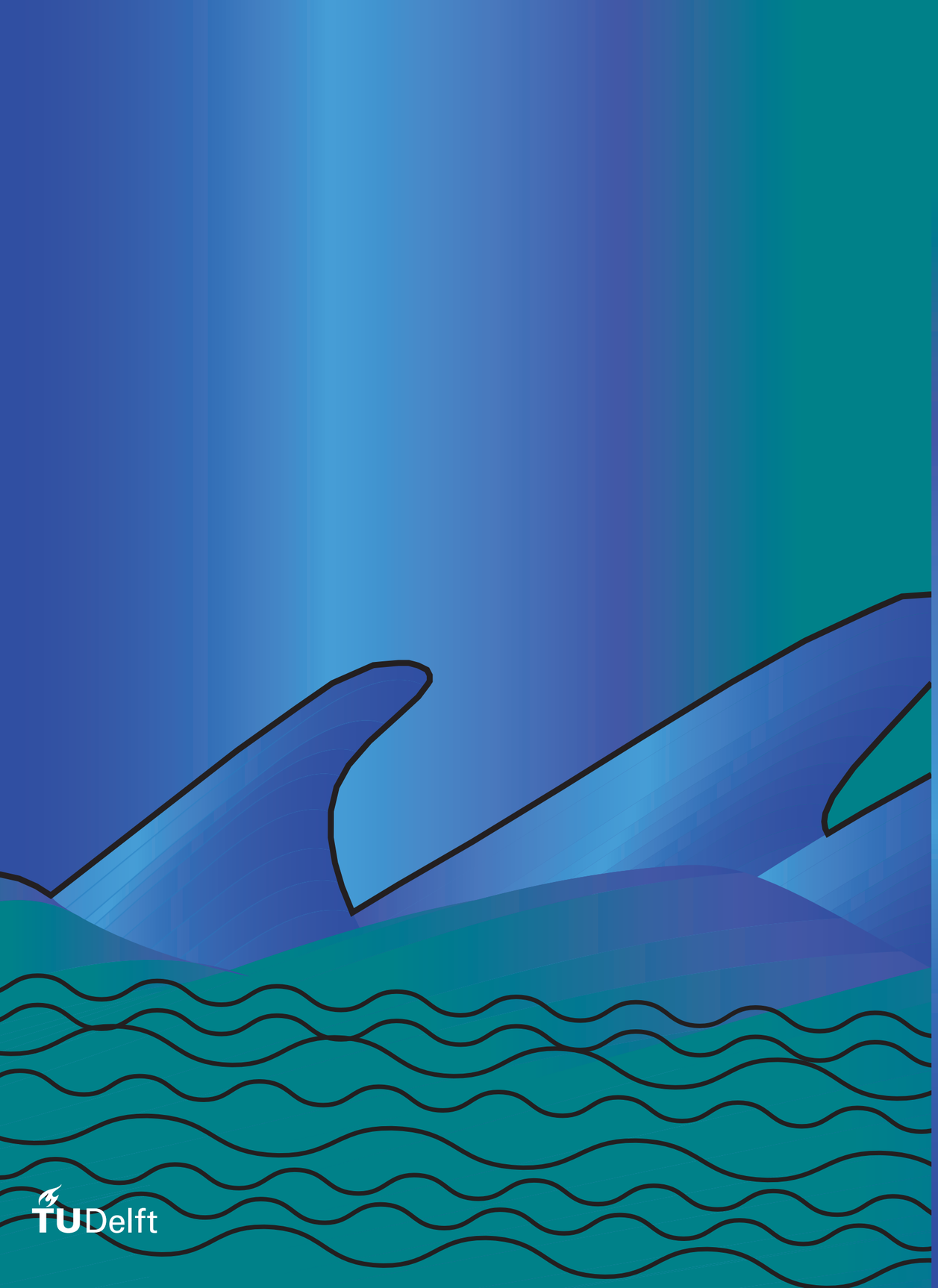

TU Delft

Modelling the changes in waveform in combined wave-current flow

Tolga Cömert

May, 2019

Modelling the changes in waveform in combined wave-current flow

by

Tolga Cömert

to obtain the degree of Master of Science

at the Delft University of Technology,

to be defended publicly on May 14, 2019 at 15:00.

Thesis committee: Dr. M. F. S. Tissier, chair/daily supervisor
Ir. F. P. de Wit, daily supervisor
Ir. J. Bosboom
Prof. Dr. Ir. A. J. H. M. Reniers
Dr. Ir. M. Zijlema

Tolga Cömert
Modelling the changes in waveform in combined wave-current flow
Delft University of Technology
Faculty of Civil Engineering and Geosciences (CiTG)
Department of Hydraulic Engineering (HE)
Environmental Fluid Mechanics (EFM)
Stevinweg 1, 2628 CN Delft
Postbus 5048, 2600 GA Delft

اللَّهُ الَّذِي سَخَّرَ لَكُمُ الْبَحْرَ لِتَجْرِيَ الْفُلْكُ فِيهِ بِأَمْرِهِ وَلِتَبْتَغُوا مِنْ فَضْلِهِ وَلَعَلَّكُمْ تَشْكُرُون

'It is Allah who subjected to you the sea so that ships may sail upon it by His command and that you may seek of His bounty; and perhaps you will be grateful' – ***Quran [45:12]***

Abstract

Combined wave-current flow is defined as the flow in which waves and currents are present together. Currents opposite to the wave direction are defined as opposing currents, while currents following the wave are defined as following currents. In general, waves in the presence of currents undergo a Doppler shift. As a result, waves have an absolute and relative frequency and the choice is mainly contingent on the frame of reference. Consequently, wave lengths are compressed (expanded) for an opposing (following) current. The importance of these effects generally depends on the spatial form of the current, which is governed by the bathymetry. Uniform (non-uniform) currents are present in the case of a uniform (non-uniform) bathymetry. For spatially uniform currents, waves are only Doppler shifted. For spatially non-uniform currents, the relative frequency increases (decreases) in the presence of opposing currents (following currents) when the current velocity is increasing in the direction of the wave. As a result, the wave amplitude increases (decreases) and the wave gets further compressed (extended). Wave blocking occurs when wave amplification leads to wave breaking.

In this research, combined wave-current flow was modelled with the non-hydrostatic wave-flow model SWASH in 2DV. The primary goal was to investigate the changes in waveform. In this research, the waveform was characterized by skewness, asymmetry and wave height. The secondary goal was to improve the present SWASH model and facilitate easier modelling of combined wave-current flow. Simultaneous input of waves and currents at the boundaries is not possible by default in the present SWASH release. Therefore, the WCS (Waves in Current Scaling) method was developed and implemented in SWASH. The WCS method provides scope for imposing regular or irregular waves in the presence of currents. One of its main features is an advanced scaling procedure at the outflow boundary: currents at either (1) the numerical wave maker in the case of opposing currents or at (2) the discharge boundary in the case of following currents are scaled to obtain mass conservation in the numerical domain.

Model results of uniform and non-uniform bathymetry demonstrated a constant wave height evolution over the domain. A general framework of modelling was created to ensure proper modelling of combined wave-current flow with the new SWASH model. Rules of thumb were created based on a sensitivity analysis of the spatial discretization and time step. It was found that for stable and accurate model results, 1) 75 or less gridcells per wave length, 2) 10 layers and 3) 4000 or more time steps per wave period were sufficient. Furthermore, SWASH was validated on the modelling of the vertical structure in combined wave-current flows. Measurements of the experiments by Klopman (1994) were used for validation. Time-averaged flow velocity profiles of the current- and wave-only cases were, in general, accurate in comparison to the measurements. A new implementation of the $k-\epsilon$ model showed that turbulent kinetic energy was suppressed, while in the present SWASH quantities of k were steadily increasing in time. For the combined wave-current flow cases, model results at the measuring position of Klopman (1994) were poor. Results at the wave maker boundary were more accurate, as the WCS method is a boundary condition method. As the fit was poor in general, a deeper analysis into the interactions between bottom, wave and current is needed. Lastly, SWASH was validated on its capability of modelling combined wave-current flow for non-uniform bathymetries. The opposing current case by Ma et al. (2017) was modelled in SWASH and model results were subsequently compared with experimental data. The trend in the model results were in good agreement with skewness, asymmetry and wave height profiles over the domain. Additionally, wave spectra at several

locations in the experimental domain were compared with model results. Model results were fairly accurate.

A key finding of this study was that the upwind scheme generates inaccurate model results of combined wave-current flow. The discretization of the water depth and the horizontal advection in the horizontal momentum equation were important. Use of the upwind scheme for these discretizations generally led to either increases or decreases in the wave height evolution over the domain, depending on the current direction. To conserve energy, a mimetic discretization is needed. A solution was implemented in the SWASH model by exclusively using the central difference scheme for the discretizations. Time steps were relatively small due to the use of the leapfrog scheme. Although this provided more accurate model results for the horizontal domain, it also led to improper modelling of the vertical structure of the flow. Interestingly, results of the vertical structure for a model with the upwind scheme were significantly more accurate. However, it is debatable whether experiments, for instance by Klopman (1994), are modelled properly in 2DV. Three dimensional effects have to be included for an appropriate velocity profile.

This study shows that SWASH was to some extent capable of modelling combined wave-current flow. The wave height evolution over the domain was modelled fairly accurate. However, model results of the vertical structure of the flow were poor, indicating that the model was not correctly resolving (physical) processes in the vertical. It is recommended to further analyse the effects of numerical schemes on the model results. Furthermore, the WCS method proved to be a useful addition, as model skill scores were mostly positive. Thus, the method should be expanded to 3D domains for further validation. In general, SWASH should be further developed to allow accurate modelling of combined wave-current flow. For instance, a new sponge layer technique is needed, as the present technique was not completely working for combined wave-current flow.

Acknowledgements

After many months of hard work, I am proud to show you the results of my thesis research. During this time, I improved my technical and analytical skills, but more importantly, I learned new things about myself. Research is exploring the unknown and for many, this might sound grim and most of all difficult. How do you investigate something you hardly have any knowledge about? For me, this is what makes research interesting. I find exploring and analysing physical phenomena that are not understood yet exciting. This is best understood with the following metaphor: when solving a Sudoku puzzle, the start is easy, but the mid-part gradually becomes more tough, until you find that one breakthrough, leading to a very rewarding end. As a result, I experienced many ups and downs, but my time-averaged progress would resemble an upwards linear slope.

This thesis work would have not been possible without the contribution of many people. If I have forgotten any names, please forgive me and know that I am very appreciative of your help.

Marion and Floris, expressing my gratitude on paper is not enough to show your involvement and passion for this research we have done together the past year. Marion and her seemingly infinite pool of knowledge about this thesis topic helped me a great deal, especially during the interpretation of my results. Her feedback and sharp comments improved this thesis tremendously. Floris was not too long ago dealing with SWASH and its complex mathematical and computational core. His experience and knowledge of SWASH and general modelling practices made my difficult times with the model bearable. With his initial idea, we were able to derive and validate the method presented in this thesis. I am thankful to both of you for our weekly meetings which pushed me to keep on track. Thank you for guiding me through this challenging but intriguing topic.

Judith, not only did you teach me a ton of stuff during your amazing lectures, but your critical thinking and constant 'why' and 'how' questions forced me to change my mindset. It is easy to state that I will achieve something, but actually thinking how is the difficult but most critical part. Your way of explaining concepts is astonishing, as I often understand you immediately. Thank you very much for your commitment and time.

Ad is not only a great lecturer but also an incredible researcher. A large part of the results we obtained would not be possible without your help. Your way of decomposing a problem and linking it with the methodology is a skill that helped me at many moments. Thank you for being part of this research.

Marcel, I am very grateful that even with the toughest SWASH problems you were there to help me. Your intelligence is unlimited as was your commitment to this work. I am still amazed by your computer skills and I hope that one day, I might reach your level. I hope the contributions we made will further advance SWASH and make it an even greater model than it is. I want to thank you for your involvement.

My stay in office room 2.92.1 was very enjoyable due to the presence of fellow MSc and PhD students. Thank you Said, Lennard, Ruben, Hugo and Ascha for the many laughs and talks we had. Thanks to everyone on the 2nd floor and Waterlab for the fun talks during lunch breaks. Furthermore, I want to thank Said, Alaqel and Choco for reading my report and giving constructive feedback. Many thanks to Otti for helping me with administrative issues and planning of meetings. Special thanks to Carine for providing the figure with an overview of SWASH routines.

I would like to thank my parents and my little sister for their unconditional love and support during all my years of study. Above all, I want to thank Allah, the almighty, for granting me the opportunity, determination and strength to do my research and for blessing me with great people who have been my support in my personal and professional life, Alhamdoelillah.

Enjoy reading!

Tolga Cömert
May 2019, Delft

Contents

1 Introduction

1.1 Context

1.1.1 General information regarding combined wave-current flow

Combined wave-current flow is defined as the propagation of free-surface waves in the presence of currents. If currents propagate in the same direction as the wave, they are characterized as *following currents*. When currents propagate against the wave, they are characterized as *opposing currents*. All of these currents may demonstrate spatial differences in the case of a non-uniform bathymetry. Accordingly, a distinction is made between waves on spatially uniform and non-uniform currents. This is the same as the distinction between combined wave-current flow for a uniform and non-uniform bathmetry, as bathymetry and the spatial structure of the current are directly related to each other by mass conservation.

By definition, any type of wave or current may be present in wave-current flow, e.g. tidal waves (wave), river outflow (current) etc. This research is limited to the most common types of waves and currents near the coast and in experimental studies. Incoming waves at the coast are usually generated at the ocean (swell) or during local storms (wind waves) and waves in laboratories are generated with wave makers. In general, the assumption for currents is that the temporal and spatial scales are much larger than those for waves, thus a steady state is assumed (Jonsson et al., 1970; Peregrine, 1976; Wang et al., 2018). Currents varying in time are not within the scope of this research.

The study of combined wave-current flow has been an active research area in the past couple of decades. This is evident from the occurrence of many experimental studies (e.g. Kemp and Simons, 1982, 1983; Lai et al., 1989; Umeyama, 2005). The general objectives are to study wave-current related phenomena and to obtain data sets to validate numerical models. These experimental studies frequently demonstrate the occurrence of phenomena that cannot be explained by theory or still lack a physical and mathematical background in existing wave-current models. Therefore, the emphasis in this research is put on the modelling practices of combined wave-current flow.

1.1.2 Examples of combined wave-current flow in nature

Many examples of combined wave-current flow are found in the natural environment. Tidal inlets are large natural systems at which incoming waves meet following (opposing) currents during flood (ebb) tide. During extreme events, such as wave blocking in case of waves meeting a non-uniform opposing current, wave heights can significantly amplify. Ships are then more prone to rough wave conditions and capsizing might occur during the breaking of these amplified waves (Chawla and Kirby, 2002). Analysis shows that the non-linear interaction between waves and (tidal) currents induces sediment import into tidal basins (Elias et al., 2006). These non-linear interactions may also have a considerable influence on cross-shore sediment transport (Klopman, 1992), but due to lack of in-depth knowledge, more research is needed (Elias et al., 2006).

Another example in coastal and open ocean waters is the occurrence of freak waves (waves with wave heights approximately $2.2H_s$ (Dean, 1990)). Freak waves form threats to navigation vessels and

marine structures (Wu and Yao, 2004). The presence of strong opposing currents might be one of the dominating factors in the generation of this type of wave, but this remains uncertain (e.g. Hjelmervik and Trulsen, 2009; Lavrenov and Porubov, 2006; S. Yan et al., 2010).

More knowledge regarding combined wave-current flow can also be of great importance for other research fields. Combined wave-current flow is analogous to the occurrence of phenomena around black holes (Euvé et al., 2015; Schützhold and Unruh, 2002). With the use of wave-current models, new insights into the related phenomena can be gained.

1.1.3 Hydrodynamics and sediment dynamics in combined wave-current flow

The examples in the previous section show the relevance, importance and broadness of the research scope in combined wave-current flow. Within this study, emphasis is put on the hydrodynamics of combined wave-current flow. Understanding the hydrodynamics is important, as it makes provision for further studies on the sediment transport in combined wave-current flow.

Inherently, the hydrodynamics of combined wave-current flow are to a large extent the same as for wave- and current-only flows. However, the most noticeable difference between these flows is the wave-current interaction present in combined wave-current flow. The influence of wave-current interactions on flow, soil and structures has been extensively studied (e.g. C. W. Li and K. Yan, 2007; Y. Li and Lin, 2010; J. Yu and Slinn, 2003, amongst others). Studies show that including wave-current interactions in the hydrodynamics generally leads to different results than a superposition of the wave- and current-only results. Including wave-current interactions in the numerical modelling of combined wave-current flow is therefore important.

Sediment dynamics largely depend on the hydrodynamics. In general, waves and currents are important sediment transport mechanisms. The main rule of thumb is that waves stir up the sediment, whereas currents mix and transport the sediment (Bijker, 1992). However, this is only the case for the current related transport. Wave-related fluxes can also be present, e.g. asymmetric waves in shallow water with higher peak velocities at the wave crest relative to lower peak velocities at the wave through (van Rijn and Havinga, 1995; van Rijn et al., 1993). Unravelling sediment transport with all of these contributions included, i.e. wave related transport, remains difficult.

A list of advances in sediment transport modelling under wave-current interactions is formulated by Lu et al. (2015). Their main conclusion is that future research in this topic should focus on better understanding of the non-linear processes involved in wave-current interactions and quantitative descriptions of suspended sediment transport for different combinations of current, wave and sediment size.

1.1.4 Problem statement

As there is a lot to be discovered in the hydrodynamics in combined wave-current flow, not many useful findings can be applied in sediment transport. For instance, the bed shear stress in combined wave-current flow has been subject to debate as many different models exist (e.g. Bijker, 1967; Christoffersen and Jonsson, 1985; Grant and Madsen, 1979, amongst others) and each one leads to different results, which demonstrates the lack of a (fundamental) physical description (Soulsby et al., 1993).

The superposition of solutions for wave- and current-only flows is (in most cases) not possible due to the non-linear interaction between the waves and currents (Kemp and Simons, 1982). Tools, such as numerical models, are therefore used to better understand the physical processes in combined wave-current flow. A distinction can be made between computational fluid dynamics (CFD), phase-averaged and phase-resolving models. CFD models are too restricted to the fluid and moreover complex to use. Phase-averaged models, such as SWAN (Booij et al., 1999), take wave-current flow into account, but many unknowns remain in the intra-wave scale. Phase-resolving models solve at the intra-wave

scale with relatively low computational effort. Combined wave-current flow can therefore be modelled efficiently and accurately. Phase-resolving models of the Boussinesq-type have been widely used (e.g Chen et al., 1998, 2003), but they are, to some extent, limited as only depth-averaged values are returned. However, phase-resolving models that incorporate the RANS equations can resolve the vertical.

1.2 Research objectives

1.2.1 Research goals

The primary goal of this research is to investigate the changes in waveform in combined wave-current flow. Waveforms, i.e. the shape of waves, implicitly give information regarding flow parameters, such as the velocity. For instance, waveforms can be used as initial estimators for the effects of waves on suspended sediment transport. For this research, the waveform is characterized by skewness, asymmetry (both third order moments depending on the axis of interest (Elgar, 1987)) and wave height.

The secondary goal is to create the base for a new tool for future applications, including the modelling of suspended sediment transport in combined wave-current flow. The horizontal domain is restricted to 1D. In 2DH/3D, the wave-current angle is the angle between the main directions of both mechanisms. It can induce refraction of the wave by the current and influence the strength of the interaction between both of them. These types of 2DH/3D effects are ignored. However, the newly developed method in this research is easily expandable to 2D domains.

In this research, the non-hydrostatic wave-flow model SWASH (Zijlema et al., 2011) is developed and validated regarding its performance in modelling combined wave-current flow. A new method is developed in SWASH, which allows easier modelling of waves and currents simultaneously. Results for the spatial structure of combined wave-current flow will be validated with experimental data. An additional benefit of using SWASH is that the model is capable of modelling sediment transport. In general, there have been many studies related to modelling sediment transport in, for instance, the vicinity of a tidal inlet (Dodet et al., 2013, amongst many others), but no numerical studies have been performed with the use of a phase-resolving wave-flow-sediment model. Although this is not the topic of this research, future research can focus on further development of the techniques used in this research to include the modelling of sediment transport.

1.2.2 Research questions

Based on the overall aim of this research, the following research question and sub-questions are defined:

Main research question

What is the validity of SWASH in modelling combined wave-current flow for uniform and non-uniform bathymetries in 2DV for opposing and following currents?

Sub-questions

- Which variables in combined wave-current flow induce changes in the waveform?
- How can the present SWASH model be extended to facilitate the modelling of combined wave-current flow?
- To what extent can SWASH be used to model combined wave-current flow for uniform and non-uniform bathymetries in 2DV for opposing and following currents?

1.3 Research method

The general methodology of this research is given in a chronological order:

1) A literature study will be performed to gain in-depth knowledge regarding wave-current interactions. A review of theory regarding combined wave-current flow for uniform and non-uniform bathymetries will be made. Findings in experimental research will be highlighted.

2) The model limitations of the present SWASH release with combined wave-current flow will be analysed. A new method will be developed within the model to allow a much easier and proper integration of combined wave-current flow.

3) The new SWASH model will be validated based on basic cases and experimental data. Agreements and shortcomings will be discussed and improvements of the method outside the scope of this research will be recommended. Validation will be performed with data of the vertical structure and spatial evolution of wave height, skewness and asymmetry.

1.4 Outline

In this chapter, an introduction was given into combined wave-current flow. The research objective has been defined and elaborated on. In Chapter 2, background information is given on combined wave-current flow and findings in experimental studies.

In Chapter 3, the new method in SWASH is presented. Additional model settings and validation parameters are discussed. The results with the new method are shown in Chapter 4. Basic cases for uniform and non-uniform bathymetries are used and compared with analytical solutions.

The first validation of model results is performed in Chapter 5. Emphasis is put on the vertical structure in combined wave-current flow. Chapter 6 focuses on the spatial evolution of the waveform. This is done by validation with experimental data.

In Chapter 7, interesting results are discussed and the validity of this research is generalized. Finally, in Chapter 8, the research questions are addressed and further recommendations are given. Supplementary materials (figures, tables, context) are provided in appendices.

2 Background information

This chapter provides background information relevant to combined wave-current flow. Traditional theories for waves are applicable for combined wave-current flow, but a shift in paradigm is required, as waves are now propagating on top of currents.

In Section 2.1, general equations for waves on currents are discussed. A distinction is made between waves on uniform and non-uniform currents. Both of them are assessed in Sections 2.2 and 2.3 respectively. Techniques, such as calculating wave parameters in the presence of currents, are demonstrated.

Based on findings in experimental research, features of wave-current interactions are examined in Section 2.4. Observed phenomena, for instance blocking of waves, are highlighted. A general overview of relevant wave-current interaction mechanisms is given in Section 2.5. Lastly, a summary of the chapter is given in Section 2.6.

2.1 General theory on combined wave-current flow

2.1.1 Frame of reference

In combined wave-current flow, the frame of reference is an important starting point. If the wave is viewed by a non-moving observer, the movement of the wave together with the total movement enforced by the current are observed. Values in this non-moving, i.e. stationary, frame of reference are denoted with subscript $_a$.

The other option is to define a frame of reference that moves with the wave itself. In this moving, i.e. relative, frame of reference, values are denoted with subscript $_r$. Note that the current is still physically present, but omitted from the perspective of the observer.

2.1.2 Wave parameters in presence of currents

In general, the interaction between a wave and a current is characterized by the Doppler shift endured by the wave:

$$\omega = \sigma + kU, \tag{2.1}$$

where ω is the absolute wave frequency, σ is the relative wave frequency (also known as intrinsic frequency), k is the wave number and U is the depth-averaged current velocity. If this equation is differentiated with respect to k, the result is:

$$c_{g,a} = c_{g,r} + U, \tag{2.2}$$

where $c_{g,a}$ is the absolute group velocity ($= \frac{\partial \omega}{\partial k}$) and $c_{g,r}$ is the relative group velocity ($= \frac{\partial \sigma}{\partial k}$). Depending on the frame of reference, either one of the velocities is valid.

The relative wave frequency is usually expressed as a function of the wave number:

$$\sigma = \sqrt{gk \tanh(kd)}, \tag{2.3}$$

where d is the water depth. Substituting this expression in Equation 2.1, results in an equation where the absolute wave frequency is explicitly a function of the wave number. This equation is also known as the dispersion relation in the presence of currents.

2.1.3 Change in relative wave frequency

Generally, the absolute wave frequency is known and therefore fixed. The relative frequency, i.e. the wave length, can change depending on the current. A distinction can be made between three cases: 1) no current, 2) spatially uniform current (see Section 2.2) and 3) spatially non-uniform current (see Section 2.3).

1. In a no current case, the second term on the RHS of Equation 2.1 reduces to zero, which means that the absolute and relative frequencies are equal. This is the basic case, for which all expressions, derived from any wave theory, are completely valid and applicable.
2. For a spatially uniform current, the absolute wave frequency is larger (smaller) than the relative wave frequency in case of a following (opposing) current. The wave length changes as a result: for a following (opposing) current, the wave length increases (decreases). Expressions derived from wave theories need to be modified in order to get consistent results.
3. In the final case, a spatially non-uniform current, the change in wave frequency depends on the change of the current. Spatially varying currents can occur when there is a constriction or expansion, either vertically or horizontally, in the flow pattern. Examples are, amongst others, submerged bars where the current has higher velocities on top of the bar due to mass conservation. For a wave with an opposing current that increases in strength along the wave ray, the wave length decreases while the amplitude increases. An extreme case is wave blocking. During this event, the energy of the wave is completely blocked by the current. In Equation 2.2, the absolute group velocity then reduces to zero. For a wave with a following current, the wave length increases and the amplitude decreases. These effects are reversed when the current is not increasing, but rather decreasing in strength.

2.1.4 Applicability of linear wave theory

It is important to realise that in combined wave-current flow, the physical characteristics of waves remain the same. For instance, shortening of the wave, present in a *uniform* bathymetry, does not lead to a reduction of the wave amplitudes. The change in wave amplitude is independent of the choice of frame of reference. Wave amplitudes are only altered if there are spatial gradients in, for instance, bathymetry or currents.

There is no conservation of energy for waves in combined wave-current flow due to the energy transfer between the waves and current. However, there is conservation of wave action, N. Wave action is defined as the ratio between wave energy and relative frequency, i.e. $\frac{E}{\sigma}$.

Linear wave theory is still useful for waves in the presence of currents. However, additional adaptations are needed to gain the correct expressions. A detailed derivation is given in Hedges (1987). Only relevant expressions for this research are repeated here. The expression for the horizontal orbital velocity is:

$$u_{orb}(x,z,t) = \sigma a \left(\frac{\cosh(k(d+z))}{\sinh(kd)} \right) \sin(\omega t - kx), \tag{2.4}$$

where a is the wave amplitude and z is the vertical distance from the mean water level (upwards is positive). The difference from regular linear wave theory is the use of the relative wave frequency for the velocity amplitude, which is physically reasonable, as the wave undergoes a Doppler shift.

The wave action balance for a 1D domain without frequency shifting is defined as:

$$\frac{\partial N(x,t)}{\partial t} + \frac{\partial c_g N(x,t)}{\partial x} = \frac{S(x,t)}{\sigma}, \tag{2.5}$$

where N is the wave action, c_g is the group velocity in x-direction and S is a summation of the source terms. If steady conditions without source terms are assumed, the wave action balance can be simplified to:

$$\frac{\partial c_g N(x,t)}{\partial x} = 0. \tag{2.6}$$

This equation shows that the wave action flux does not change in space and should therefore be equal everywhere in the domain. A solution, integrated in space, is provided by Hedges (1987):

$$\frac{\rho g H^2}{8\sigma}(U + nc_r) = \text{constant}, \tag{2.7}$$

where H is the wave height and n is the factor between the group and phase velocity of a wave.

2.2 Waves in presence of uniform current

2.2.1 Graphical solution by Jonsson et al. (1970)

As was mentioned in Section 2.1, the dispersion relation remains valid for a wave in the presence of a uniform current. Jonsson et al. (1970) provide by means of a graphical method the iterative procedure to calculate wave lengths in presence of currents. The equation derived is:

$$\sqrt{\frac{d}{L}\tanh(kd)} = \sqrt{\frac{d}{L_0}}\left[1 - \frac{U\sin(\beta)T_a}{h}\frac{d}{L}\right], \tag{2.8}$$

where L is the wave length, L_0 is the deep water wave length and β is the angle between the wave ray and the current vector. This angle can be omitted, as β equals zero for the cases in this research. However, for this general analysis, this simplification is not taken into account.

Equation 2.8 can be solved iteratively or with the use of a graph such as the one in Figure 2.1. Equation 2.8 is reformulated in the form $F(h/L) = G(h/L)$, where F and G are arbitrary functions with argument h/L. F is unique and can be determined with the use of wave tables. G is, however, different, as it depends on the characteristics of the current and appears as a straight line in the graphical method.

Three cases are identified: 1, 2 and 3. Case 3 is divided in subcases a, b and c. Results are shown in Figure 2.1. Note that the vertical axis shows either the solution of the F or G function and the horizontal axis is the argument h/L. In case 1, the current is following, while in case 3 the current is opposing. In case 2, the current velocity equals zero and is, therefore, not relevant to the scope of this research.

The general result can be summarized for two cases: when the current and the wave propagate in the same direction, the wave length increases. When the current and the wave propagate in opposite directions, the wave length decreases. Neglecting these differences with waves on still water ($U = 0$) can lead to a source of errors (Peregrine, 1976).

2.2.2 Analytical solution by Peregrine (1976)

Peregrine (1976) expands further on the work of Jonsson et al. (1970) by providing a new mathematical analysis. Equation 2.1 is rewritten such that $m = \omega - \vec{k} \cdot \vec{U}$ with $m = \pm\sigma$. Note that the variables are now 2D.

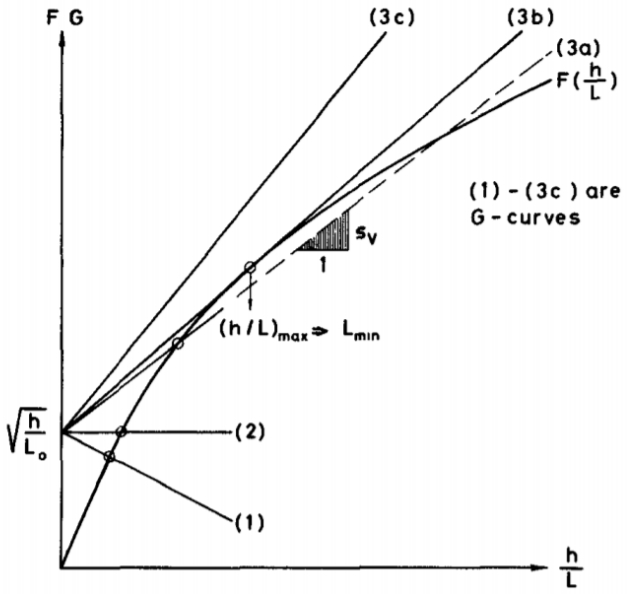

Fig. 2.1.: Graphical representation of Equation 2.8 from Jonsson et al. (1970). F and G are substitute variables for the left-hand and right-hand side respectively. With this figure, the wave length can be determined for waves in presence of currents by finding the ratio of h/L for intersections between the substitute variables (F = curve, G = straight). Taken from Jonsson et al. (1970).

Figure 2.2 shows a diametral section, i.e. cross-section in a circle with form of the possible solutions, where the horizontal axis is the wave number made relative to the current with a unit vector e and the vertical axis shows the solutions for m in the case of $U \neq 0$ and $k \not\propto U$. Only solutions to Equation 2.1 are of interest, thus, the trace of the plane of $m = \omega - \overrightarrow{k} \cdot \overrightarrow{U}$ is also shown.

Points A, B, C and D are intersection points and represent a physical state of the flow: for the cases in this research, points A and B are interesting to analyse. Point A is a wave in the direction of the current (positive axis), which results in an absolute wave frequency larger than the relative wave frequency (see Equation 2.1). At point B, the wave has an opposing current and the absolute frequency is smaller than the relative frequency. Both points demonstrate a shift in their frequency, which in the previous sections was defined as the Doppler shift.

2.3 Wave in presence of non-uniform current

For spatially varying currents, the change in current leads to changes in wave properties. The most evident case is a wave propagating against an opposing current. The wave is forced back by the current, but the group velocity of the waves is usually high enough, such that the current velocity can be overcome.

2.3.1 Change in amplitude

Longuet-Higgins and Stewart (1960) demonstrate by means of a mathematical analysis the change in waveform of short gravity waves on currents and (relatively) long waves. The rate of transfer of energy, R_x, across a fixed surface in space (only one axis) is found to be equal to:

$$R_x = Ec_g + EU + S_xU + \frac{1}{2}\rho d(U + E/c\rho d)^3, \tag{2.9}$$

where S_x is the radiation stress. It is S_xU, ignored in previous derivations, that includes the interaction between a wave and current. It represents the work done by the current against the radiation stress due to the wave motion. Using this extra term, Longuet-Higgins and Stewart (1960) formulate that the

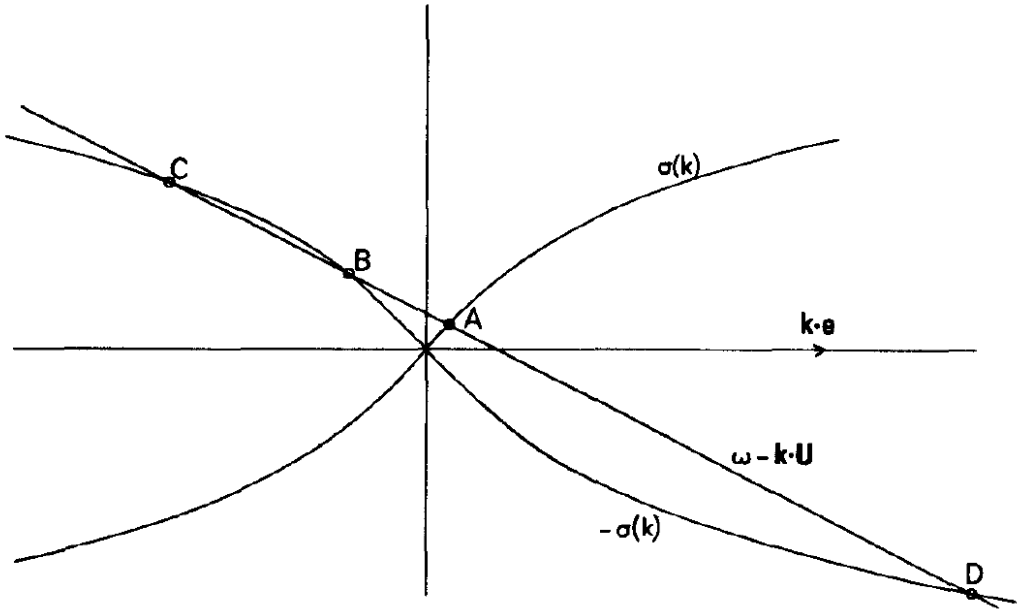

Fig. 2.2.: For multiple values of vector k, solutions of the dispersion relation are given. Equation 2.1 is considered in (k, m) space. Taken from Peregrine (1976).

work done against the radiation stress is converted into short-wave energy, which means an increase of the short wave amplitude.

In a following publication, Longuet-Higgins and Stewart (1961) derive the change in wave amplitude for a non-uniform current by using Equation 2.9. The expression found is:

$$\frac{a}{a_0} = \left[\frac{c_0(c_0 + 2U_0)}{c(c + 2U)}\right]^{\frac{1}{2}}, \tag{2.10}$$

where the quantities denoted by subscript $_0$ are still water values. This equation demonstrates that for opposing currents, the waves are amplified exponentially while for following currents, the wave amplitude decreases similar to a square root relation.

2.3.2 Definition of wave blocking

At the wave blocking point, waves are blocked from propagating further. Peregrine (1976) demonstrates by means of the conservation of wave action that the condition for a blocking point is met for $U = -\frac{1}{4}c$, where c is the phase velocity of the waves for still water. Points B and C (see Figure 2.2) might converge, which means that the group velocity of the waves equals the current velocity. The point at which this property holds, is, thus, called the wave blocking point and its characteristic equation is:

$$c_{g,r} + U = 0. \tag{2.11}$$

Leading up to the wave blocking point, wave lengths are shortened, leading to an amplification of the wave amplitude. As a results, waves are steepened. Wave breaking occurs for full wave blocking, but it is also observed when conditions nearly meet the required ratio for blocking (Lai et al., 1989).

2.3.3 Wave reflection at wave blocking point

Shyu and Phillips (1990) and Trulsen and Mei (1993) demonstrate that due to the increase of the intrinsic frequency of the wave, the relative propagation velocity of the waves at a certain moment equals the current velocity, after which wave reflection takes place at the blocking point. This is due to the further increase of the intrinsic frequency, leading to propagation in the direction of the current.

When the capillary effect is also taken into account, a second reflection may occur if the intrinsic frequency increases up to capillarity. Note that wave reflection is only of importance for small wave amplitudes. Due to the increase in wave steepness, wave breaking takes place at or before the blocking point and no/very little wave reflection takes place (Chawla and Kirby, 2002).

The amount of waves reflected has been approximated by Stiassnie and Dagan (1979) for the case of non-uniform slowly varying currents. When the current velocity at the blocking point is approaching the maximum current velocity, not all waves will be reflected, meaning that there is partial wave reflection at the wave blocking point.

2.4 Experimental research

Experiments in combined wave-current flow are rare, as the experimental setup is difficult to realise. Without proper care, simultaneous generation of waves and currents might lead to the presence of secondary effects such as recirculating flow due to insufficient wave and current absorption. This makes validation of numerical models difficult. Between experiments, a distinction is made between experiments focussed on the vertical structure of combined wave-current flow and experiments analysing parameters in the horizontal domain.

2.4.1 Vertical structure of combined wave-current flow

Bakker and van Doorn (1978) were one of the first researchers that looked at the vertical structure of a combined wave-current flow. Their aim was to gain data and validate a new mathematical model that could model the turbulent bottom boundary layer. One of their main findings was that a simple superposition between the mean velocity distribution of a current and mean velocity distribution of a wave is not correct, as the combined wave-current flow showed significant differences in the mean velocity profile.

Experiments by Kemp and Simons (1982, 1983) focused more on the locations in the upper layer and near the bed in a combined wave-current flow. For a following current, it was found that the bed shear stress was significantly increased for a rough bed. The mean velocity, compared to a current-only case, was lower, but the turbulent intensities were much larger for a rough bed. For a smooth bed, the same results were found but the magnitudes were considerably smaller. For both beds, the turbulent boundary layer was reduced in thickness.

For opposing currents, Kemp and Simons (1982, 1983) found that for a rough bed, the apparent roughness and shear stress (a measure for the bed roughness in combined wave-current flow) were substantially increased, while the mean velocity decreased. In general, it was found that the mean velocities in the upper layer were retarded for a following current and increased for an opposing current.

Klopman (1994) (a detailed description is given in Section 3.3.1) measured the same effect in his experiments, which led to the development of a generalized Lagrangian mean model by Groeneweg (1999). This model was validated with experimental data, indicating that the model is capable of modelling combined wave-current flow.

An assessment was made of the observed change in mean velocity profile based on two theoretical explanations: one based on the local force balance in the longitudinal direction and the other on secondary circulations in the cross-sectional plane (Groeneweg and Battjes, 2003). Results showed that the longitudinal component of the wave-induced driving force was substantially dominant over the cross-sectional components (Groeneweg and Battjes, 2003).

Umeyama (2005) performed detailed experiments to assess the Reynolds stresses and velocity distributions in combined wave-current flow. Results of the velocity profiles are shown in Figure 2.3. The

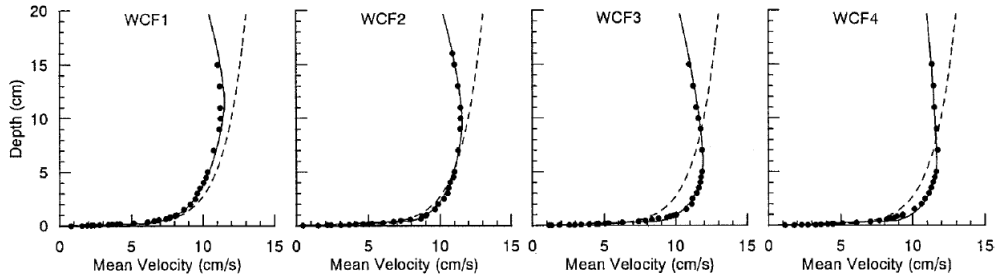

(a) The mean velocity profiles for following currents.

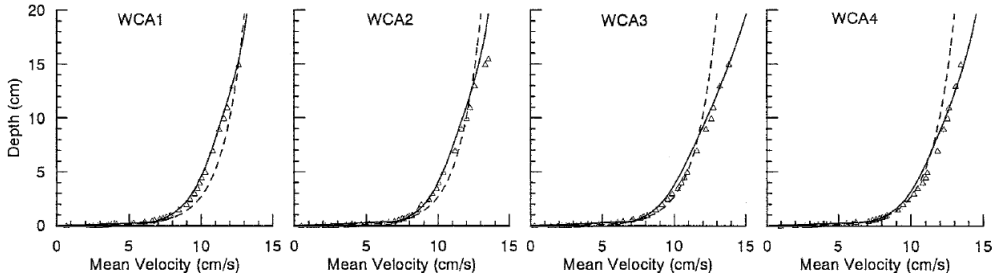

(b) The mean velocity profiles for opposing currents.

Fig. 2.3.: Measurements as obtained by Umeyama (2005). Higher test numbers usually mean larger and longer waves. The measurements are shown by data points (circular for following and triangular for opposing). Model results by Umeyama (2005) are shown with the black line. The measurement results clearly show the deviation with the logarithmic profile (dashed line), typically obtained for open channel flows. Taken from Umeyama (2005).

velocity distributions for following (opposing) currents show a relatively higher (lower) velocity near the bed and a lower (higher) velocity above a certain height (Umeyama, 2005).

The combined wave-current Reynolds stresses, a measure for the turbulence in the flow, slowly decreases from the bed for an opposing current. For a following current, there is a rapid decrease and even a point at which the sign of the Reynold stress changes.

2.4.2 Horizontal structure of combined wave-current flow

Lai et al. (1989) set up experiments in a wave tank. Waves were generated by wave makers on both ends of the tank. The currents were generated by a pump at the left end of the tank, resulting in waves that propagated following (left end) or trailing (right end) the current. Measurement devices, such as a Doppler velocimeter and capacitance probes, were used to measure every experiment. The current profile was measured at various depths and the measurements of the slope of the surface were converted to the wave number and phase velocity. Figure 2.4 shows the experimental setup.

The experiments were carried out for non-breaking and breaking waves. The shortening of the wave length was observed for gently breaking waves, as well as a shift in the intrinsic frequency. In the case of wave blocking, the theoretical blockage limit point of $\overline{u}/C \approx 1/4$ was found, confirming results of past research (e.g. Y. Y. Yu, 1952).

Another result obtained by this study, which was not performed previously at that time, was the effect of spatially varying currents. The end conclusions were that (1) the kinematic conservation of the waves was confirmed for the steady state condition ($\frac{\partial k}{\partial t} + \nabla n = 0$, with k the wave number and n the apparent frequency, can be reduced to $\nabla n = 0$ in steady state) and (2) variations of characteristics of waves propagating against currents agree well with predicted values by use of the kinematic conservation and the dispersion relation (Lai et al., 1989).

Briggs et al. (1997) researched wave-current interaction in inlets by using laboratory experiments. Regular and irregular waves were studied with and without ebb (opposing) and flood (following)

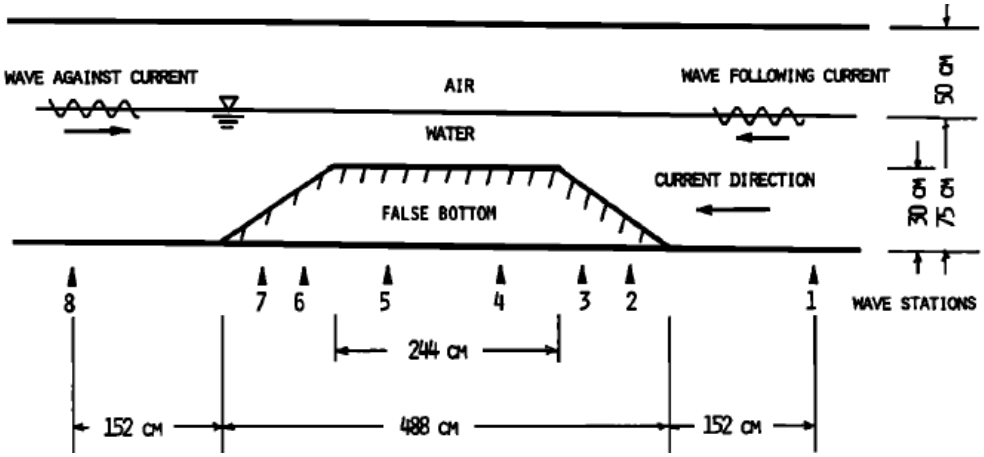

Fig. 2.4.: Schematic view of experimental setup by Lai et al. (1989). The maximum and minimum water depth were $0.75\ m$ and $0.35\ m$ respectively. The current was imposed from right to left. Waves were imposed at the left and right end of the flume. The false bottom was used to create a current field with spatially varying velocity. Time series were generated at 8 wave stations. Taken from Lai et al. (1989).

currents. Results showed that wave breaking occurred for the larger wave heights. With the use of the numerical model REFDIF, changes in the wave parameter in presence of currents were computed. The model predictions were in very good agreement with the measurements.

One of their main findings was that higher frequency components were generated in case of ebb currents. This growth took place at a non-linear rate with the current velocity. These components were occasionally blocked, leading to gentle wave breaking. The spectral shape of the waves remained the same, except in cases with severe wave breaking. All higher frequency components were completely blocked, resulting in a change of the spectral shape by reduction of the energy in the wave spectrum (Briggs et al., 1997). The increase of higher frequency components was similar to wave-only experiments for shoaling (Briggs and Smith, 1990; Smith and Vincent, 1992).

Chawla and Kirby (1999) used an experimental setup in which a three-dimensional structure was responsible for the spatial non-uniformity of the current. At one end, waves were generated with a wave paddle, while at the other end currents were generated with a pump. An inlet was created to avoid the additional focusing of the waves on laterally spreading jets.

The setup was created such that wave blocking occurred close to the narrow part of the inlet (see Figure 2.5). Monochromatic waves with varying wave heights were used for each experiment run.

The results demonstrated wave reflection from the blocking point for even the smallest amplitudes. Theoretical models did not agree well with measured values due to non-linear effects, i.e. amplification of the wave amplitude, at the wave blocking point (Chawla and Kirby, 1999). Furthermore, amplitude dispersion is an important process in wave blocking. Amplitude dispersion is defined as waves having different phase velocities for different wave amplitudes. Depending on the initial wave amplitude and frequency, monochromatic wave-current interactions lead either to (1) blocking and reflection, (2) blocking and breaking at blocking point, (3) passage of wave through the maximum current due to amplitude dispersion but still wave breaking and thus blocking and (4) energy transfer to lower frequencies where wave blocking does not occur (Chawla and Kirby, 1999).

Chawla and Kirby (2002) continued their experimental research by analysing the differences between monochromatic and random waves in combined wave-current flow. Models with a wave slope criterion, i.e. maximum wave slope allowed, matched measurement data very well (Chawla and Kirby, 2002).

The importance of non-linear effects are seen in the dispersion relation and energy shift to lower frequencies. Current-limited breaking is found to be very different for monochromatic and random

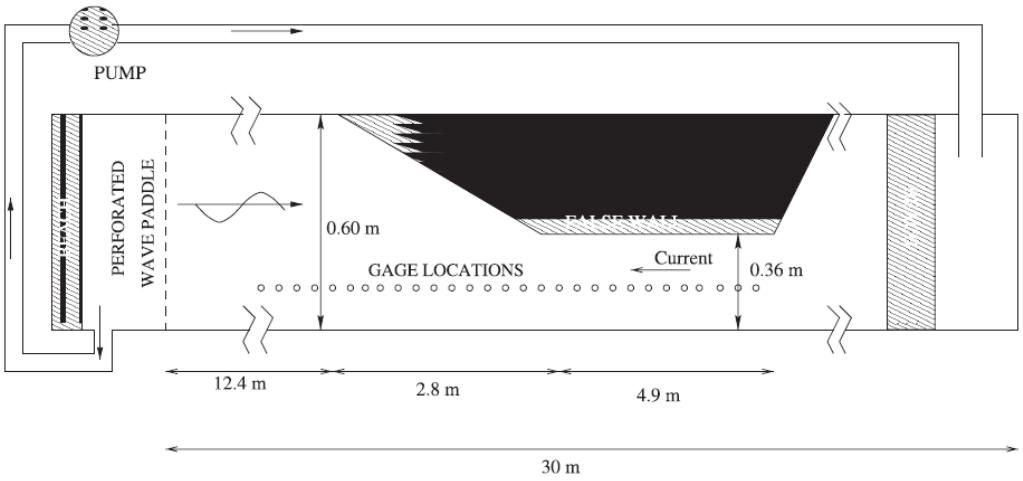

Fig. 2.5.: Schematic view of experimental setup by Chawla and Kirby (2002). The maximum and minimum width were $0.60\ m$ and $0.36\ m$ respectively. Waves and currents were generated at the left and right end of the flume, respectively. A false wall was used to create a spatially varying current. Time series were generated at numerous gage locations in the flume. Taken from Chawla and Kirby (2002).

waves, while energy dissipation from depth-limited breaking is the same for both. This is again found to be related to the non-linearity of wave steepening and energy shift in the energy spectra.

Fernando et al. (2011) used a wave basin to study the effects of wave-current interactions on formation of bed ripples. Current velocity profiles were measured in detail and used to validate the theoretical models for wave-current flows. The models managed to predict the current velocities well in case of small wave heights, however, for moderate and large wave heights, the models were inadequate in predicting the near-surface current velocities.

2.5 Overview wave-current phenomena

To conclude, a brief overview of all relevant phenomena regarding wave-current interaction is given (e.g. Drost et al., 2018; Romero et al., 2017; Wolf and Prandle, 1999).

- When waves propagate perpendicular to the current ($\theta = \frac{\pi}{2} + n\pi$ with θ the angle between wave and current and $n \in N^+$), the systems are not influenced by each other. This can be seen from Equation 2.1 in vector form: the dot product of $\overrightarrow{k} \cdot \overrightarrow{U}$ can be written as $|k||U|cos(\theta)$.
- For following currents, the wave length increases. For spatially non-uniform current, wave heights tend to decrease.
- For opposing currents, the wave length decreases. For spatially non-uniform current, wave heights tend to increase. Wave blocking occurs at the point where the relative group velocity is equal to the current velocity.
- For both directions of the current, due to the frequency dispersion, a Doppler shift is found. If the current is stationary in time, the absolute frequency (ω) should be constant. If the current is spatially uniform, the intrinsic frequency (σ) should be constant. If both frequencies show changes in time, the currents are non-stationary and non-uniform (Wolf and Prandle, 1999).
- In case of non-uniform currents, current-induced refraction takes place in a similar fashion to depth-induced refraction
- The bed shear experienced by waves tends to be larger in presence of currents (Wolf and Prandle, 1999). However, due to the large variety in results of different models (Soulsby et al., 1993), more knowledge is needed regarding the bottom boundary layer in combined wave-current flow.

The wave-current interactions can also be divided into two groups (Lai et al., 1989). A distinction is made between strong and weak interactions. Strong interactions are related to changes of the waves

by the current detectable within one wave period or wave length (Lai et al., 1989). Most of the effects mentioned in the previous sections can be placed in this group. The weak interactions are defined as changes of the waves by the current detectable through long-term evolution of the waves (Lai et al., 1989). Their effects are however relatively small, such that they are hardly observed in the field.

2.6 Key findings

The following conclusions are drawn:

- The frame of reference in combined wave-current flow is either defined from a non-moving perspective, the absolute frame of reference, or from a moving perspective, the relative frame of reference. It is important to realise which of the two are used as the equations can be different in formulation between both frames.
- Waves in the presence of a current are Doppler shifted. This means that the wave has an absolute and relative wave frequency. For uniform opposing currents, the absolute wave frequency is smaller than the relative wave frequency. This means that the wave length is smaller compared to the wave length in still water. For following currents, the opposite holds.
- Linear wave theory is still applicable for waves in the presence of a current, but small changes in the formulations are needed. In general, wave action (and not wave energy) is conserved in combined wave-current flow.
- The properties of waves in the presence of a non-uniform current change depending on the magnitude of the current. For an increasing opposing (following) current, the wave length shortens (lengthens) and the wave amplitude increases (decreases).
- Wave blocking is defined as the point at which the relative group velocity of the waves equal the velocity of the current. Wave breaking takes place and for small-amplitude waves, wave reflection can take place at the blocking point.
- The time-averaged velocity profile for combined wave-current flow is significantly different from the logarithmic profile typically observed in flows. A clear vertical shear is observed near the surface for both following and opposing currents. Several theories exist for the origin of this vertical shear, but there is still a lack of confirmation of the source.
- Experimental research has confirmed that the theoretical blockage limit for waves in the presence of non-uniform opposing currents holds. In general, energy transfer between wave components can lead to different forms of blocking.

A summary of the essential background information is provided in the following table. This table can be used to assess the effects of the variables in combined wave-current flow on the waveform with respect to a wave-only flow. In the table, u_b is the velocity at the maximum or minimum point in a non-uniform bathymetry and u_i is the velocity at the beginning of the domain.

Bathymetry	Current	Wave length	Wave height
Uniform	Opposing	$\downarrow$	constant
	Following	$\uparrow$	constant
Non-uniform	Opposing, $u_b > u_i$	$\downarrow$	$\uparrow$
	Opposing, $u_b < u_i$	$\uparrow$	$\downarrow$
	Following, $u_b > u_i$	$\uparrow$	$\downarrow$
	Following, $u_b < u_i$	$\downarrow$	$\uparrow$

3 Methodology

This chapter contains information regarding the modelling tool SWASH and the newly developed method for modelling combined wave-current flow. This tool will be used as the model for simulations in later chapters.

In Section 3.1, a brief description of SWASH is given with the main components of the model. Relevant SWASH modules for further chapters are considered in detail. The limitation in modelling combined wave-current flow in the present SWASH release is discussed in Section 3.2. A newly developed method for SWASH, the wave in current scaling method (WCS), is derived and assessed. Section 3.3 gives an overview of the experiments used for the validation with the WCS method. In Section 3.4, methods used in assessing waveforms and changes in wavesforms are shown. For future use by students and researchers, a short manual is provided in Appendix A.

3.1 Non-hydrostatic wave-flow model SWASH

SWASH[1,2] is an open source model based on the non-hydrostatic shallow water equations. It numerically solves the Reynolds-averaged Navier-Stokes (RANS) equations based on several assumptions:

- The vertical scale is much smaller than the horizontal scale, hence the shallow water equations.
- The flow is incompressible, which means that the divergence of the flow velocity field is zero ($\nabla \cdot \vec{u} = 0$). In other words, the density remains constant along streamlines (or changes depending on use of equation of state).
- The hydrostatic pressure assumption is valid, which means that the variation in pressure in the vertical is only a function of the height of the water column above a certain point. SWASH is, however, also capable of modelling non-hydrostatic pressures. This is generally important when variations in the vertical are relevant.
- The Boussinesq approximation is applied, which means that density variations are small and a constant reference density is assumed.
- SWASH makes use of the σ-grid (also known as terrain-following layers) as its vertical coordinate system. A z-grid can also be obtained by defining the thickness of the layers in the vertical.

The following sections will provide information regarding SWASH and important parts of the model for this research. For a more detailed description, reference is made to relevant literature (Stelling and Duinmeijer, 2003; Stelling and Zijlema, 2003; The SWASH team, 2018; Zijlema and Stelling, 2005, 2008; Zijlema et al., 2011).

[1] At the time of this research, SWASH version 5.01
[2] SWASH = Simulating WAves till SHore

3.1.1 Governing equations

For a 2DV framework bounded by a free surface ($z = \zeta(x,t)$) and bottom ($z = -d(x)$), the governing equations are (Rijnsdorp et al., 2014):

$$\frac{\partial u}{\partial t} + \frac{\partial uu}{\partial x} + \frac{\partial wu}{\partial z} = -\frac{1}{\rho}\frac{\partial (p_h + p_{nh})}{\partial x} + \frac{\partial}{\partial x}\left(\nu^h \frac{\partial u}{\partial x}\right) + \frac{\partial}{\partial z}\left(\nu^v \frac{\partial u}{\partial z}\right), \tag{3.1}$$

$$\frac{\partial w}{\partial t} + \frac{\partial uw}{\partial x} + \frac{\partial ww}{\partial z} = -\frac{1}{\rho}\frac{\partial (p_h + p_{nh})}{\partial z} + \frac{\partial}{\partial x}\left(\nu^h \frac{\partial w}{\partial x}\right) + \frac{\partial}{\partial z}\left(\nu^v \frac{\partial w}{\partial z}\right) - g, \tag{3.2}$$

$$\frac{\partial u}{\partial x} + \frac{\partial w}{\partial z} = 0, \tag{3.3}$$

$$\frac{\partial \zeta}{\partial t} + \frac{\partial}{\partial x}\int_{-d}^{\zeta} u dz = 0, \tag{3.4}$$

where t is time, x and z are Cartesian coordinates (with $z = 0$ at the still water level), $\zeta(x,t)$ is the surface elevation measured from the still water level, $d(x)$ is the water depth, $u(x,z,t)$ is the horizontal velocity, $w(x,z,t)$ is the vertical velocity, p_h and p_{nh} are the hydrostatic and non-hydrostatic pressures respectively, ν^h and ν^v are the horizontal and vertical eddy viscosities respectively, and g is the gravitational acceleration.

Particles cannot leave the surface and penetrate through the bottom, thus kinematic and dynamic boundary conditions are prescribed at the free surface and bottom:

$$w(x, z = \zeta, t) = \frac{\partial \zeta}{\partial t} + u\frac{\partial \zeta}{\partial x}, \tag{3.5}$$

$$w(x, z = -d, t) = -u\frac{\partial d}{\partial x}. \tag{3.6}$$

When the bottom stress is substantial, an extra term is added to the horizontal momentum equation (see Equation 3.1) in the form of $\tau_b = c_f \frac{u|u|}{d}$, where τ_b is the bottom shear stress and c_f is a dimensionless friction coefficient.

For this research, only the law of the wall is used to determine the bottom friction (Nezu and Rodi, 1986). In the case of a rough bed, SWASH needs the Nikuradse roughness height k_s as an additional input parameter. In the case of a smooth bed, this is not needed.

3.1.2 Numerical implementation

Spatial grid and vertical pressure

In general, a regular 1D grid is assumed with equidistant grid points (Zijlema et al., 2011). A staggered grid is applied, where the velocities and water levels are described separately on different grid points, hence the central difference scheme is applied for the spatial discretization. For the time integration, the midpoint rule is applied. The combination of these methods is known as the leapfrog scheme or Hansen scheme (Hansen, 1956) and it is second order accurate in both space and time.

Depending on the type of discretization used for the vertical pressure gradient, the grid has different orientations. The main difference arises when using either the classical central differences scheme or the implicit Keller-box scheme. The former is primarily used for flows where the vertical structure is important. The latter is beneficial to use for a proper wave propagation if the amount of layers needed is significantly less compared with central differences (Zijlema et al., 2011).

The difference between the schemes in grid schematization is the location of the non-hydrostatic pressure, which is either at the cell centre for central differences or at the face for the implicit Keller-box scheme (Zijlema and Stelling, 2005). In this research, the implicit Keller-box scheme will be used when the number of layers K is less than or equal to 3; central differences will be applied for amounts larger than this.

Discretization of the water depth

Initial model results showed that the wave height evolution was decreasing (increasing) for uniform opposing (following) currents. It was found that the choice of numerical scheme for the water depth might contribute to this effect. For accurate model results, the water depth should be discretized with the central difference scheme. The default choice in SWASH is the upwind scheme, which generally did not provide satisfying results. More details are provided in Appendix B. Note that this is only applied in simulations for combined wave-current flow.

Discretization of advection terms in momentum equations

The discretization of the advection terms in the momentum equations, i.e. $\frac{\partial uu}{\partial x}$, $\frac{\partial wu}{\partial z}$, $\frac{\partial uw}{\partial x}$ and $\frac{\partial ww}{\partial z}$, is important for the accuracy of model results. All advection terms should be discretized with the central difference scheme for accurate model results. More details are provided in Appendix B.

Exclusively, a new formulation for the discretization of the horizontal advection term in the horizontal momentum equation is used in this research. In the present SWASH release, the horizontal advection in the horizontal momentum equation is time-integrated with the predictor-corrector scheme of MacCormack. The space discretization is approximated by either first order upwind or higher order scheme (Zijlema et al., 2011). In the new formulation, only the predictor step is used with the central difference scheme instead of the upwind scheme. Note that this is only applied in simulations for combined wave-current flow.

Stability criterion

The simulations shown in this research always use an explicit scheme for the time integration. The CFL condition is one of the requirements that should be met to ensure stability of the numerical solution. For 1D, the CFL condition is defined as:

$$Cr = \frac{\Delta t \left(\sqrt{gd} + |u|\right)}{\Delta x} \leq 1, \tag{3.7}$$

where Cr the Courant number, Δt is the time step and Δx is the grid size in x-direction. A range of Courant numbers can be defined in SWASH. For instance, it is recommended to use a $Cr_{min} = 0.2$ and $Cr_{max} = 0.5$ for high non-linear waves (The SWASH team, 2018). As currents might significantly alter waves, the maximum Courant number is equal to 0.5 for all simulations in this research.

SWASH calculates a new time step when the user-defined time step violates the CFL condition. When the time step is smaller than required, SWASH automatically doubles the time step to decrease computational effort. However, due to the use of the central difference scheme, time steps might be much smaller than values according to the CFL condition. For stability reasons (Appendix B), the minimum Courant number has been set to a small number, i.e. 10^{-15}, in order to avoid doubling of the time step.

3.1.3 Boundary conditions

Waves can be imposed in SWASH with numerous boundary condition types. The most common ones are the water level, velocity and weakly reflective boundary types. Since the research interest lies in modelling waves and currents at the same time, a water level boundary condition type is not applicable as only the water level is prescribed.

Weakly reflective boundary condition

The weakly reflective boundary, as a numerical wave maker boundary, is used to enforce a non-reflective boundary at which only outgoing waves are allowed. It is commonly known as a radiation boundary since waves are absorbed (depending on the characteristic of the wave). In SWASH, the weakly reflective boundary is defined as:

$$u_b = \pm\sqrt{\frac{g}{d}}(2\zeta_b - \zeta) \tag{3.8}$$

where u is the velocity, d is the water depth at the boundary and ζ is the water level. Terms with subscript b refer to the values at the boundary. This boundary condition is derived from a combination of the Sommerfeld radiation condition and the 1D continuity equation (Blayo and Debreu, 2005).

Unfortunately, the weakly reflective boundary condition is not applicable in the simulations for this research. Combined wave-current flow introduces a water level gradient to enforce the flow. The difference between gradient and still water level at the boundary leads to the imposition of secondary waves, in the numerical model, that aim to compensate for this difference. This is, however, physically not correct as these secondary waves are not actually present in combined wave-current flow. Thus, a weakly reflective boundary type is omitted from simulations in following sections.

Velocity boundary condition

The boundary condition of main interest is the velocity boundary condition. SWASH can calculate the velocity profile according to a logarithmic, hyperbolic cosine or uniform distribution over the vertical, i.e. the water depth. For waves in general, the hyperbolic cosine distribution will be used in this research. According to linear wave theory, the horizontal particle velocity is defined as:

$$u(x,z,t) = \omega a\left(\frac{\cosh(k(d+z))}{\sinh(kd)}\right)\sin(\omega t - kx). \tag{3.9}$$

In the numerical implementation, SWASH integrates this equation over the entire water depth for a depth-averaged simulation. For multi-layered simulations, the integration is performed per layer and a correction factor, taking into account when the current water depth is not equal to the still water depth, is used. With the use of this correction factor, SWASH correctly produces the Stokes drift, i.e. mass transport due to wave.

Stokes drift

The Stokes drift is defined as the residual motion of particles resulting in a net mass transport in the direction of the wave propagation (Stokes, 1847). If the wave is located in the inner shelf, i.e. outside the surfzone near the coast, the Stokes drift is piecewise compensated by a Eulerian flow. For instance, if measurements would be made in a fixed place (Eulerian), one would measure the return flow that is compensating the Stokes drift due to wave propagation. The net movement of particles would, therefore, be zero.

However, the Stokes drift has a different profile in the surf zone. The compensation leads to a net movement of particles. In the upper half of the flow, particles are mostly transported in the direction of the wave and in the lower half, particles are transported against the wave direction. The Lagrangian Stokes drift in the inner shelf can be calculated with:

$$\overline{u}_{st} = \omega k a^2 \frac{\cosh(2k(d+z))}{2\sinh^2(kd)}. \tag{3.10}$$

Non-linear waves

Non-linear waves cannot be imposed appropriately in SWASH, as the hyperbolic cosine profile for the wave is based on linear wave theory. Generally, linearisation is sufficient when parameters ak, a/h and a/k^2h^3 are much smaller than 1. The first parameter indicates the wave steepness ($ak = \frac{H}{2} \cdot \frac{2\pi}{L} \approx \frac{H}{L}$), the second parameter requires a wave amplitude much smaller than the water depth and the third parameter, also known as the Ursell number (Ursell, 1953), indicates the degree of non-linearity of waves. Future development of SWASH will focus on the option to impose non-linear waves. For this research, several methods to generate time-series of non-linear waves were used, which are further discussed in Appendix C.

Irregular waves

Regular as well as irregular waves can be imposed in SWASH. Imposing regular waves is rather straightforward in the aforementioned boundary conditions. For irregular waves, it is assumed that the conditions are stationary, Gaussian which allows the use of Fourier series to describe the waves. Random phases are generated with the use of a seed number (which can be modified in the SWASH input file) and subsequent random number. SWASH needs the shape of the spectrum and allows three options: a PM spectrum (Pierson Jr. and Moskowitz, 1964), a JONSWAP spectrum (K. Hasselmann et al., 1973) or a TMA spectrum (Hughes, 1984).

For spectra in general, it is prescribed to allow enough wave components, N, for a proper generation of the random wave signal. For a JONSWAP spectrum, the following equation can be used (The SWASH team, 2018):

$$N = \frac{f_{max} - f_{min}}{\Delta f}, \qquad \text{with } \Delta f = \frac{1}{T_{cycle}}, \tag{3.11}$$

where f is the frequency of the wave, T_{cycle} is the cycle period in waves are generated from a spectrum and f_{max} and f_{min} are the maximum and minimum frequencies of the wave spectrum respectively. For a JONSWAP spectrum, f_{max} and f_{min} are $3f_p$ and $0.5f_p$, respectively, with f_p the peak period. The recommended amount of wave components is between 100 and 300, as amounts larger than this can increase computational time significantly.

Evanescent modes can be generated when imposing a spectrum in SWASH. A cut-off frequency is used to remove these modes. This frequency is larger for more layers and lower for increasing water depths.

Discharge boundary condition

Currents are imposed using the discharge boundary condition. This is rather straightforward in SWASH, as there are only options for logarithmic or uniform distribution profiles. The most commonly used one is the logarithmic profile, since it is the typical velocity profile found for open channel flows.

3.1.4 Vertical mixing

Standard $k - \epsilon$ model

In SWASH, vertical mixing can be accounted for using the $k - \epsilon$ model as described by Launder and Spalding (1974). The mean flow characteristics are used to take into account the effects of turbulence

Tab. 3.1.: Standard model constants, as used in $k-\epsilon$ model. Taken from Launder and Spalding (1974).

C_μ	C_1	C_2	σ_k	σ_ϵ
0.09	1.44	1.92	1.0	1.3

(Nieuwstadt et al., 2016). The $k-\epsilon$ model makes use of two transport equations: one for the turbulent kinetic energy, k, and one for the rate of dissipation of turbulence energy, ϵ:

$$\frac{D\epsilon}{Dt} = \frac{1}{\rho}\frac{\partial}{\partial x_k}\left[\frac{\mu_t}{\sigma_\epsilon}\frac{\partial \epsilon}{\partial x_k}\right] + \frac{C_1 \mu_t}{\rho}\left(\frac{\partial U_i}{\partial x_k} + \frac{\partial U_k}{\partial x_k}\right)\frac{\partial U_i}{\partial x_k} - C_2\frac{\epsilon^2}{tke}, \tag{3.12}$$

$$\frac{Dk}{Dt} = \frac{1}{\rho}\frac{\partial}{\partial x_k}\left[\frac{\mu_t}{\sigma_k}\frac{\partial tke}{\partial x_k}\right] + \frac{\mu_t}{\rho}\left(\frac{\partial U_i}{\partial x_k} + \frac{\partial U_k}{\partial x_k}\right)\frac{\partial U_i}{\partial x_k} - \epsilon. \tag{3.13}$$

For definitions and derivation, reference is made to the original publication (Launder and Spalding, 1974). These equations can be solved to determine both variables, which in turn can be used to determine turbulence terms on the scale of the mean flow. The turbulent eddy viscosity ν^v can then be calculated as $C_\mu \rho k^2/\epsilon$.

The $k-\epsilon$ model is a two-equation turbulence model that can be applied for any flow, provided that the model constants are calibrated correctly. The original creators of the model suggested the values in Table 3.1, which were based on a large amount of experiments for free turbulent flows. There are some differences for other types of flows (e.g. axisymmetric jets), but as this research mainly focuses on combined wave-current flow, the model constants will be left unchanged.

Extension of $k-\epsilon$ model in SWASH

Recent work by Larsen and Fuhrman (2018) demonstrates that all commonly used two-equation turbulence models are unconditionally unstable in regions with nearly potential flow. As a result, turbulent kinetic energy and thus eddy viscosity values growth exponentially, leading to an overproduction of generated turbulence for waves.

They propose a new formulation which deals with this problem. The $k-\epsilon$ model can be stabilized by modifying the definition of the eddy viscosity:

$$\nu^v = \frac{C_\mu k^2}{\widetilde{\epsilon}}, \qquad \text{with } \widetilde{\epsilon} = max\left(\epsilon, \lambda_2 \frac{C_2}{C_1}\frac{p_0}{p_\Omega}\epsilon\right), \tag{3.14}$$

$$p_0 = 2S_{ij}S_{ij}, \qquad \text{with } S_{ij} = \frac{1}{2}\left(\frac{\partial u_i}{\partial x_j}\right), \tag{3.15}$$

$$p_\Omega = 2\Omega_{ij}\Omega_{ij}, \qquad \text{with } \Omega_{ij} = \frac{1}{2}\left(\frac{\partial u_i}{\partial x_j}\right), \tag{3.16}$$

where λ_2 is a damping coefficient, p_0 is the shear production for turbulence, p_Ω is the shear production for turbulence in case of potential flow (where $p_\Omega << p_0$ holds), S_{ij} is the strain rate tensor and Ω_{ij} is the rotation rate tensor.

The coefficient λ_2 is, in a physical sense, the threshold for regions where potential flow is present. When the flow close to the bottom is analysed, the standard $k-\epsilon$ model is still valid in its entirety. However, close to the surface, where usually potential flow is present, i.e. waves, the limiter in the new formulation stops the overproduction of turbulent kinetic energy and thus viscosity. This significantly improves the modelling results of surface waves. This new formulation has been implemented in SWASH with $\lambda_2 = 0.2$ as a model constant. An assessment of its effects on model results is shown in Section 5.2.2.

3.1.5 Sponge layer

Waves in SWASH can be absorbed with different techniques. The sponge layer is one of the recommended choices for short waves. Radiation conditions, such as the Sommerfield condition, only work well for long waves.

The water levels and velocities inside the sponge layer are modified according to a weighing function, which takes into account the distance from the point within the sponge layer to the end of the sponge layer (left or right end depends on wave direction). The expressions used are (Mayer et al., 1998):

$$\eta = (1-\gamma)\eta + \gamma\eta_p, \tag{3.17}$$

$$u = (1-\gamma)u + \gamma u_p, \tag{3.18}$$

with

$$\gamma(x) = b\beta^3 + (1-b)\beta^6, \tag{3.19}$$

$$\beta = \frac{|x - x_{start}|}{|x_{end} - x_{start}|}, \tag{3.20}$$

where η is the water level, η_p and u_p are the water level and velocity at the end of the sponge layer respectively, γ is the weighing function, b is the parameter that determines the growth rate of the relaxation and β is the relative distance in the sponge layer with $\beta = 1$ at the end. In SWASH, b is equal to 0.5 by default.

If Equation 3.3 holds, the sponge layer technique reduces the vertical velocity indirectly. As the effects of wave-current interactions on the vertical velocity are not fully known, reflection can be completely eliminated by also dampening the vertical velocity.

The sponge layer technique is extended for this research by including the dampening of the vertical velocity, w. The following equation is implemented in SWASH:

$$w = (1-\gamma)w + \gamma w_p. \tag{3.21}$$

3.2 Wave in current scaling method (WCS)

In this section, a newly developed method for SWASH is presented for modelling of combined wave-current flow. This method is called 'wave in current scaling' (hereinafter referred to as WCS) as it is in its most basic form scaling the waves and currents such that wave-current interactions (e.g. Doppler shift, Chapter 2) are accounted for. The limitations and earlier solutions in SWASH are briefly discussed. The WCS method will be presented for both opposing and following currents, as there are some small differences between.

3.2.1 Constraints in present SWASH release

Modelling limitations

Combined wave-current flow can be highly non-linear, especially in cases with non-uniform currents in space and time. For a first-order approximation, the velocity signal of a combined wave-current flow can be seen as the summation of an oscillating velocity due to the wave and a velocity due to the current. In numerical models, the velocity signal will therefore be a composite of the magnitude for both signals. Note that no changes of the direction of the current, i.e. no flow reversal, are assumed.

Examples of velocity signals are shown in Figure 3.1. A logarithmic velocity profile is typical for a mean flow, as the friction between bed and flow with the no-slip boundary condition leads to non-uniform profiles in the vertical. Neglecting the discontinuities in velocity profiles between turbulent and viscous boundary layers, such a flow can be well approximated with a logarithmic profile.

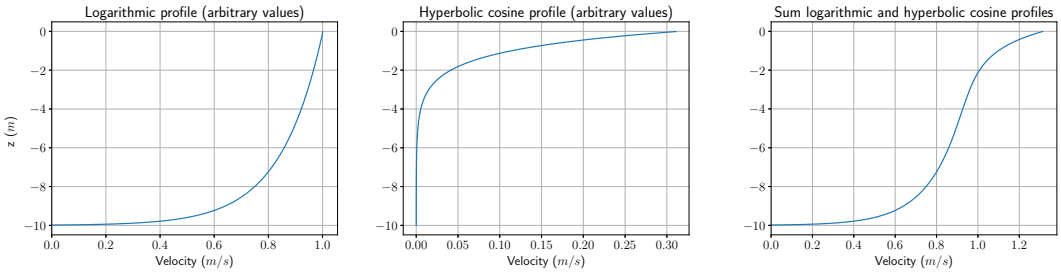

(a) Logarithmic velocity profile.

(b) Hyperbolic cosine velocity profile.

(c) Summation of logarithmic and hyperbolic velocity profiles.

Fig. 3.1.: Example of the interaction between logarithmic and hyperbolic cosine profiles. The y-axis is the water depth and the x-axis is the velocity. Values were arbitrarily chosen.

According to linear wave theory, a wave has a hyperbolic cosine profile in the vertical. This is substantially different from a logarithmic profile. For this analysis, the interest mainly lies in superposition of these velocity signals.

It should be stressed that SWASH is capable of simulating wave-current interactions. However, imposing waves and currents *simultaneously* at the boundary in the present SWASH release is not possible due to the default boundary conditions. They do not allow the proper imposition of waves and currents simultaneously.

Equation 3.9 demonstrates the limitation of SWASH. To simulate a case involving both waves and currents, there is no term accounting for a mean flow due to the current. As only one boundary condition can be specified at each boundary, it is not possible to account either (1) for a mean flow with a numerical wave maker or (2) waves when imposing a flow.

In the present SWASH release, the only possible way of imposing waves and currents simultaneously is to impose user-created time series. These time series have to include orbital velocities (taking into account the Doppler shift), current velocities and an initial velocity field. This becomes a rather heavy task to perform for a substantial amount of simulations with the likelihood of making pre-processing errors.

Earlier method by de Wit (2016)

A previous solution in SWASH, proposed by de Wit (2016), was implemented to account for alongshore currents. To model a velocity due to a tidal wave, the tide can be modelled as a time-averaged water level gradient in the momentum equation (Ruessink et al., 2001). Since the time scale of tidal waves is much larger than typical short wave periods at the coast, time-averaging has barely an impact on the solution. However, when a water level gradient is imposed in the model, discontinuities occur, e.g., when using cyclic boundary conditions. Therefore, de Wit (2016) proposed the use of the time-averaged pressure gradient, defined as the pseudo gradient.

The standard pressure gradient as described by SWASH is:

$$\frac{1}{\rho}\frac{\partial(p_h + p_{nh})}{\partial x}, \tag{3.22}$$

for which de Wit (2016) proposed to add the pseudo gradient, uniform over the domain, in the following manner:

$$\frac{1}{\rho}\frac{\partial(p_h + p_{nh})}{\partial x} + \frac{1}{\rho}\overline{\frac{\partial p_{tide}}{\partial x}}. \tag{3.23}$$

For the cases studied by de Wit (2016), SWASH was successful in modelling the correct velocities for alongshore currents with this method. However, for cross shore domains, difficulties arise with the pseudo gradient because the bathymetry changes much faster.

From a physical standpoint, the pseudo gradient method is invalid for a rapidly changing bathymetry. One can derive from the horizontal momentum equation, assuming steady-state conditions with no advection and diffusion, the velocity as a function of amongst others the pressure due to the tidal wave and water depth:

$$u = -\sqrt{\frac{\overline{p_{tide}} g d}{c_f}}. \tag{3.24}$$

Using the experimental setup by Ma et al. (2017) (see Figure 3.5) as an example, the water depth is $0.45\ m$ at both sides of the flume and the water depth on top of the submerged breakwater is $0.1\ m$. The discharge is equal everywhere, thus based on mass conservation, velocities on top of the submerged breakwater are larger than in the deeper parts. Since the pseudo gradient is constant in the domain, the velocity only scales with the water depth according to Equation 3.24 (assuming spatially uniform friction). This means that the velocity on top of the breakwater will be smaller, as the water depth is smaller, which is fundamentally not correct. Together with some additional difficulties, the pseudo gradient is therefore not suited for our modelling purposes.

3.2.2 General framework WCS method

It is clear that there is a need for a method that accounts for waves and currents simultaneously in the case of rapidly changing bathymetries. Furthermore, the method should be straightforward to implement in simulations, i.e. efficient and straightforward to use.

The WCS method is a new implementation in SWASH that allows the modelling of combined wave-current flow. It is based on the idea that the velocity signal is composed of both the horizontal particle velocity due to the wave and the velocity due to the current (see Section 3.2.1). The WCS method is applicable for both regular and irregular waves. Note that the WCS method is only implemented for combined wave-current simulations: for current- and wave-only simulations, the numerical implementation falls back to the default SWASH routines. Furthermore, results with the WCS method are denoted with the use of 'new SWASH model' or just 'WCS method'.

Assumptions

The WCS method starts with the assumption that the *time-averaged* inflow and outflow discharges are equal. Time-averaging is defined in terms of wave cycles, which results in discharges without the influence of the wave. This ensures mass conservation in the domain. A starting point is the schematized model from Figure 3.2, which we assume to be multi-layered in our 1D, i.e. 2DV, model. The q at both boundaries is thus equal when averaged over time and either left- or right-oriented, depending on the direction of the current.

The discharge is the product of velocity and water depth. In general, one could alter a discharge to the desired value by either modifying the water depth or velocity. Here, we assume that only the velocity signal may be modified, i.e. the water depth is not adapted and only the velocity is prone to changes.

We assume the same orientation of boundary conditions as used in experimental research (see Section 2.4). Therefore, the WCS method assumes that on the left end a velocity boundary condition (numerical wave maker) is used and at the right end, a discharge boundary condition is used (see Figure 3.2). This always holds, i.e. opposing and following currents have the same boundary conditions at the same locations. To absorb the waves, a sponge layer is used at the right end of the domain with a length equal to approximately three times the (peak) wave length.

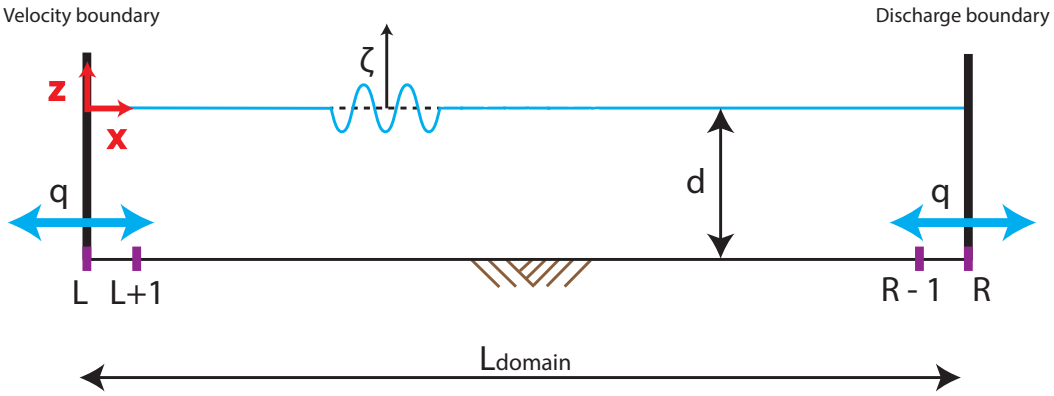

Fig. 3.2.: Schematized model of a typical numerical domain with length L_{domain}, now with the addition of the WCS method. The (z, x)-axes are defined at the still water depth d at the left end of the domain. The surface level, ζ, is defined at the still water depth d. The discharge, q, is imposed at both velocity and discharge boundaries. The double headed arrows denote that water either enters or leaves the domain. For the derivations, L is the grid point at the left boundary and $L+1$ is the grid point next to it. The same holds for grid points R and $R+1$, defined at the right end of the domain.

The combined wave-current flow has a non-uniform velocity profile, thus continuity in the velocity profiles at the boundaries is needed. At the inflow boundary, continuity is always preserved (assuming no reflection) since the flow is imposed with our method. However, continuity of the velocity profile at the *outflow* boundary is the biggest concern. The WCS method deals with this differently based on the type of current (opposing or following), but in general, the velocity profile at the grid point right before the outflow boundary is used in defining the conditions at the outflow boundary. The derivation is given in the following sections. For the derivations, the symbols used are demonstrated in Figure 3.2.

Iterative solver for wave number

Finally, the WCS method corrects for the wave amplitude (by using the relative wave frequency in the particle velocity, Equation 2.4) and wave length (according to the Doppler shift, Equation 2.1). This is performed by iteratively solving the dispersion relation in presence of currents (see Equations 2.1 and 2.3 combined) with an iterative solver.

The initial estimate for the wave number can be found by, for instance, using the dispersion relation without currents. Many approximations exist and there is an existing procedure in SWASH that can be used for this purpose. However, the difference between the dispersion relation with and without currents increases with increasing currents, which can be computationally heavy.

Therefore, an initial estimator, as described by Fenton and McKee (1990), will be used. They provide explicit approximations to Equation 2.1 for all types of waves. The initial estimator is based on whether the wave is short or long according to the ratio $T\sqrt{g/d}$ where T is the absolute wave period. If this ratio is smaller than 4, the following approximation is used:

$$k = \frac{4\omega^2/g}{\left(1+\sqrt{1+4\bar{u}\omega/g}\right)^2}. \tag{3.25}$$

If this does not hold, the waves are long and thus the following approximation used is:

$$kd = \frac{\omega\sqrt{d/g}}{1+F} + \frac{1}{6}\frac{(\omega\sqrt{d/g})^3}{(1+F)^4} + \frac{(11-19F)}{360(1+F)^7}(\omega\sqrt{d/g})^5, \tag{3.26}$$

where F is the Froude number ($= \frac{\bar{u}}{\sqrt{gd}}$). This equation is an infinite series, but here, following Fenton and McKee (1990), the cut-off is taken at the third term. Dividing the terms at the RHS by the water depth will give the wave number in presence of a current.

Although the initial estimators provide reliable estimates, there is still a margin of error with the correct values. The error is the absolute difference between the given absolute frequency (input of model) and the absolute frequency calculated with the iterative solver. This error should be reasonably small, in the order of 10^{-2}. The algorithm provided by Fenton and McKee (1990) will be used as the iterative solver. After an initial estimate is made by use of either Equation 3.25 or 3.26, the solution can be approximated further with the following equation:

$$k_{n+1}d = \frac{2\omega\sqrt{d/g}\sqrt{k_n d\tanh(k_n d)} - k_n d\tanh(k_n d) + k_n^2 d^2\,\mathrm{sech}^2(k_n d)}{2F\sqrt{k_n d\tanh(k_n d)} + \tanh(k_n d) + k_n d\,\mathrm{sech}^2(k_n d)}, \tag{3.27}$$

where k_{n+1} is the wave number after one iterative step in which k_n is used. The equation may look complicated but computationally wise, it is very efficient.

3.2.3 WCS method for opposing current

An opposing current is initialized by a current propagating from right to left and a wave propagating from left to right. At the discharge boundary no modifications are needed. The flow velocity profile is altered due to presence of the sponge layer absorbing the incoming waves at this boundary. Therefore, some extra domain space should be used in front of the sponge layer to give the discharge adaptation time. One can also reduce the adaptation time by imposing a discharge with a logarithmic velocity profile, but the WCS method allows the user to have a choice between this option and a uniform velocity profile.

The velocity at the discharge boundary condition is thus defined as:

$$u_R(k_{lay}) = \frac{q_R}{d_R(k_{lay})}, \tag{3.28}$$

where R is the grid point at which the discharge (right) boundary is located and k_{lay} is the layer (number).

At the velocity boundary, the WCS method alters the boundary condition, such that waves are propagating into the domain. The incoming current is propagating out of the domain. The flow velocity signal at grid point L (Figure 3.2) is a summation of the velocities due to the current and waves and we are only interested in the former to allow proper outflow of the current. To ensure continuity, we use the flow velocity signal at grid point $L + 1$, to which we apply a Reynolds decomposition to find the current velocity:

$$u_{L+1} = \overline{u_{L+1}} + u_{\prime,L+1}, \tag{3.29}$$

where u_{L+1} is the composition of both current and wave velocities, $\overline{u_{L+1}}$ is the mean current velocity and $u_{\prime,L+1}$ is the velocity due to waves. In SWASH, this equation is implemented by means of a forward moving average applied to u_{L+1}:

$$u^{n+1}_{L+1,mov} = u^{n}_{L+1,mov} - \frac{\Delta t}{T_{mov}}(u^{n}_{L+1,mov} - u^{n}_{L+1}), \tag{3.30}$$

where $u^{n+1}_{L+1,mov}$ and $u^{n}_{L+1,mov}$ are the the moving average velocities at time steps $n+1$ and n respectively, Δt is the time step, T_{mov} is the period over which the velocity signal is averaged and u^{n}_{L+1} is the (undisturbed) velocity signal. In Equation 3.29, $\overline{u_{L+1}}$ is the same as $u^{n+1}_{L+1,mov}$ in Equation 3.30. We now have obtained the flow velocity profile we want to impose at grid point L.

For the iterative solver (see Equation 3.27), we need the undisturbed water depth at the boundary, i.e. no influence of waves visible at grid point L. The still water depth cannot be used due the development

of a water level gradient in combined wave-current flow. The water depth also needs to be decomposed in mean and fluctuating components. Following the same procedure as for the velocity, we can obtain the moving average water depth at the numerical wave maker (grid point L), $d_{L,mov}$:

$$d_{L,mov}^{n+1} = d_{L,mov}^{n} - \frac{\Delta t}{T_{mov}}(d_{L,mov}^{n} - d_{L}^{n}). \tag{3.31}$$

Our first assumption in the WCS method is the time-averaged in- and outflow discharges being equal to each other. Formally, we can define this as:

$$\overline{q_L} = \overline{q_R}, \tag{3.32}$$

where the bar represents time-averaged values. At the discharge boundary, we know what the magnitude of the discharge is. The only unknown is the discharge at the numerical wave maker, which we can define as:

$$\overline{q_L} = \sum_{k_{lay}=1}^{K} \overline{u(k_{lay})} \cdot \overline{h(k_{lay})}, \tag{3.33}$$

where K is the total amount of layers and u and h are the velocity and layer thickness respectively. This is essentially the definition of a discharge, i.e. velocity times water depth.

To make sure that Equation 3.32 always holds, we use the moving average velocity $\overline{u_{L+1}}$ in a scaled form at grid point L. We introduce the scaling factor α_{WCS} in the following relation:

$$\overline{u_L(k_{lay})} = \alpha_{WCS} \cdot \overline{u_{L+1}(k_{lay})}, \tag{3.34}$$

and combined with Equations 3.29 - 3.33, we can find the following expression for α_{WCS}:

$$\alpha_{WCS} = \frac{q_R}{\sum_{k_{lay}=1}^{K} \overline{u_{L+1,mov}(k_{lay})} \cdot \overline{d_{L,mov}(k_{lay})}}. \tag{3.35}$$

Substituting Equation 3.35 in Equation 3.34 finally gives the velocity of the current at multiple layers. The velocity signal imposed at the numerical wave maker is now a combination between the expression for the current velocity and Equation 2.4:

$$u_L(k_{lay}, t) = \sigma a \left(\frac{\cosh(k(d_{L,mov} + z))}{\sinh(k d_{L,mov})} \right) \sin(\omega t) + \overline{u_L(k_{lay}, t)}. \tag{3.36}$$

The velocity is described as a function of the layer. This means that the WCS method applies a global assumption (*total discharge*), but solves at each layer separately.

To summarize, the WCS method for opposing currents uses several procedures to decompose the velocity next to the numerical wave maker in steady (current) and oscillating (wave) parts. This velocity is then used at the numerical wave maker after being scaled to have matching discharges at both ends of the domain. The waves are imposed by accounting for the Doppler shift due to the current.

3.2.4 WCS method for following current

The main difference between the WCS method for a following and opposing current is the approach and not so much the tools. Some of the equations in Section 3.2.3 are reused, but at different locations.

Starting at the discharge boundary, we do not have to deal with waves any more, as they are absorbed by the sponge layer. This implies that moving averages for the velocities and water depth are not needed. We still want to ensure continuity between velocity profiles at the outflow boundary, thus the

velocity profile at grid point $R-1$ is scaled, such that the discharge is equal to the scaled velocity at grid point R times the water depth:

$$u^R(k_{lay}) = \alpha_{WCS} \cdot u_{R-1}(k_{lay}), \tag{3.37}$$

with

$$\alpha_{WCS} = \frac{q_R}{\sum_{k=1}^{K} u_{R-1}(k_{lay}) \cdot d_R(k_{lay})}. \tag{3.38}$$

Note that the velocity and water depth at grid point $R-1$ and R, respectively, are the instantaneous values. Moving averages are not used at this boundary.

At the numerical wave maker, the wave and the current propagate in the same direction. For the Doppler shift calculations, we still need a moving average for the water depth at grid point L, which is the same as Equation 3.31.

For following currents, we opt to always choose for a logarithmic profile of the current. SWASH calculates the logarithmic velocity profile based on the following expression for turbulent flows (Nezu and Rodi, 1986):

$$\frac{u(z)}{u_*} = \frac{1}{\kappa} \log(\frac{z}{z_0}), \tag{3.39}$$

where $u(z)$ is the flow velocity, u_* is the shear velocity, κ is the von Kármán constant and z_0 is an integration constant near the wall/bottom.

The boundary condition for the numerical wave maker is the same as Equation 3.36, but with $\overline{u_L(k_{lay}, t)}$ replaced by Equation 3.39.

3.2.5 Moving average period in WCS method

A moving averaging period, T_{mov}, of 10 waves is usually stable and leads to accurate model results. This is based on the results of a sensitivity analysis (see Section D.1). This number of wave periods is, therefore, the default option in SWASH. If the wave is monochromatic, T_{mov} is equal to the wave period. In the case of irregular waves, T_{mov} is equal to the peak wave period.

3.2.6 Additional details and results for WCS method

The general work flow scheme is summarized and provided in Figure 3.3. The new commands for using the WCS method in SWASH are shown in Section D.2. For comparison, combined wave-current flow modelling with and without the WCS method is given in Section D.3. The WCS method is preferred based on the amount of additional work that has been automatized in comparison to modelling with the present SWASH release. To conclude, a summary of the results for the extension of the WCS method to a 3D domain is given in Section D.4. Note that this domain size is outside the scope of this research. However, a derivation is provided, as it might prove to be useful for future research with the WCS method.

3.3 Validation of WCS method with experimental data

Validation of the WCS method is performed with two types of experiments. Experimental data obtained by Klopman (1994) is validated with the WCS method. This is data concerning the vertical structure in combined wave-current flow for a uniform bathymetry. The second part of the validation is performed with experimental data from Ma et al. (2017). Their dataset demonstrates the spatial evolution of waves in a following or opposing current for a non-uniform bathymetry.

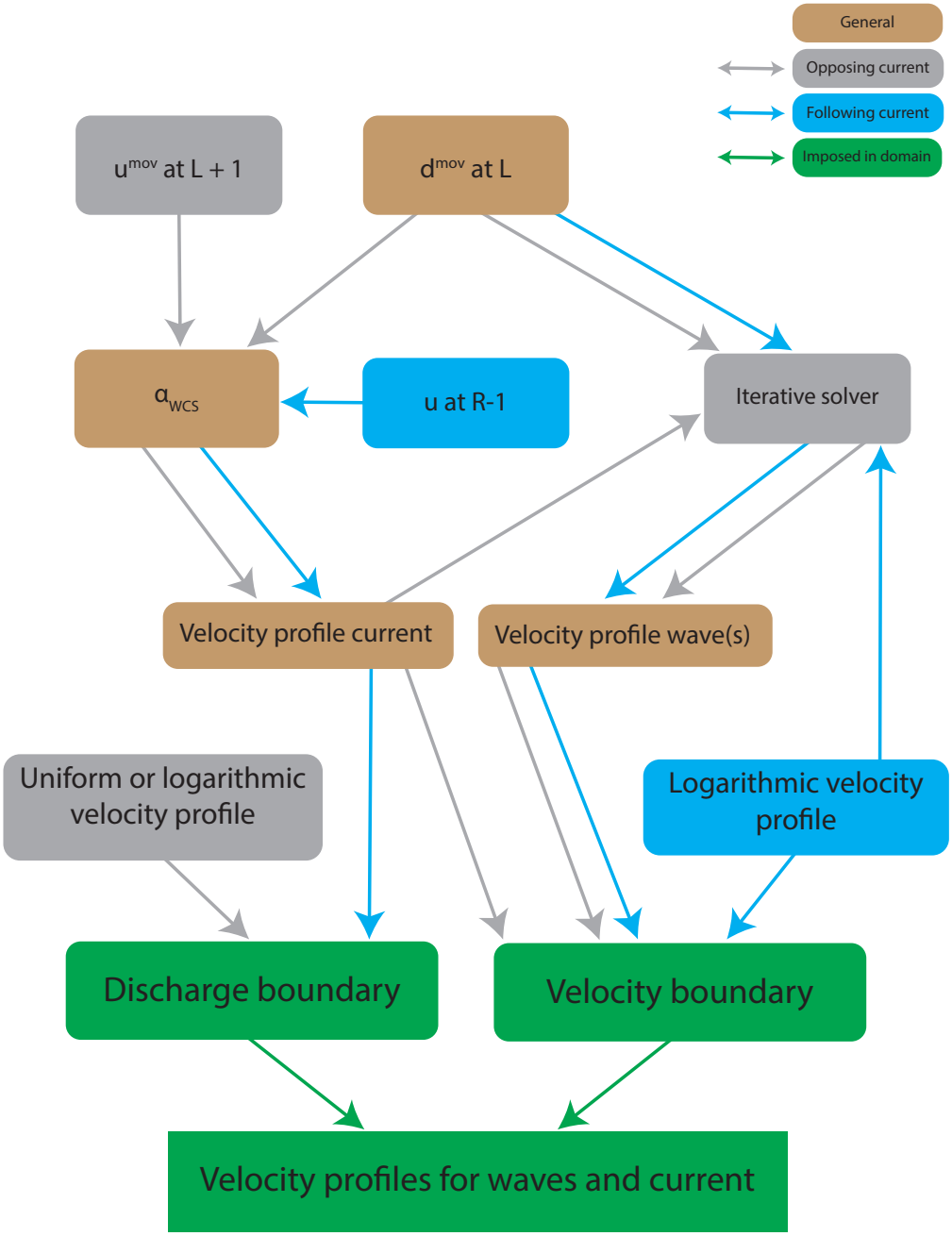

Fig. 3.3.: Work flow scheme of WCS method. The boxes and arrows denote general and distinct features between opposing and following currents.

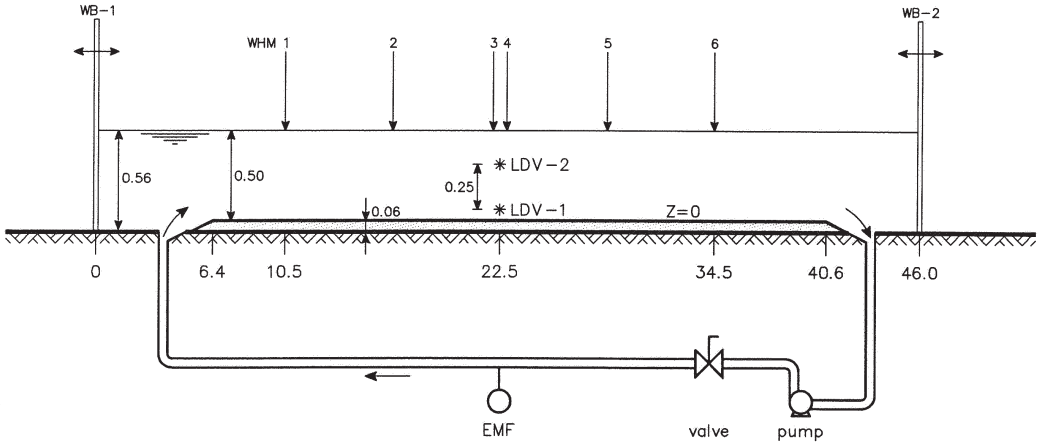

Fig. 3.4.: Schematic view of experimental setup by Klopman (1994). Measures are in meters. The horizontal and vertical scale are $1:250$ and $1:25$ respectively. Waves were generated and absorbed at the left and right end of the flume, respectively. The current was generated with the use of a flow-circulation circuit. The water depth was $0.5\ m$. Measurements were taken with the use of a LDV meter at the halfway point and wave height meters at different positions in the flume. Taken from Klopman (1994).

3.3.1 Experimental work by Klopman (1994)

Klopman (1994) performed laboratory experiments on combined wave-current flow. The main goal was to obtain data to validate mathematical models developed for combined wave-current flow. Previous experiments focused on the bottom boundary layer and not so much the vertical structure of combined wave-current flow.

Klopman (1994) put emphasis on the vertical structure of the mean flow driving forces. Next to typical monochromatic waves, other wave conditions were used. Experiments were conducted for following and opposing currents with monochromatic, bi-chromatic and random waves.

The experimental setup used by by Klopman (1994) is demonstrated in Figure 3.4. The main channel has a length of $46\ m$, a width of $1.0\ m$ and a depth of $0.5\ m$. The bed was roughened with a custom-made false bed. Coarse sand with a grain size of approximately $2\ mm$ was pasted on the bed. Analysis of test series resulted in a Nikuradse roughness height k_s of $1.2\ mm$.

Wave boards capable of generating and absorbing waves were present at both ends of the channel. Waves were generated according to second-order Stokes theory (Klopman and van Leeuwen, 1990). Due to time restriction, only the monochromatic test cases were used in the validation of the WCS method.

Note that monochromatic wave[3] is a misused definition, as the waves are of second order. This implicitly means that more than one wave is needed to compose the wave signals. Therefore, only the wave parameters of the carrier wave are used. The wave period and wave amplitude were $1.44\ s$ and $0.06\ m$ respectively.

The discharge was imposed with the use of a flow-circulation circuit. The inflow and outflow of the discharge took place at boxes located in the channel bottom. The boxes consisted of a perforated plate and they were filled with marbles to generate turbulence as little as possible. The discharge was monitored with the use of a electric-magnetic discharge meter. The mean current velocity in the experiments was $0.16\ m/s$, which gives a discharge of $0.08\ m^2/s$.

Measurements were performed at one cross-section in the channel, located exactly in the middle. To measure the vertical structure, a Laser Doppler velocimetry (LDV) was used. To reduce the duration of

[3] Wave with spectrum containing only one frequency

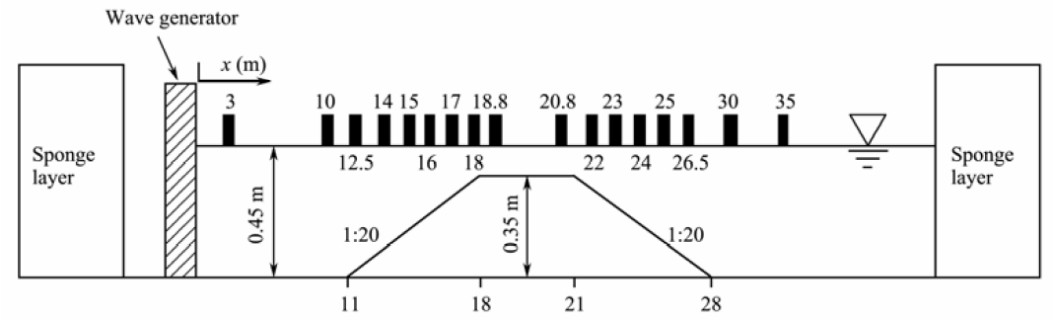

Fig. 3.5.: Schematic view of experimental setup by Ma et al. (2017). Measures are in meters. Waves were generated and absorbed at the left and right end of the flume, respectively. Currents were generated with axial pumps at both ends of the flume. A submerged breakwater with side slopes of $1/20$ was placed in the middle. The maximum and minimum water depth were $0.45\ m$ and $0.1\ m$ respectively. Taken from Ma et al. (2017).

the experiments, two LDV systems were used. Wave height meters were spread out over the flume to measure wave height at different locations. The minimum test duration was $600\ s$.

3.3.2 Experimental work by Ma et al. (2017)

Experiments by Ma et al. (2017) focused on the wave transformation of waves in combined wave-current flow over a submerged breakwater. They were conducted in a wave-current flume with length $50\ m$, width $3\ m$ and height $0.7\ m$. The experimental setup is demonstrated in Figure 3.5. The water depth used in the experiments was $0.45\ m$.

Waves were generated by means of a hydraulically driven piston-type wave maker at the left end of the flume. Axial pumps at both ends of the flume were used to simulate currents. At both ends of the flume, wave absorbers were installed to prevent reflection of the waves. The data was recorded as time series of the water surface elevations. Measurements were obtained by use of capacitance gauges at different locations in the flume. The absolute accuracy of each gauge is in the order of $\pm 1\ mm$ (Dong et al., 2014).

In the validation for the WCS method, a test experiment with an opposing current is used. Waves were generated by means of a JONSWAP spectrum with a T_p of $1.0\ s$ and a H_s of $0.05\ m$. The current velocity at the boundary was $0.03\ m/s$, which gives a discharge of $0.0135\ m^2/s$. With the use of continuity, the maximum velocity on top of the submerged breakwater is equal to $0.3\ m/s$.

3.3.3 Model performance

To assess the performance of SWASH in comparison with experimental data, the root mean square error, RMSE, is used as a measure of accuracy (Caruana and Niculescu-Mizil, 2006; Sutherland et al., 2004; Sutskever et al., 2014). It is defined as:

$$\text{RMSE} = \sqrt{\frac{1}{N}\sum_{n=1}^{N}(X_p - X_o)^2}, \tag{3.40}$$

where N is the amount of observations and X_p and X_o are the predicted and observed quantities respectively. To interpret the model results in terms of a comparison with a baseline model, a skill score is used (e.g. Bosboom et al., 2014; Reniers et al., 2006; Rijnsdorp et al., 2014). The model skill score is defined as:

$$\text{Skill} = 1 - \sqrt{\frac{\frac{1}{N}\sum_{n=1}^{N}(X_p - X_o)^2}{\frac{1}{N}\sum_{n=1}^{N}(X_{p,baseline} - X_o)^2}}, \tag{3.41}$$

where $X_{p,baseline}$ is the predicted quantity by the baseline model. By this definition, the skill score can vary from $-\infty$ to 1. If the skill score is positive (negative), the model provides better (poorer) predictions in comparison to the baseline model (Bosboom et al., 2014).

3.4 Waveform parameters

As mentioned in Section 1.2.1, the waveform in this research is characterized by use of skewness, asymmetry and wave height. The same definitions, as described by de Wit et al. (2017), are used. The skewness, Sk, and asymmetry, As, can be calculated from time series with the following equations:

$$Sk = \frac{\left\langle \zeta^3 \right\rangle}{\left\langle \zeta^2 \right\rangle^{3/2}}, \tag{3.42}$$

$$As = \frac{\left\langle H(\zeta^3) \right\rangle}{\left\langle \zeta^2 \right\rangle^{3/2}}, \tag{3.43}$$

where ζ is the surface elevation, $H(\zeta)$ is the imaginary part of the Hilbert transform (Elgar, 1987) and $\langle ... \rangle$ denotes time-averaging.

The wave height is calculated from time series. For this purpose, a spectral analysis is used (Falnes, 2007). In case of random waves, i.e. use of a wave spectrum, a low-, high- or band-pass filter can used to remove unwanted higher and lower frequencies (Holloway, 1958). For instance, noise signals can be generated when the imposed signal at the wave maker boundary is not matching the governing equations. If the frequency is smaller than the minimum frequency in a spectrum, a cut-off frequency can be applied to filter these signals.

4 Numerical settings and spatial discretization for modelling combined wave-current flow

This chapter considers model results obtained with the newly implemented WCS method. This is done for uniform and non-uniform bathymetries. The goal of this chapter is to determine to what extent the new SWASH model is capable of modelling combined wave-current flow. Test cases with variations in the numerical settings and spatial discretization are simulated, as these are important for accuracy and stability reasons.

The approach in the assessment of the model is discussed in Section 4.1. The setup of the model is given in Section 4.2. A distinction is made between the numerical domains for uniform and non-uniform bathymetries. The setup of the sensitivity analysis is shown in Section 4.3. The results of the uniform and non-uniform bathymetry cases are discussed in Section 4.4 and 4.5 respectively. A general framework for the modelling of combined wave-current flow in SWASH is provided in Section 4.6. Lastly, the effect of the sponge layer on model results is discussed in Section 4.7. A summary of the results of this chapter is given in Section 4.8.

4.1 Model assessment

Model results are assessed in this chapter to form a general framework for the modelling of combined wave-current flow in SWASH. The starting point is a base model with spatial discretization and time step settings based on rules of thumb (The SWASH team, 2018). A sensitivity analysis was performed, since it is not known whether these rules of thumb are optimized for combined wave-current flow modelling. Therefore, the spatial discretization and time step were varied with values based on general modelling guidelines, computational effort and expert judgement.

Theoretical predictions and analytical solutions were used as hypotheses. The assessed quantities of the model results were the wave height evolution over the domain and time-averaged velocity profiles. More specifically, the wave height evolution was used to determine whether a change in the horizontal discretization and time step led to better or poorer results in comparison to the base model. For comparison, simulations without currents were also run. The time-averaged velocity profiles were used to highlight differences in the vertical structure. The goal was to determine a vertical discretization, such that model results would not significantly differentiate for more or less layers.

It could be the case that there might be differences in stability and accuracy between model results of uniform and non-uniform bathymetries. Accordingly, a distinction was made for model results of uniform and non-uniform bathymetries.

4.2 Model setup

A numerical model was set up for the simulations in uniform and non-uniform bathymetry. The domain sizes are given in Sections 4.2.1 and 4.2.2. General model settings are given in Section 4.2.3.

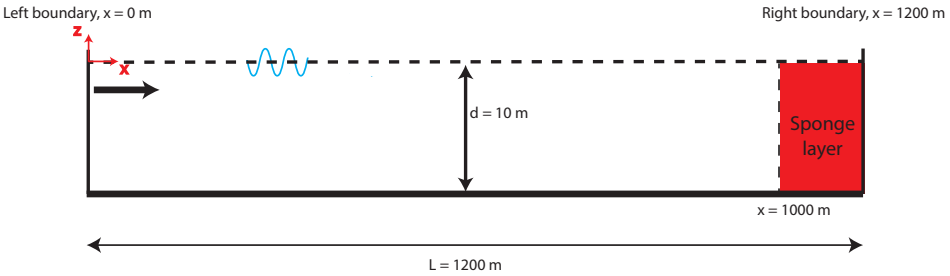

(a) Sketch of the numerical model used for the case with uniform bathymetry. The length of the domain was $1200\ m$. Waves were generated at the left boundary and absorbed with a sponge layer next to the boundary at the right. A uniform current was imposed at the right boundary. The water depth was $10\ m$.

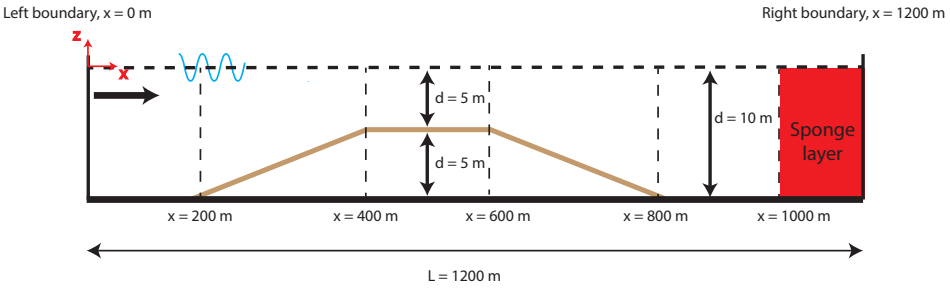

(b) Sketch of the numerical model used for the case with non-uniform bathymetry. The length of the domain was $1200\ m$. Waves were generated at the left boundary and absorbed with a sponge layer next to the boundary at the right. A uniform current was imposed at the right boundary. The submerged breakwater is placed at the halfway point with side slopes of $1/20$. The dimensions are not to scale. The maximum and minimum water depth were $10\ m$ and $5\ m$ respectively.

Fig. 4.1.: The numerical domains for the uniform and non-uniform bathymetry cases.

4.2.1 Numerical domain for uniform bathymetry

A sketch of the model setup is given in Figure 4.1a. The length of the domain L_D and the still water depth d were $1000\ m$ and $10\ m$ respectively. The discharges, q, were set at $-5\ m^2/s$ and $5\ m^2/s$ for the opposing and following currents respectively. Consequently, the velocities were $-0.5\ m/s$ and $0.5\ m/s$. Spin up was reduced by imposing an initial velocity equal to the velocity of the current.

4.2.2 Numerical domain for non-uniform bathymetry

A sketch of the model setup is given in Figure 4.1b. It is the same model as for the uniform bathymetry case. However, a submerged breakwater was now present in the domain. The submerged breakwater had a side slope of $1/20$ at both sides. The length of the side slopes was $200\ m$, which was also the length of the shallow part on top of the submerged breakwater. The left and right slopes are, hereinafter, referred to as the shoaling and deshoaling areas. The water depth in the shallow part was equal to $5\ m$ and the discharges from the uniform bathymetry case were used again.

4.2.3 General model settings

Boundary conditions

For the WCS method, velocity and discharge boundary conditions were used at the left and right end of the domain, respectively. At the velocity boundary condition, a monochromatic wave was imposed on the current. The wave had a period of $8\ s$, yielding a wave length of approximately $71\ m$. The wave height was $0.1\ m$. At the discharge boundary condition, the value was set equal to the magnitude of the discharge of the current.

Sponge layer

A sponge layer was imposed in both domains, see Figure 4.1. The sponge layer had a length of $200\ m$, resulting in a total domain length of $1200\ m$ for both uniform and non-uniform bathymetries.

Spatial discretization and time step

The recommended number of gridcells per wave is between 50 and 100. Although these are values for irregular waves, it is assumed that the same holds for monochromatic waves. Consequently, 75 grid cells per wave length were assumed for the baseline model. It followed that the number of gridcells mxc in the domain was equal to 1200. This resulted in a spatial resolution, Δx, of $1\ m$. Note that the wave length is calculated without the presence of currents. In comparison to still water, the wave length in the presence of currents is larger or smaller, thus, the number of gridcells per wave is higher or lower. The general recommendation is to calculate the wave length in the presence of currents and determine the deviation from the still water wave length. If the model results are not satisfactory and the deviation is large, the number of gridcells should be calculated with the wave length in the presence of currents.

The number of layers depends on the vertical flow structure and wave transformation. The vertical flow structure is important in this research, as it is used in the validation part. For a proper vertical flow structure, the recommended number of layers is 10. Wave transformation is important as well, since skewness, asymmetry and the wave height evolution will be studied for a non-uniform bathymetry. The number of layers mainly depends on the kd value, i.e. the dimensionless depth, because it determines the importance of linear wave dispersion. Based on the boundary conditions, a kd value of 0.88 can be found and correspondingly, at least 2 layers are needed. In general, the vertical flow structure is normative for the required number of layers. However, it is still important to verify the dimensionless depth, which is done in further chapters.

According to the CFL criterion (see Equation 3.7), the maximum time step is 0.045. Note that the velocity of the current is taken into account. However, for stability reasons, the time step needed for the central difference scheme (see Section 3.1.2) might be much smaller. On that account, a safe estimate of $0.002\ s$ was made based on initial model results.

Bottom friction and viscosity

Friction was taken into account with the logarithmic law of the wall. Conditions were assumed to be smooth. Vertical viscosity was modelled with the use of the $k-\epsilon$ model.

Simulation time

For reliable model output, spin up should be avoided. Furthermore, the number of waves should be in the order of 300 for a proper post-processing analysis (de Wit, 2016; The SWASH team, 2018). Initial model results indicated that the spin up time was in the order of $10\ min$. The simulation time for 300 waves is $40\ min$. Therefore, the total simulation time was 50 minutes. The flow velocity profiles were generated at $x = 500\ m$ for both uniform and non-uniform batymetries.

Tab. 4.1.: The model settings used in the sensitivity analysis of the new SWASH model.

	Values
Number of gridpoints per wave length	30, 50, 100, 150
Number of layers	5, 20
Number of time steps per wave period	1000, 2000, 10000, 20000

4.3 Sensitivity analysis setup

In this section, the setup for the sensitivity analysis is given. Note that for the assessment, only values of one model setting were changed in the base model. Furthermore, time efficiency is an important consideration in the assessment. Models, such as SWASH, should produce reliable results at low computational effort and time. Due to the use of the central difference scheme in the new model, time steps are much smaller compared to the discretizations with upwind schemes. Therefore, the spatial discretization should be fine enough to capture all processes within combined wave-current flow, but at the same time, not lead to unreasonably large computational times. This was taken into account in the setup of the sensitivity analysis.

For the horizontal discretization, the effects of the number of gridcells per wave length were assessed with different values. The minimum number of gridcells for proper modelling was estimated at 30. The maximum number was 150, as larger numbers would lead to unreasonably large computational times. For the vertical discretization, only two different configurations were made: 5 and 20 layers. A lower number of layers than 5 leads to an insufficient resolution to properly solve the vertical flow structure. A higher number of layers would lead to unreasonably large computational times. For the time step, the amount of time steps per wave period, mct, was used to compare simulations. In the base model, mct was equal to 4000. A range of values was tested in the sensitivity analysis. An overview of all the values is given in Table 4.1.

4.4 Model results for uniform bathymetry

4.4.1 Analytical solution

The analytical solution for the wave is derived from linear wave theory and the Doppler shift (see Section 2.2). The wave height in the domain should remain constant. The same holds for the absolute wave frequency. However, the relative wave frequency is different, as the wave is, compared to still water, either lengthened or shortened. For the opposing current, the relative wave frequency is $0.83\ rad/s$. This means that the wave length in the relative frame of reference is equal to approximately $65\ m$. For the following current, the relative wave frequency is $0.74\ rad/s$, yielding a relative wave length of approximately $75\ m$.

4.4.2 Results of base model

Model results of the base model indicate that the wave height in the presence of currents is modelled rather accurate. The wave height evolution for the opposing and following current is shown in Figure 4.2. Wave height evolutions for the currents and no current cases are matching closely. The model results confirm the hypothesis that the wave height in the presence of currents is approximately equal to the wave height in still water. Moreover, the wave height in the presence of currents is roughly constant in the domain. A spatial zero-crossing analysis revealed that in the case of an opposing (following) current, the compressed (expanded) wave length was approximately equal to the analytical value of the previous section.

Wiggles, as observed in all wave height profiles, were present in the model results. It is known that SWASH is prone to generating output with these wiggles[1], thus this issue is not related to the modelling

[1] Personal communication with F. P. de Wit (2019)

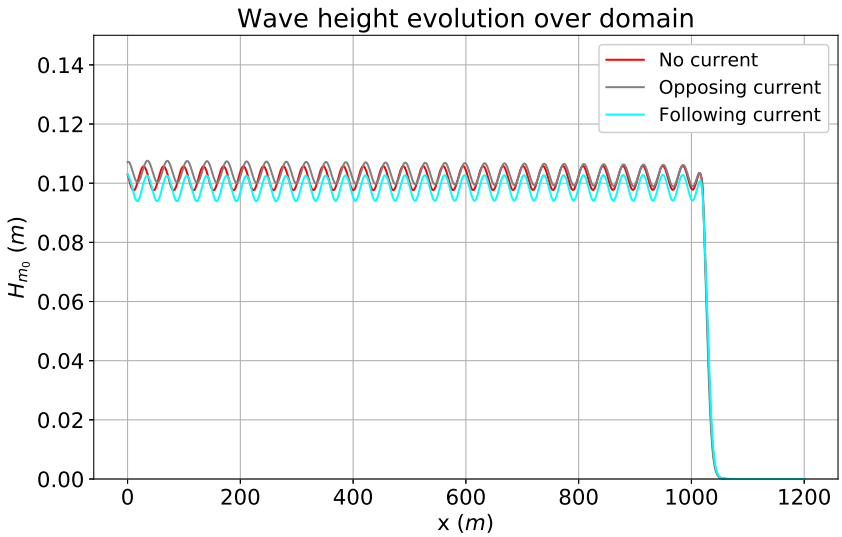

Fig. 4.2.: The evolution of the wave height in the presence of an opposing and following current for a uniform bathymetry. The results for the no current case are also provided. The wave heights in the sponge layer are zero, since the wave is absorbed.

of combined wave-current flow. For the most part, the wave height evolution for both currents was approximately constant, but a slight increase and decrease was observed. As mentioned in Chapter 3, the use of upwind schemes led to these types of increases and decreases of the wave height. There is a possibility that in one of the SWASH routines, an upwind routine is still present. Due to time constraints, this was not verified, but it can be safely assumed that these increases or decreases are negligibly small in comparison to the wave height. Lastly, the wave heights are modelled fairly accurate by the WCS method, but there is no clear match in the results of opposing and following currents. One of the identified reasons was the use of the moving average. For opposing currents, two moving averages at the inlet boundary are used, whereas for following currents, one moving average at the outflow boundary is used. Generally, the wave height for the opposing current is larger than the imposed wave height. The opposite holds for the wave height in the presence of a following current. However, results indicate that these differences are negligibly small. It is still a good check to calculate the wave height in initial model simulations. If the wave height is not sufficient, the value can be increased or decreased. This procedure was applied in previous research (de Wit, 2016; Dobrochinski, 2014).

4.4.3 Results of different orientations of horizontal discretization

The effect of different gridcells per wave length is shown in Figure 4.3. More gridcells per wave length led to larger wave heights, which was more apparent in the case of the opposing current. For both opposing and following currents, model results were stable for 75 or less gridcells per wave length. For 100 or more gridcells per wave length, model results were unstable. The CFL criterion was met in all cases, thus numerical stability should be ensured.

Water level profiles at different moments in time demonstrated the presence of instabilities. This was only found for the unstable models. It remains unknown whether these instabilities occur due to the use of the WCS method, the central difference scheme or a combination of both. Additional runs with lower time steps led to stable model output. However, the differences with the analytical solution were significant, thus lowering the time step leads to stable, but inaccurate model results. Another possible cause is the omission of the limited numerical dissipation obtained with the BDF scheme. Since the central difference scheme is exclusively used, disturbances are not avoided anymore (Zijlema et al.,

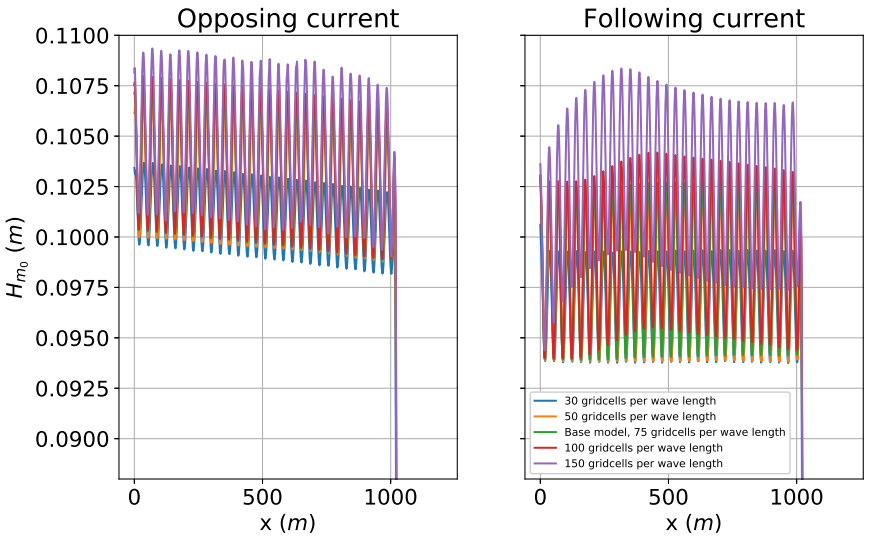

Fig. 4.3.: The evolution of the wave height in the presence of an opposing (left) and following (right) current for a uniform bathymetry. Results are shown for different number of gridcells per wave length. Note that results are zoomed in for $0.085\ m < H_{m_0} < 0.11\ m$.

2011). It could also be the case that aliasing, i.e. perpetual gain, due to time integration is leading to a blow up of the model results (Edwards, 2007).

4.4.4 Results of different orientations of vertical discretization

The time-averaged flow velocity profiles are shown in Figure 4.4. Results demonstrate that the differences between the number of layers is relatively small. For the opposing current, 10 or more layers seem to be sufficient to capture the vertical structure at the upper part of the water column. Near the bottom, no substantial differences are found. For the opposing current, the differences between the number of layers is negligible. Furthermore, an analysis of the wave height and its evolution over the domain was made. The conclusion was that the wave height and evolution were approximately the same for all cases. This implies that the number of layers does not affect the wave height at this range of vertical grid sizes.

4.4.5 Results of different orientations of time step

Results of different numbers of time steps per wave, mct, period are shown in Figure 4.5. For both opposing and following currents, the model results were unstable for $mct = 1000$. For $mct \geq 2000$, model results were stable for both current directions. However, different numbers of time steps still led to substantially different wave heights in the domain. The most apparent difference was the shape and magnitude of the wiggles in the model results. For larger mct, wiggles were smaller. In fact, the wave height evolution was considerably close to the analytical solution for $mct = 20000$. The same was observed for the following current case. This suggests that the wiggles in the model results are a function of the time step, for which it holds that smaller time steps lead to smaller wiggles. More research on the generation of these wiggles would be useful to reduce their extent, or even completely avoid them.

4.5 Model results for non-uniform bathymetry

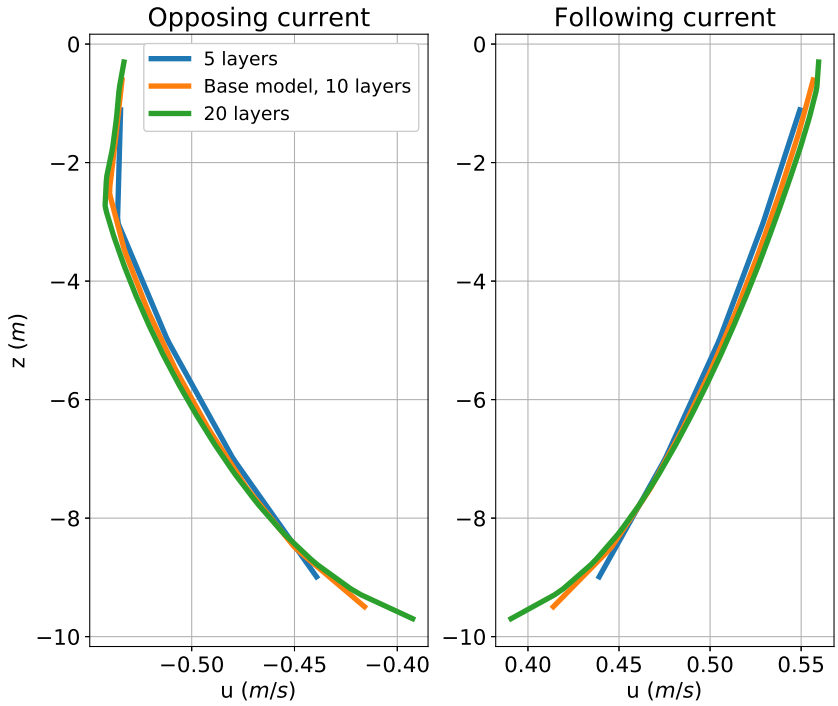

Fig. 4.4.: The time-averaged flow velocity profiles for an opposing (left) and following (right) current in a uniform bathymetry. Results are shown for different numbers of layers. The model results were first interpolated on to a fixed z-grid and afterwards time-averaged for 300 waves.

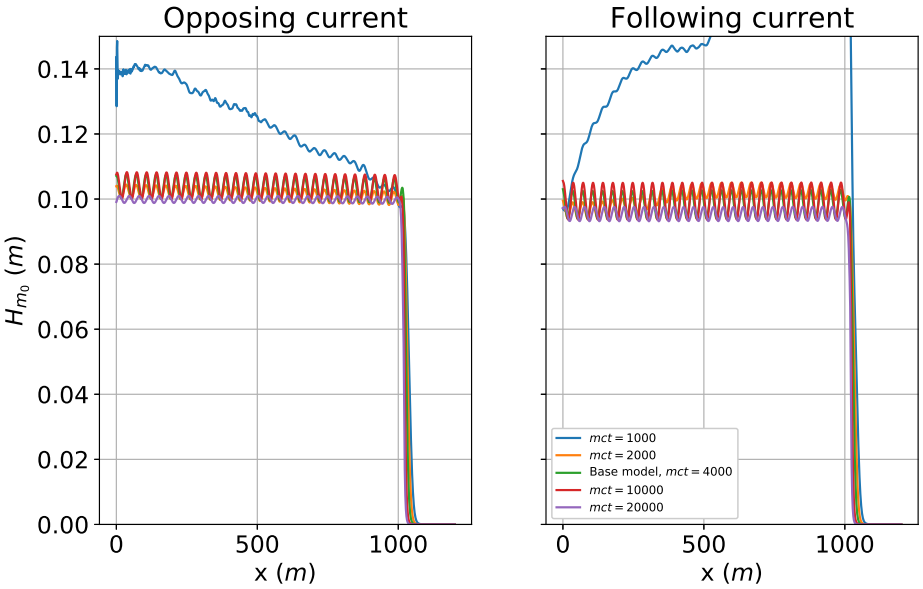

Fig. 4.5.: The evolution of the wave height over the domain for an opposing (left) and following (right) current in a uniform bathymetry. Results are shown for different numbers of time steps per wave period.

4.5.1 Analytical solution

The analytical solution for the non-uniform bathymetry model can be derived based on the conservation of wave action. The complete derivation and analysis of the results are given in Appendix E. A key assumption was that frictional effects were ignored. This was done for simplicity. However, the analytical solution will not completely match the model results, as bottom friction is present in the numerical model.

To summarize, the wave height in all cases changed due to depth-induced shoaling. For the case without currents, the wave height increased in the shoaling zone. In the deshoaling zone, the wave height decreased back to its initial value. For the cases with currents, the wave height was also altered by the current. In the presence of an opposing current, the wave length decreased in the shoaling area. As a result, wave heights increased. In the deshoaling area, the wave length and wave heights returned to their initial values. The same effects were observed for a following current, but in reverse, thus the wave height decreased and increased in the shoaling and deshoaling areas respectively.

4.5.2 Results of base model

The results of the base model are shown in Figure 4.6. In general, the magnitudes of the modelled wave heights were decent. It is difficult to make reasonable conclusions, as the wiggles in the model results were larger than the differences between the wave heights of the analytical and modelled results. Therefore, the focus is set on the trend of the model results. The trend of the wave height evolution is the resulting line when the wiggles are averaged out. Interestingly, the trend was predicted quite well in comparison to the analytical solution.

- In the case of no currents, the trend demonstrated an overestimation of the wave height compared to the analytical solution.
- In the following current case, the modelled trend was slightly underestimated over the entire domain. Similar results were also found in Section 4.4.2, but the difference is more apparent in the case of non-uniform bathymetries. Interestingly, the small increase of the wave height on top of the submerged breakwater is present in the trend of the results. This indicates that the model is producing the correct order of magnitudes of the shoaling factor, due to the decrease in water depth, and the deshoaling factor, due to the following current.
- In the opposing current case, the trend of the modelled wave heights were closely matching to the analytical solution, except for the shoaling zone and shallow part on the top of the submerged breakwater. The wave heights at these locations were slightly overestimated. Furthermore, the general trend of the results indicates that there was a slight decrease of the wave height over the domain. This decrease might be present due to frictional effects at the bottom. However, the amplitudes of the waves are substantially smaller than the water depth, thus no significant dissipation is expected. As the difference in wave height between the begin and the end of the domain is about $2\ \%$, it is assumed that model results are acceptable. However, these model results indicate that the governing equations are not fully energy conservative.

4.5.3 Results of different orientations of horizontal discretization

Model results of different gridcells per wave length are shown in Figure 4.7. In general, results are similar to the findings of Section 4.4.3. For both opposing and following currents, model results were stable for 75 or less gridcells per wave length. The size of the wiggles decreased for less gridcells per wave length. For 100 or more gridcells per wave length, model results were unstable.

4.5.4 Results of different orientations of vertical discretization

The time-averaged flow velocity profiles are shown in Figure 4.8. The number of layers does not have a significant effect on the model output. Model results of the opposing and the following current are

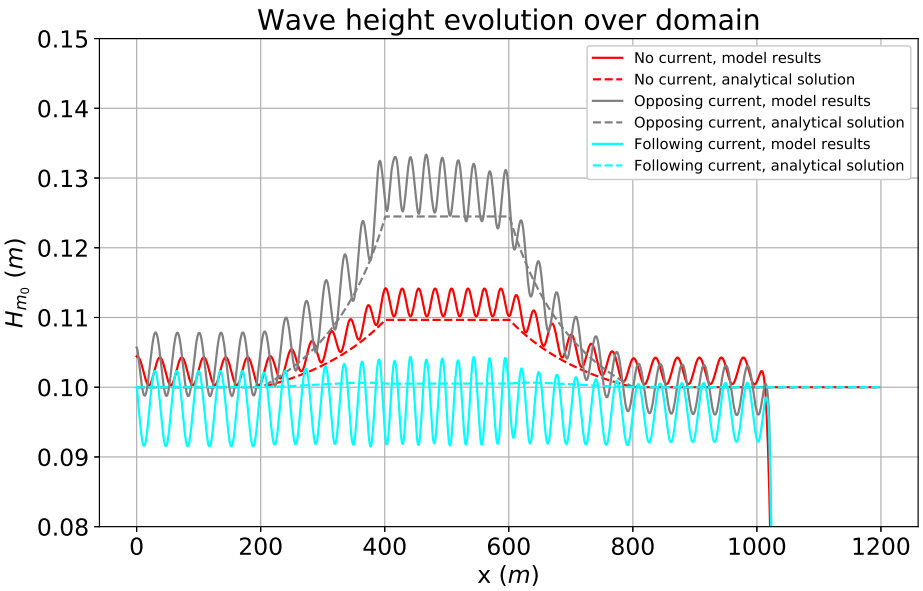

Fig. 4.6.: The evolution of the wave height in the presence of an opposing and following current for a non-uniform bathymetry. The results for the no current case are also provided. The wave heights in the sponge layer are zero, since the wave is absorbed.

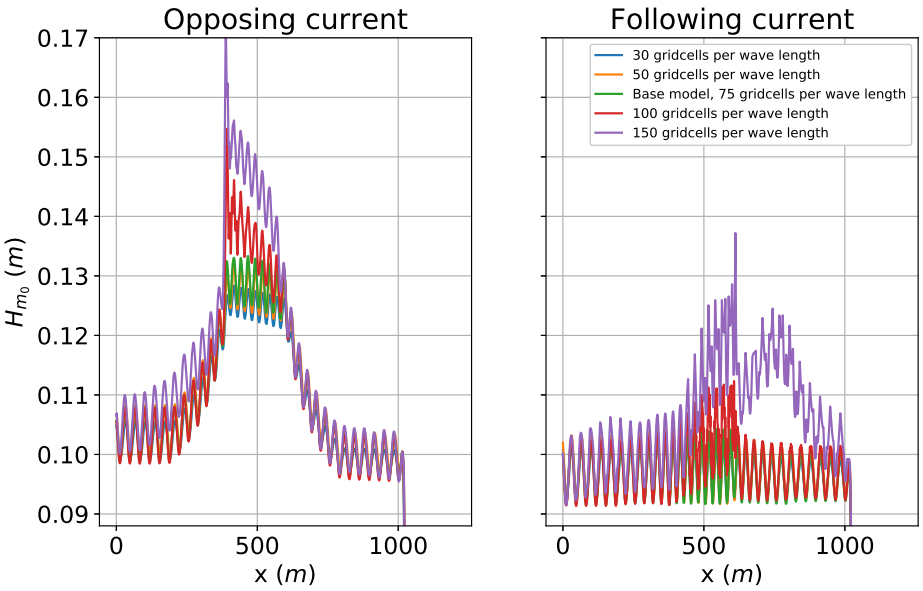

Fig. 4.7.: The evolution of the wave height in the presence of an opposing (left) and following (right) current for a non-uniform bathymetry. Results are shown for different number of gridcells per wave length. Note that results are zoomed in for $0.085\ m < H_{m_0} < 0.11\ m$.

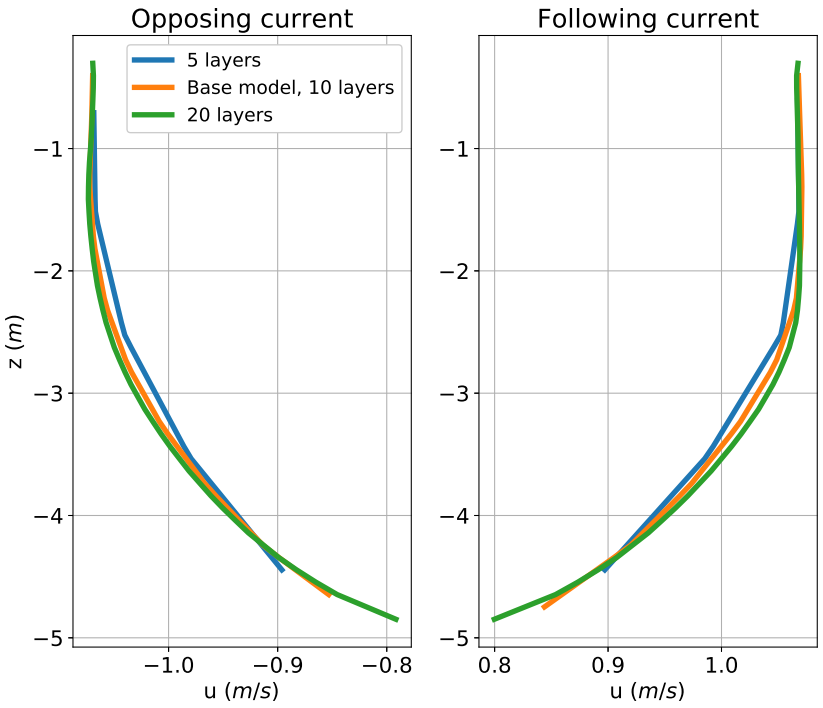

Fig. 4.8.: The time-averaged flow velocity profiles for an opposing (left) and following (right) current for a non-uniform bathymetry. Results are shown for different numbers of layers. The model results were first interpolated on to a fixed z-grid and afterwards time-averaged for 300 waves.

nearly the same. An analysis of the wave height and its evolution over the domain revealed that the wave height and evolution were approximately the same between all cases.

4.5.5 Results of different orientations of time step

The influence of mct on the model results is demonstrated in Figure 4.9. For both opposing and following currents, the model results were unstable for $mct \leq 2000$. The model results remained stable for both current directions for for $mct \geq 4000$. The different numbers of time steps had the same effect on the wave height and wiggles as found in Section 4.4.5, thus, for larger mct, the wiggles were smaller and the wave height evolution was fairly close to the analytical solution.

4.6 General framework for modelling combined wave-current flow

Based on the results of Section 4.4 and 4.5, a general framework is made for modelling combined wave-current flow. Note that the rules of thumb are developed for wave parameters in still water. In general, model results were similar for uniform and non-uniform bathmetries. In the general framework, the lowest value between these two bathymetries was chosen as the normative value. Additional simulations revealed that the WCS method in combination with this general framework also provided accurate results in the case of irregular waves. This is important for the model approach in Chapter 6.

4.6.1 Rules of thumb for spatial discretization

Present rules of thumb for the spatial dicretization in SWASH proved to be useful. The recommended number of gridcells per wave length were sufficient to capture the wave characteristics and provide reliable model output. The same was found for the number of layers. However, for an increasing

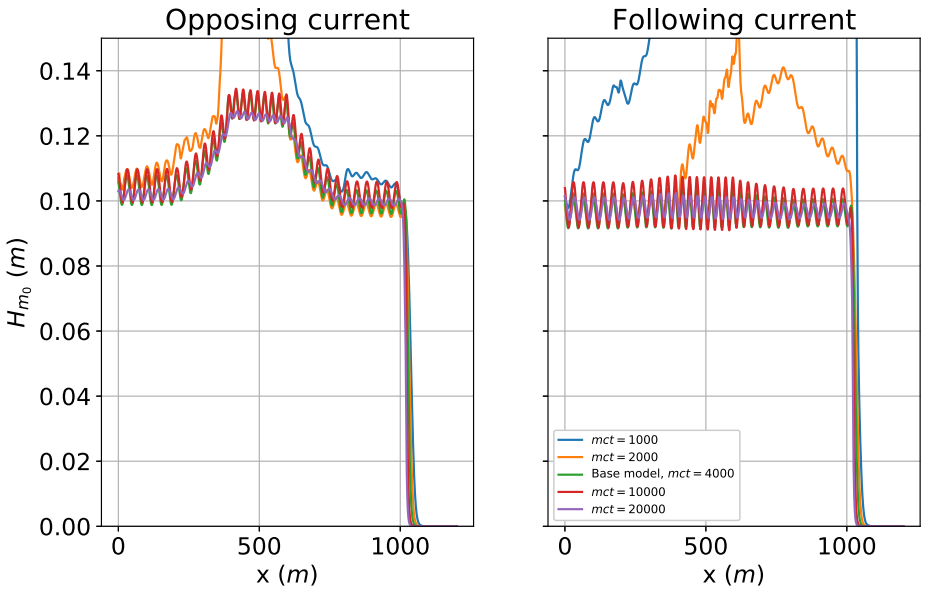

Fig. 4.9.: The evolution of the wave height over the domain for an opposing (left) and following (right) current for a non-uniform bathymetry. Results are shown for different number of time steps per wave period.

number of gridcells per wave length, model results were unstable. This was found for values of 100 and 150. Thus, it is recommended to use 75 gridcells per wave length. The choice in number of layers mostly depends on the desired vertical resolution. For 20 layers or less, it is certain that model results are stable and accurate.

4.6.2 Rules of thumb for time step

The CFL criterion is not normative in the new model. The model results were unstable for time steps as yielded by the CFL criterion. A new quantity mct was introduced, which is the number of time steps per wave period. This proved to be more useful, as model output indicated that for $mct \geq 4000$, the results were satisfactory. The size of the wiggles in the model output can be reduced by using a larger mct. However, this leads to exceedingly large computational times, reducing the feasibility of the model. Therefore, it is recommended to use $mct = 10000$ for accurate and reliable model results.

4.6.3 Limitations of general framework

This framework was tested and in general, accurate model results were obtained. However, it must be noted that the presented values might not work for every case. Some limitations are:

- Model results might not be stable for every non-uniform batymetry. The model results of uniform and non-uniform bathymetries with $mct = 2000$ were stable for the former, but unstable for the latter. This indicates that the shape of the non-uniform bathymetry has an influence on the stability of model results.
- For relatively fine grids, the new model produces unstable results. Therefore, a very detailed resolution in the horizontal domain is not possible, which limits the new model to some extent.
- The number of layers might also be restricted by a maximum number, but this was not analysed.
- The velocity of the current might have a considerable influence on the wave length. Differences with still water might be large enough for unstable model results.
- The rules of thumb are based on simulations that have a ratio current velocity over phase velocity of $|U/c| \approx 0.06$. Consequently, models with other ratio's do not necessarily yield stable and accurate results.

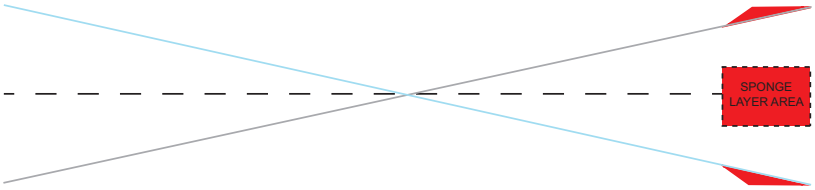

Fig. 4.10.: The losses due to the use of a sponge layer in case of combined wave-current flow in SWASH. The dashed line represents a mean water level. The gray line represents the water level gradient in case of an opposing current, while the blue line represents that of a following current.

The general recommendation is to use the proposed rules of thumb, check water level and velocity profiles in the domain and, accordingly, control whether results are stable.

4.7 Sponge layer effects on model results

Initial model results of current-only simulations showed that a water level gradient developed in the domain. This water level gradient acts as the driving force for the current. Unfortunately, due to the use of a sponge layer, the volume of water in the domain was either increasing or decreasing. The difference between gain or loss of volume depends on the type of current. Typical SWASH simulations are for wave-only cases where the mean water level is generally a flat line when time-averaged. The sponge layer works well in those cases. Nevertheless, the present sponge layer technique does not work well for domains containing a gradient in water level.

The effect, caused by the sponge layer, is present due to relatively large gradients in the water level and velocity profiles. Figure 4.10 can be used to explain the volume increase and decrease. In the case of an opposing current, the water level has a positive upwards slope in the domain (starting from the left end). As was explained in Section 3.1.5, the sponge layer in SWASH dampens out values inside the sponge layer based on the value at the end of the sponge layer and relative distance to this end. As a result, the water levels and velocities in the sponge layer flatten out to a straight, horizontal line. The red area (Figure 4.10) appears in the solution. This red area is the extra amount of volume added to the simulation. The process is reflected for the following current, for which the red area represents a volume decrease. In general, these volume changes can be visualised in time. Results are shown in Figure 4.11. As expected, a volume decrease in time takes place for the following current, while for the opposing currents the volume increases.

It is assumed for further simulations that this effect, caused by the sponge layer, is relatively small in comparison to the imposed wave heights and water level gradients. Furthermore, the volume increase and decrease is in comparison to the total volume of water in the domain negligibly small. However, recommendations for improvement of the sponge layer technique are given in Chapter 8.

4.8 Conclusion

From this chapter, the following conclusions are drawn:

- Simulations of uniform and non-uniform bathymetries were run with the new SWASH model. Present rules of thumb were used in the model setup. In general, results were fairly accurate in comparison to the analytical solution.
- Model results indicated the presence of wiggles. It is known from previous research that SWASH is prone to generating these wiggles and results of the no current case also showed these wiggles. As this is a fundamental issue with the model, no further analysis was made to find the cause of this behaviour. Combined wave-current flow simulations demonstrated that the wiggles were increasing in size for more gridcells per wave length and more time steps within one wave period.

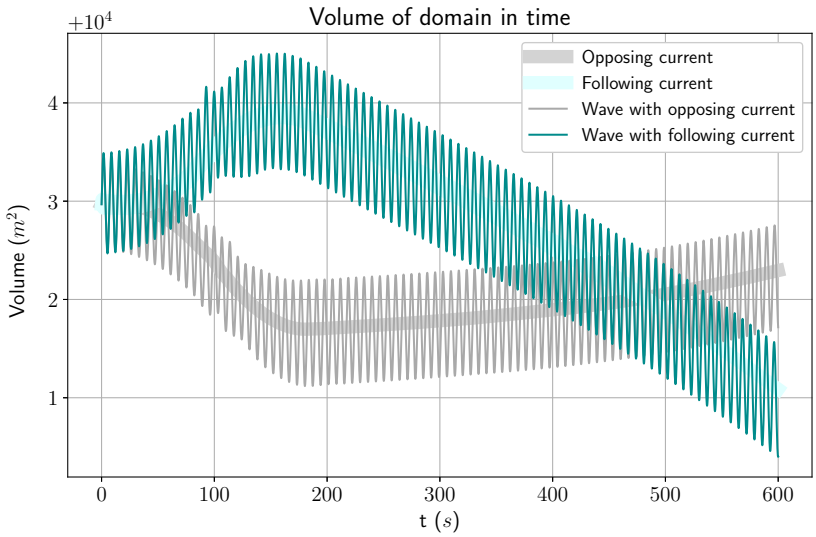

Fig. 4.11.: The volume of the domain in time for the current-only and combined wave-current flow simulations. The initial rise (drop) for the following (opposing) current is due to the water level adapting to an equilibrium.

- A sensitivity analysis was performed to test the limits of the new model. The spatial discretization and the time step were the tuning parameters. Results showed that the number of gridcells per wave length could lead to numerically unstable results. This was found for values larger than 100. It is still unknown why this occurs, however, possible causes were identified. The number of layers does not have a significant influence on the time-averaged flow velocity profiles. The number of time steps per wave period determines the accuracy and stability of the model results. For high values, wave heights were close to matching analytical solutions. For low values, accuracy of the results decreased and the model was more prone to instabilities. In general, the model produced unstable results for $mct \leq 2000$.
- Based on the results of the sensitivity analysis, a general framework was created for the new model. The goal of this framework was to reduce the probability of unstable model runs and find optimized rules of thumb for spatial discretization and time steps. Furthermore, computational times should be relatively comparable to the present SWASH release. In general, the rules of thumb for stable and accurate model results are:
  1. 75 or less gridcells per wave length
  2. 20 or less layers
  3. 4000 or more time steps per wave period.
- The use of a sponge layer leads to a volume increase or decrease in the results. However, the effect on model results was negligibly small.

5 Validation of combined wave-current flow for uniform bathymetry: experiment by Klopman (1994)

This chapter reveals model results with the WCS method of experiments conducted by Klopman (1994). The goal of this chapter is to determine how capable SWASH is in reproducing experimental data for a case with uniform bathymetry. During the analysis of the initial results, several bugs were found in SWASH 5.01. The model was updated to get rid of these bugs, thus the model used hereinafter is referred to as SWASH 5.01*A*.

The setup for validation is shown in Section 5.1. A summary of the model results of the current- and wave only simulations is provided in Section 5.2. For more details regarding the analysis, reference is made to Appendix F. Model results of the combined wave-current flow case for opposing and following currents are analysed in Section 5.3. Velocity profiles of the opposing and following current cases are described in detail. A summary of the key findings is given in 5.4.

5.1 Validation approach

Details regarding the experiments conducted by Klopman (1994) can be found in Section 3.3.1. For the validation of the WCS method, the current-only, wave-only and combined monochromatic wave-flow cases were used. All cases were approximated as 2DV in SWASH, as there were no variations in the horizontal direction perpendicular to the main axis of the wave flume.

The following steps were completed sequentially:

1. Currents only
   a) Present SWASH release
      i. Following current
      ii. Opposing current
   b) WCS method
      i. Following current
      ii. Opposing current
2. Waves only
   a) SWASH
   b) User-generated time series
3. Waves and currents
   a) Opposing current
   b) Following current

The goal is to first ensure proper modelling of the current- and wave-only cases. Any underlying problem with the model can be assessed and solved. This reduces, to some extent, the possibility of errors in the combined wave-current flow simulations. Another objective for the current- and wave-only cases is to compare the performance of the present SWASH release and the new model with the WCS method.

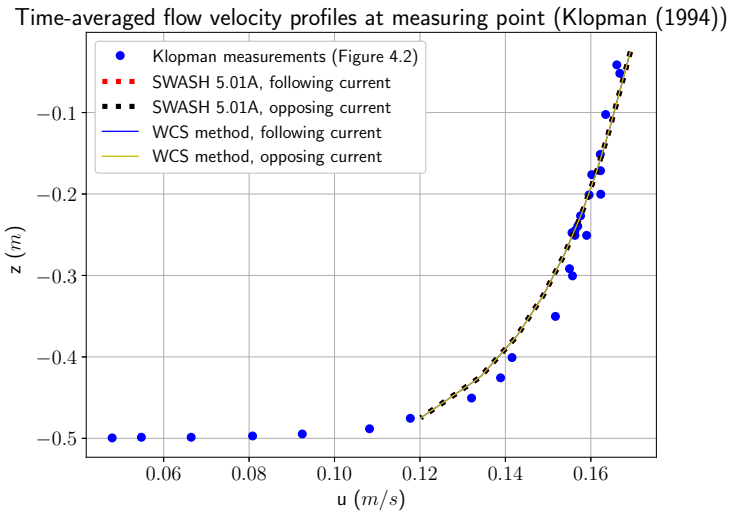

Fig. 5.1.: The time-averaged flow velocity profiles for SWASH 5.01A and the WCS method. Both methods are used to simulate a following and opposing current. The results were first interpolated on to a fixed z-grid and afterwards time-averaged between $t = 10\ min$ and $t = 20\ min$. As the results match each other, some lines are overlapping and not visible.

5.2 Model results of current- and wave-only experiments

The detailed analysis of model results of the current- and wave-only experiments is given in Appendix F. Key findings are presented in this section.

5.2.1 Velocity profiles of current-only experiment

Current-only simulations were performed with the present SWASH release as well as the WCS method (both SWASH versions hereinafter referred to as models). Klopman (1994) only used one direction for the currents. However, for the simulations, both directions were modelled with both models. This was done to assess whether results were symmetric and, thus, independent of direction. Furthermore, a distinction was made between numerical domains with and without a sponge layer.

Without sponge layer

Time-averaged flow velocity profiles were generated with the present SWASH release and the WCS method. Results are summarized in Figure 5.1. It is clear from these results that both models produce the same output. Furthermore, model output is the same for opposing and following currents. This means that the model results are symmetric, thus the general direction of the current has no negative effects on the results.

With sponge layer

Results of the cases with sponge layer are shown in Figure 5.2. Differences are now present between the present SWASH release and the WCS method, which was not the case in the simulations without sponge layer. There is also a substantial difference between current directions. Two possible causes were identified. Water level profiles (Figure F.10) are significantly different between both models as well as current directions. As a result, the water depth, and thus the flow velocity profile, was slightly larger or smaller. Furthermore, the placement of the sponge layer with respect to the current direction makes a difference. The sponge layer was placed at the right end of the numerical domain for all simulations. Results with the present SWASH release suggest that when the flow was not altered by

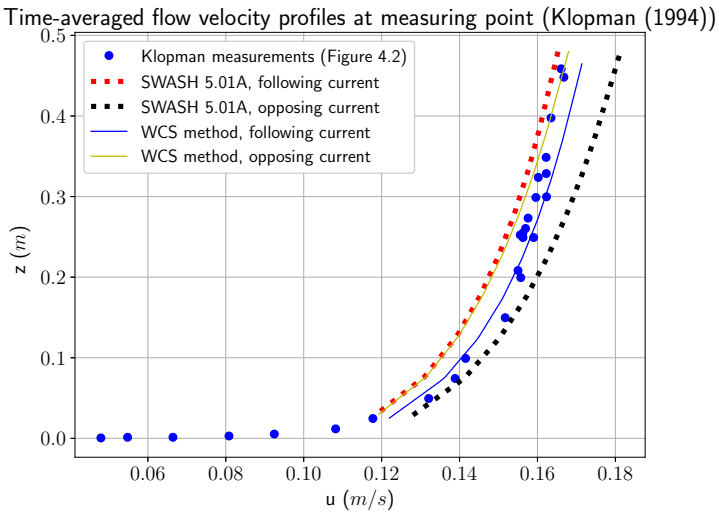

Fig. 5.2.: The time-averaged flow velocity profiles for SWASH 5.01A and the WCS method. Both methods are used to simulate a following and opposing current with a sponge layer. The results were first interpolated on to a fixed z-grid and afterwards time-averaged between $t = 10\ min$ and $t = 20\ min$.

Tab. 5.1.: The RMSE values of the model results of the current-only case of Klopman (1994). Values are obtained for the present SWASH release (SWASH 5.01A) the WCS method. Note that the values have a unit of m/s.

	SWASH 5.01A (opposing)	WCS (opposing)	SWASH 5.01A (following)	WCS (following)
Without sponge layer	0.0028	0.0031	0.0028	0.0031
With sponge layer	0.0088	0.0057	0.0060	0.0032

the sponge layer, i.e. for following currents, the flow velocity profile was only underestimated due to the increased water depth. When the flow was altered by the sponge layer, i.e. for opposing currents, the flow velocity profile was overestimated and, additionally, showed a different shape in comparison with measurements. Results with the WCS method also deal with these causes, but there remains a difference with the results of the present SWASH release. This difference is related to the water level at the outflow boundary, which for the WCS method is dynamic, i.e. it changes in time, whereas for the present SWASH release the outflow boundary is static, i.e. the water level is constant in time.

Model performance

To conclude, the performance of SWASH in modelling the current-only case of Klopman (1994) was analysed with the use of the RMSE and model skill score (see Equations 3.40 and 3.41). The output was only considered for $z > -0.45\ m$. The RMSE values are shown in Table 5.1. The baseline model for the skill score was the present SWASH release, as the goal is to assess whether the WCS method produces better results. Results are shown in Table 5.2. In all results, a distinction is made between opposing and following currents.

For the model results with and without sponge layer, no significant difference in accuracy is present between the present SWASH release and the WCS method. In general, both methods produce relatively accurate results, as all of the RMSE values are low in comparison to the magnitude of the flow velocity profiles. Model skill scores for the cases without sponge layer suggest that the WCS method produces poorer output than the present SWASH release. However, model skill scores for the cases with sponge layer indicate that the WCS method produces significantly better output. The addition of the WCS method, thus, proves to be useful, as a sponge layer is always used in the simulations for combined wave-current flow.

Tab. 5.2.: The model skill scores for the WCS method in modelling the current-only case of Klopman (1994). The baseline predictions were obtained with the present SWASH release (SWASH 5.01A).

	Opposing current	Following current
Without sponge layer	-0.113	-0.108
With sponge layer	0.351	0.463

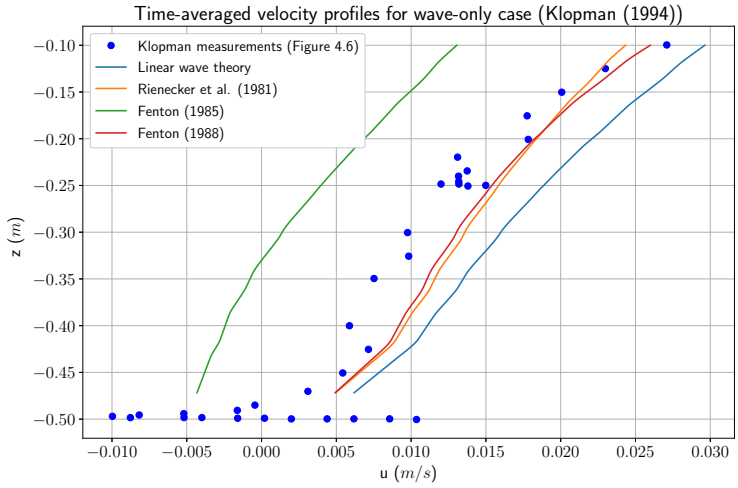

Fig. 5.3.: Data from Klopman (1994) measurements (Figure 4.6, original report) compared with model results. The model results were time-averaged and obtained for different wave conditions as specified in the figure.

5.2.2 Velocity profiles of wave-only experiment

Wave-only simulations were performed with the present SWASH release. The waves, imposed by Klopman (1994), were non-linear, thus regular linear wave theory is not sufficient to fully describe the wave. Therefore, time series were generated (Appendix C) with various methods. For comparison, the wave was also generated with default SWASH options, i.e. expressions of linear wave theory were used.

Comparison between different methods of wave generation

The time-averaged velocity profiles of the wave generation methods are shown in Figure 5.3. The obtained profiles are actually the Stokes drift profiles, as only wave flux is time-averaged. The theoretical Stokes drift profile has a similar shape as the experimental data (see Figure F.11). In general, the profiles of the model results had the same shape as the measurements and Stokes drift profile. However, the results of the wave generated with the method by Fenton (1985) significantly underestimated experimental data. The results of the waves generated with the methods by Rienecker and Fenton (1981) and Fenton (1988) had the closest fit to the measurements. The results of the wave generated with linear wave theory were fairly accurate, thus for simplicity, it was assumed that linear waves should produce satisfying results of combined wave-current flow.

Results of different number of layers

Interestingly, the number of layers had a significant influence on the time-averaged velocity profiles. The larger the number of layers were, the more shapes of the profile were deviating from measurements. More layers lead to higher resolutions near the bottom, which might be a possible cause for this effect.

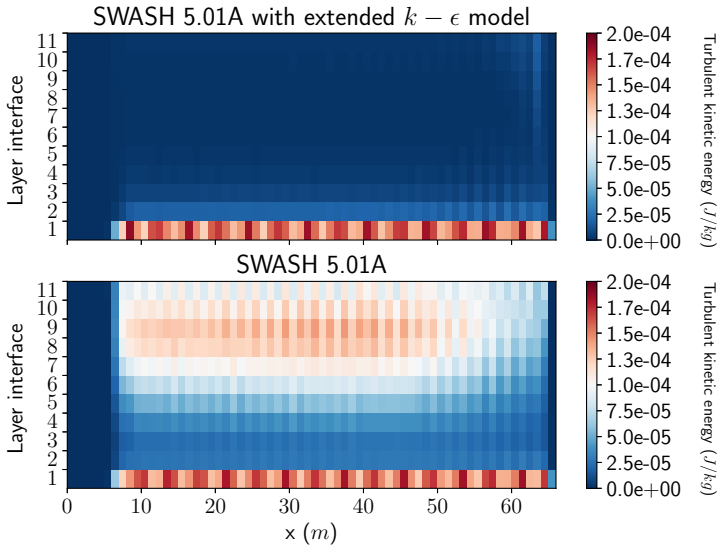

Fig. 5.4.: The turbulent kinetic energy profiles for the linear wave case generated with the present SWASH release and a new SWASH model including the extension of the $k-\epsilon$ model. The results are shown over the domain per layer interface at $t = 3\ min$. At the left end of the domain, a sponge layer with length $8\ m$ was placed.

However, the bottom friction was exactly matching for every case. No further analysis was made. To neglect these effects for the combined wave-current flow simulations, the number of layers was set to 10.

Turbulent kinetic energy

The new extension of the $k-\epsilon$ model (see Section 3.1.4) was assessed by comparing results obtained with the present SWASH release and the new model. Results of the turbulent kinetic energy profiles are shown in Figure 5.4. The results with the new model indicate that the generation of turbulent kinetic energy is suppressed. However, results with the present SWASH release demonstrate that turbulent kinetic energy values were steadily increasing in time. The increase in the turbulent kinetic energy leads to more turbulent viscosity. For model cases with large simulation times, this uncontrolled behaviour could perhaps lead to the altering of the waves and currents. Therefore, the extended $k-\epsilon$ model is a valuable addition to SWASH.

Model performance

The performance of SWASH in modelling the wave-only case of Klopman (1994) was evaluated with the RMSE and model skill score. The output was only considered for $z > -0.45\ m$. The model results with the default SWASH input were used as the baseline model for the skill score. The RMSE and model skill scores are shown in Table 5.3 and 5.4, respectively.

Results indicate that the method by Fenton (1985) produces the poorest results in terms of accuracy. Furthermore, the skill score is negative, which means that model output is poorer in predicting the experimental data compared to the linear wave. The RMSE values of the other methods and default SWASH produce fairly accurate results. The model output with the methods by Rienecker and Fenton (1981) and Fenton (1988) resulted in positive skill scores, which is logical, since the waves as imposed by Klopman (1994) were non-linear. As the results of the linear wave are reasonably accurate, the default SWASH option will be used for the combined wave-current flow simulations. Note that this means that model output will not match the experimental data. However, the interest lies in the

Tab. 5.3.: The RMSE values of the model results of the wave-only case of Klopman (1994). Values are obtained with output of the present SWASH release (SWASH 5.01A). Note that the values have a unit of $10^{-4}\ m/s$.

Linear wave	Rienecker and Fenton (1981)	Fenton (1985)	Fenton (1988)
5.4	1.4	17.9	1.0

Tab. 5.4.: The model skill scores for the present SWASH release in modelling the wave-only case of Klopman (1994). The baseline predictions was the linear wave, imposed with the default SWASH option.

Rienecker and Fenton (1981)	Fenton (1985)	Fenton (1988)
0.49	-0.82	0.56

capabilities of SWASH in modelling the vertical shear in combined wave-current flow, thus, exact matches are not of importance for this research.

5.3 Model results of combined wave-current flow experiment

5.3.1 Model setup

The model setup was to a large extent used from the current- and wave-only simulations. For a full description, reference is made to Section F.1. The imposed wave was linear, as the results of the wave-only case indicated a fairly accurate match with experimental data. The wave characteristics were kept the same, as initial model results showed accurate results of the wave height evolution. The spatial discretization and time step were determined with the general framework for modelling combined wave-current flow (see Section 4.6). For the horizontal discretization, 75 gridcells per wave were used. Accordingly, 2000 gridcells were used in the model. For the vertical discretization, 10 layers were used. To ensure stable and accurate model results, mct was equal to 10000, matching a time step of $0.000125\ s$. The total simulation time was $10\ min$ with approximately $3\ min$ spin up time.

5.3.2 Model results

Time-averaged flow velocity profiles at the measuring position of Klopman (1994) are summarized in Figure 5.5. The opposing and following current cases are discussed in the following sections. The model results and experimental data of the current-only case are included for comparison.

Opposing current

The models results of the opposing current are poor in comparison to experimental data by Klopman (1994). The data clearly demonstrates the presence of a significant vertical shear close to the surface. As demonstrated in Section 2.4, similar results were found in other experiments. However, the model results indicate that the vertical shear is approximately zero. Furthermore, the magnitude and shape of the velocity profile is significantly different from the data. Surprisingly, close to the bottom, the model results indicated the correct shape of the velocity profile. Unfortunately, flow velocities were substantially overestimated. This suggests that the bottom friction is not modelled properly, as frictional effects mainly play a role. Interestingly, one area of the vertical structure was modelled fairly accurate. For $-0.25\ m < z < -0.15\ m$, results closely matched the experimental data.

Following current

The models results of the following current are extremely poor compared to measurements. The shape of the time-averaged velocity profile conflicted with that of the measurements. Experiments suggest a

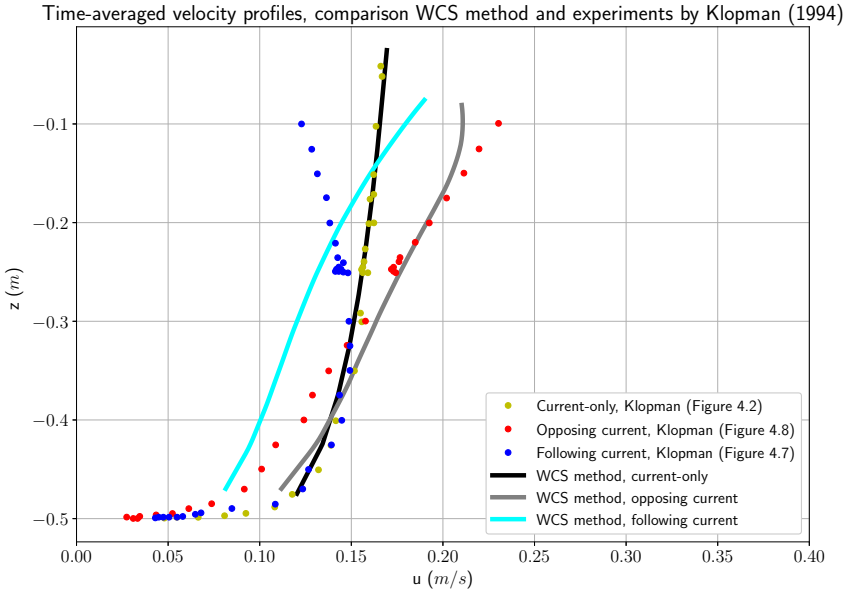

Fig. 5.5.: The time-averaged horizontal velocity profiles for the current-only, opposing current and following current cases. Model results at the measuring position of Klopman (1994) are compared with experimental data.

negative vertical shear, see Section 2.4. However, model results demonstrate a positive vertical shear, which can only be expected for an opposing current.

Model results at boundary point

The model results at the measuring position of Klopman (1994) are unsatisfactory, as the model results do not match the measurements. However, it is not certain whether the mismatch in results and measurements is due to the WCS method, the general SWASH model or a combination of both. By definition, the WCS method is a boundary condition method. Interestingly, the most accurate model results were obtained at the wave maker boundary, i.e. the velocity boundary. Results are shown, see Figure 5.6. The profile of the following current case was now partially resembling the measurements, although results are still inadequate. On the other hand, the results of the opposing current case improved a lot. The vertical shear close to the surface was not present. However, the shape of the profile is closely resembling that of the measurements. There is still a considerable difference in magnitude.

Significance of results

In general, the model results at the wave maker boundary are slightly satisfying, as SWASH demonstrates the capacity of modelling the shapes of the velocity profiles. However, the magnitude of the modelled results are highly inaccurate. Moreover, the results were significantly different at different locations in the domain. This suggests that the model is not capable of uniformly modelling the vertical structure of the flow over the domain. As the wave boundary layer is missing, the model results near the bottom were generally poor.

As was mentioned in the previous section, it is unclear whether the mismatch in validation results are due to the general components of the SWASH model or the WCS method. For the model setup, some assumptions might have a considerable influence on the results. The experiments by Klopman (1994) were approximated as 2DV. As a result, three-dimensional effects were neglected. These

Tab. 5.5.: The RMSE values of the model results of the combined wave-current flow cases of Klopman (1994). Values are obtained with output of the WCS method. Note that the values have a unit of m/s.

Opposing current	Following current
0.012	0.010

Tab. 5.6.: The model skill scores of the WCS method for the combined wave-current flow cases of Klopman (1994). The baseline predictions were the current-only model results of the present SWASH release.

Opposing current	Following current
0.543	0.422

types of effects have a considerable influence on the time-averaged velocity profiles. Dingemans et al. (1996) demonstrate by means of a numerical model based on the Craik and Leibovich equation (Craik and Leibovich, 1976) that the lateral boundaries, i.e. side walls of the wave flume, are important for the flow. Furthermore, the difference between the imposed waves in the experiment and in the numerical model could also explain the general poor fit between model results and measurements. As the imposed wave was non-linear in the experiments by Klopman (1994), non-linear wave-current interactions might be underestimated in the case of a linear wave.

5.3.3 Model performance

The RMSE and model skill scores are summarized in Table 5.5 and 5.6 respectively. The baseline model were the results of the current-only case, as it was not possible to use the same model setup and the present SWASH release for modelling combined wave-current flow. In general, the WCS method proves to be a useful addition to the present SWASH release, as model skill scores are positive. However, the accuracy of the model is not significantly high, as the RMSE values are substantial in comparison to the magnitude of the velocity profiles.

5.4 Conclusion

From this chapter, the following key points are found:

- Current-only model results
  - The present SWASH release as well as the WCS method are capable of simulating the current-only flow in the experiment of Klopman (1994). Model results were fairly accurate in comparison to experimental data.
  - When a sponge layer is added to the current-only cases, preference should given to the WCS method, as it does not lose its accuracy in modelling the flow. The results with the present SWASH release are relatively poor. The skill score for the WCS method is substantially positive.
- Wave-only model results
  - Time-averaged velocity profiles of the wave-only model results were acceptable. Four methods of wave generation were tested. In general, time series of non-linear wave theories resulted in the best fit with experimental data, as their skill score were relatively high. Surprisingly, the linear wave showed a fairly accurate match with data. However, for all cases, the wave boundary layer was not present in model results due to an insufficient vertical resolution.
  - The number of layers had a significant influence on the shape of the time-averaged velocities for the wave-only case. More layers generally resulted in more deviation of model results with measurements. Unexpectedly, the wave boundary layer was still not present for large numbers of layers.
  - The generation of turbulent kinetic energy with the present SWASH release is unbounded in time. As pointed out by Larsen & Fuhrman (2018), the standard

$k - \epsilon$ model is unconditionally unstable. This is also in line with the results in the wave-only case of the experiment of Klopman (1994). The proposed new set of limiters by Larsen & Fuhrman (2018) in the $k - \epsilon$ model demonstrates the suppression of generation of turbulent kinetic energy.

- Combined wave-current model results
  - Model results at the measuring position of Klopman (1994) were unsatisfactory. In the opposing current case, the velocity shear is generally modelled well, except near the surface. In the following current case, the velocity profile was modelled very poorly, as the shape and direction conflicted with measurements. For both cases, results of the velocity profiles near the bottom were substantially different from measurements.
  - Model results at the wave maker boundary were promising for both opposing and following currents. The vertical shear was modelled fairly accurate for the opposing current. However, there was still a significant mismatch between the velocity shear near the surface and measurements. For the following current case, the velocity profile was more accurate than at the measuring position of Klopman (1994). In general, the skill score for both opposing and following currents were highly positive.
  - In general, the model results at the wave maker boundary showed that SWASH is capable of producing the vertical structure of combined wave-current flow. However, significant differences remain between model results and measurements. Furthermore, profiles were less accurate for locations further from the wave maker boundary. One of the causes for this general mismatch might be related to the modelling approach. The 3D effects in the Klopman (1994) experiment are important for the velocity profile.

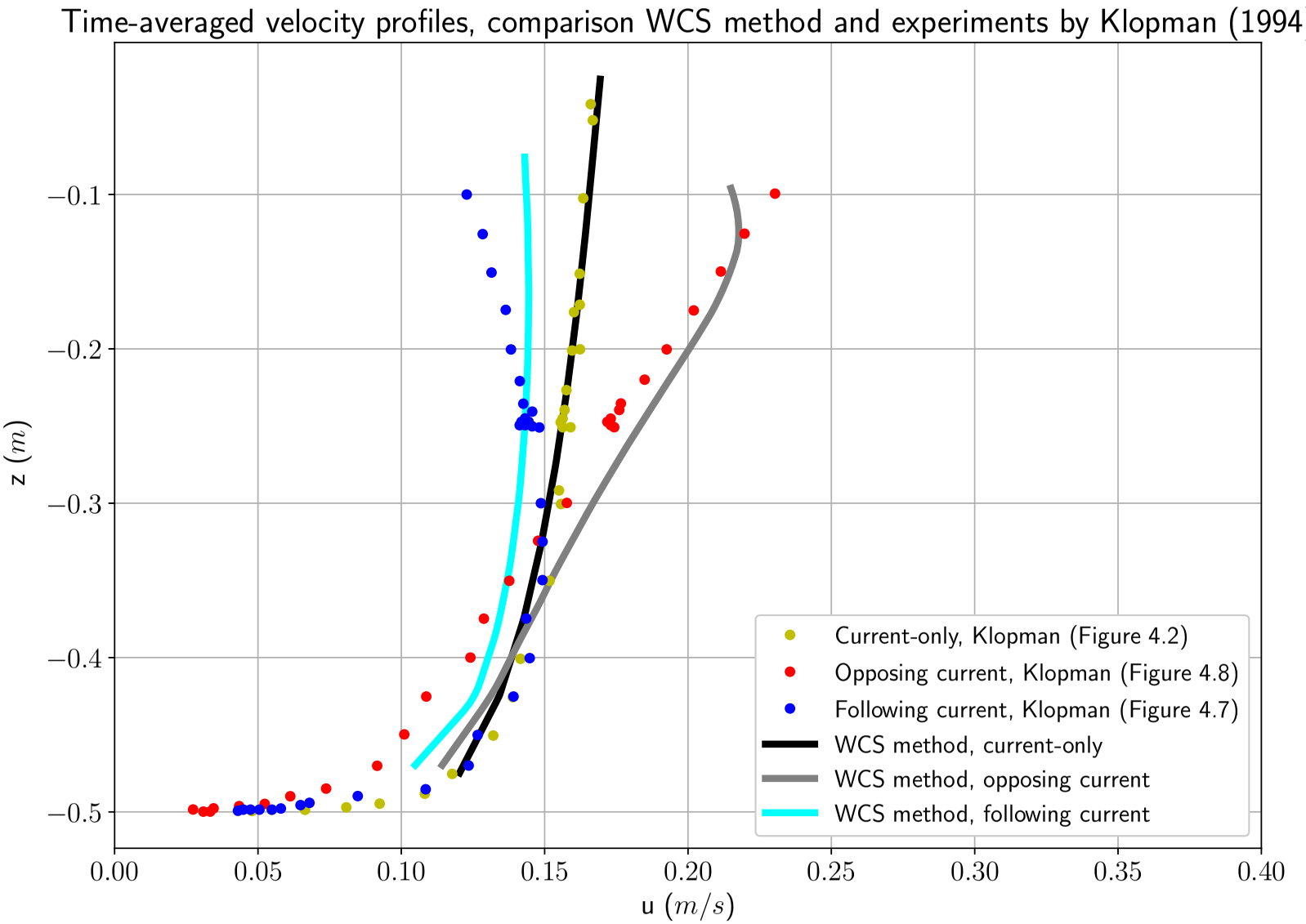

Fig. 5.6.: The time-averaged horizontal velocity profiles for the current-only, opposing current and following current cases. Model results at the wave maker boundary are compared with experimental data.

6 Validation of combined wave-current flow for non-uniform bathymetry: experiment by Ma et al. (2017)

In this chapter, the newly developed SWASH model is validated with measurements from experiments carried out by Ma et al. (2017). The goal of this chapter is to determine how capable SWASH is in producing model results of an experiment with non-uniform bathymetry.

The setup for validation is shown in Section 6.1. The model setup is provided in Section 6.2. Model results of the opposing and no current cases are analysed in Section 6.3. A summary of the key findings is given in 6.4.

6.1 Validation approach

The opposing current case by Ma et al. (2017) is validated with the new SWASH model. Details regarding the experiments can be found in Section 3.3.2. In the model output, time series were generated at several locations in the domain. With these time series, a comparison was made with experimental data. More specifically, skewness, asymmetry and wave height were calculated from the time series. As mentioned in Section 3.4, the waveform is defined with these parameters. Furthermore, wave spectra at a few locations were provided by Ma et al. (2017), thus a validation of the wave spectra was also made. For the model performance, simulations were also executed without currents. The model results were subsequently used as the baseline model. Note that the skill scores in this case only reflect on the utility of the WCS method.

6.2 Model setup

A numerical model was set up for the modelling of the experiment by Ma et al. (2017). The domain sizes are given in Sections 6.2.1. General model settings are given in Section 6.2.2.

6.2.1 Numerical domain

The experiment by Ma et al. (2017) was approximated as 2DV in SWASH. The flume had a length of $50\ m$. A sponge layer with length $5\ m$ was placed at the right end of the domain, yielding a total length of $55\ m$. A submerged breakwater was present in the flume. The submerged breakwater had a side slope of $1/20$ and length of $7\ m$ at both sides. The shallow part on top of the submerged breakwater was $3\ m$ long. The left and right slopes are, hereinafter, referred to as the shoaling and deshoaling areas. The maximum and minimum water depth were $0.45\ m$ and $0.1\ m$, respectively. A sketch of the setup for the numerical model is given in Figure 6.1.

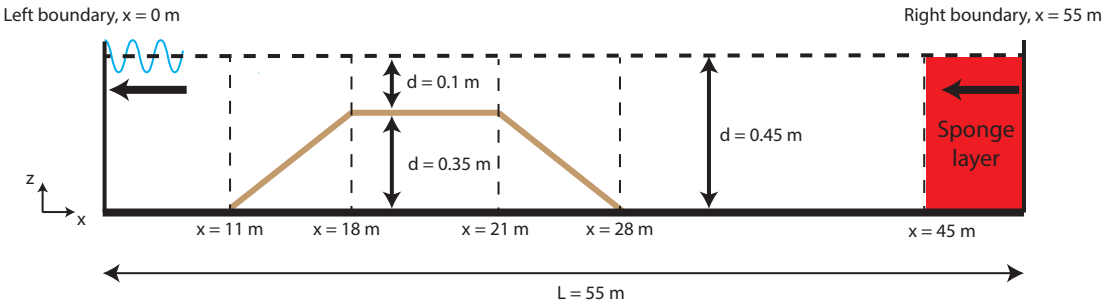

Fig. 6.1.: Sketch of the numerical model setup for the opposing current experiment by Ma et al. (2017). The length of the flume was $55\ m$. Waves were generated at the left boundary and absorbed with a sponge layer next to the boundary at the right. A uniform current was imposed at both boundaries. The black arrows show the direction of propagation of the current. The submerged breakwater was placed at the halfway point. The dimensions are not to scale. The maximum and minimum water depth were $0.45\ m$ and $0.1\ m$ respectively.

6.2.2 General model settings

Boundary conditions

Ma et al. (2017) imposed random waves by means of a JONSWAP spectrum. The same was done in SWASH at the velocity boundary. The significant wave height and peak period were $0.05\ m$ and $1.0\ s$ respectively. A default peak enhancement parameter of 3.3 was used. Furthermore, a cycle period of $80\ s$ was used, yielding a total of 200 wave components. At the discharge boundary condition, a discharge of $-0.0135\ m^2/s$ was imposed.

Spatial discretization and time step

The number of gridcells per wave length was set at 75, yielding approximately 2800 gridcells in the domain. This resulted in a horizontal resolution, Δx, of $0.02\ m$. Note that the wave length is calculated without the presence of currents. For the vertical structure, 15 layers were used.

Initial velocity field

An initial velocity field was generated to avoid large spin up times. The initial velocity in the deep parts of the domain were $-0.03\ m/s$. The velocity on top of the submerged breakwater was, accordingly, equal to $-0.135\ m/s$.

Bottom friction and viscosity

Friction was taken into account with the logarithmic law of the wall. Due to lack of information, a smooth bottom was assumed. Vertical viscosity was modelled with the use of the $k-\epsilon$ model.

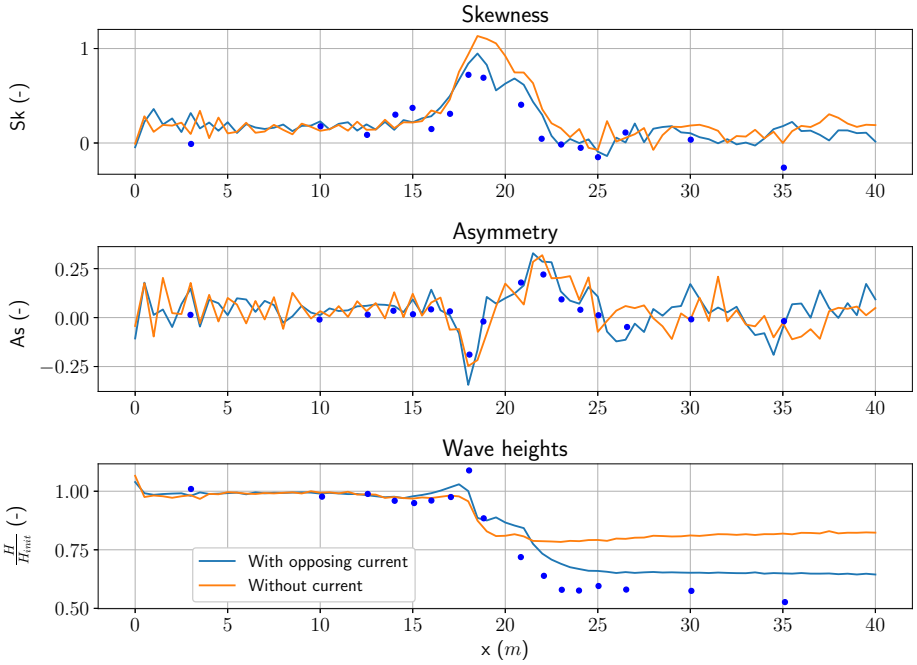

Fig. 6.2.: Skewness, asymmetry and wave height profiles over the domain based on model results are compared with measurements by Ma et al. (2017). Model results with and without a current are shown.

Simulation time

Initial model results indicated that the spin up time was in the order of $3\ min$. The simulation time for 300 peak waves is $5\ min$. Therefore, the total simulation time was 8 minutes. For the analysis of time series, the cycle periods were taken into account.

6.3 Model results

Time series at numerous locations in the domain were generated and used for the calculation of skewness, asymmetry and wave heights. Results are shown in Figure 6.2. In general, the trend of the models results were fairly accurate compared to measurements. Note that wiggles of substantial sizes were present in the skewness and asymmetry profiles for $x < 20\ m$.

6.3.1 Evolution of skewness

The results imply that skewness was prone to highly fluctuating values. As was mentioned in Section 4.4, it is known that SWASH might generate output with wiggles. It could also be the case that wiggles are present due to reflected waves. Research has shown that wave reflection takes place when the relative propagation velocity of waves equal that of the current (see Section 2.3). These reflected waves might cause significant alteration of the skewness. For the most part, conclusions regarding the magnitude of the modelled parameters are difficult to state, as these wiggles have larger deviations.

The trend of the model results is quite accurate, but there are locations in the domain where model results are significantly different from measurements. Near the wave maker boundary and sponge layer, model results were quite poor. However, near and on top of the submerged breakwater, model results were very close to the measured values. Moreover, measurements suggest that the waves were not skewed for $0\ m < x < 5\ m$. This is also expected theoretically, as the waves are propagating in the presence of a uniform current. Interestingly, the waves at the boundary developed relatively

quickly into skewed waves. This was observed close to $x \approx 1.0\ m$. After this point, the waves became positively skewed. No cause for this behaviour was found. For $x > 30\ m$, the skewness was positive. However, data suggests that the waves became negatively skewed, i.e. wave troughs and crests are peaked and flattened respectively. The model was not capable of reproducing this behaviour.

6.3.2 Evolution of asymmetry

The trend of the model results of the asymmetry were satisfactory. The trend closely matched measurements. Asymmetry was modelled quite accurate near and in the shoaling zone of the submerged breakwater, similar to results of skewness. Results in the deshoaling zone were also closely matched measurements. However, on top of the submerged breakwater, the asymmetry was positive, whereas measurements show the presence of negative values. Due to the presence of wiggles, no conclusions regarding the accuracy can be drawn.

6.3.3 Evolution of wave height

The wave height evolution is rather unsatisfactory. At the wave maker boundary, the wave height is significantly overestimated. One cause might be the default moving average period. The results imply that this was too short, as the water depth at the boundary seems to be fluctuating. For $3\ m < x < 17\ m$, results were fairly accurate compared to measurement data. The maximum wave height on top the submerged breakwater was modelled correctly. This implies that the model resolved the shoaling effects due to the depth and the current quite accurately. However, wave heights in the deshoaling zone and after were not closely matching data. Wave heights for $x > 17\ m$ were generally overestimated. This results suggests that wave breaking was likely underestimated by the model. Note that SWASH provides the option to use a wave breaking model. This option was used in the model simulation, but wave breaking was surprisingly still underestimated.

6.3.4 Comparison of wave spectra

Wave spectra were also available, thus time-series of the model results were calculated as wave spectra. Comparisons are shown in Figure 6.4. At $x = 10\ m$ and $x = 17\ m$, model results are fairly accurate. However, at $x = 22\ m$ and $x = 25\ m$, the results are relatively poor. As the wave height is overestimated for $x > 17\ m$, it is likely that the spectra contains wave components that should have been dissipated. No further analyses were made.

6.3.5 Model results without currents

In general, the presence of the current improves the fit between model results and experimental data. Results of the model without currents are interesting to compare with the previous findings. The skewness was modelled inaccurately near and on top of the submerged breakwater. In the shoaling area, model results were quite close to the measurement data. This implies that at this part of the domain, depth-induced shoaling is more dominant than effects caused by the presence of a current. The asymmetry profile was fairly accurate compared to measurements. Surprisingly, the results were at some parts of the domain, in comparison to the standard model, better.

The wave height profile for the no current model was highly inaccurate at the right side of the submerged breakwater. Although the agreement between results and data is fine for $x < 17\ m$, large discrepancies are found for $x > 21\ m$. The results of the wave height seem to be in line with the experimental findings by Beji and Battjes (1993). Due to harmonic decoupling in the deshoaling area, wave energy is redistributed over several other harmonics. As wave breaking takes place on top of the submerged breakwater, the total energy is scaled down, resulting in the smaller wave height found after propagation through this part of the domain.

Tab. 6.1.: The RMSE values of the model results of the experiment by Ma et al. (2017). Values are obtained with output of the WCS method. Note that the skewness and asymmetry have no unit, whereas the wave height has a unit of m.

	Skewness	Asymmetry	Wave height
Current	0.187	0.118	0.100
No current	0.455	0.089	0.132

Tab. 6.2.: The model skill scores of the WCS method for the experiment by Ma et al. (2017). The baseline predictions were the no current model results of the present SWASH release.

Skewness	Asymmetry	Wave height
0.59	-0.33	0.24

6.3.6 Model performance

The final model results are shown in Figure 6.3. The model performances was assessed with the use of the RMSE and model skill scores, see Tables 6.1 and 6.2. The RMSE values are substantial in comparison to the values in the domain. This is most likely due to the presence of the wiggles. As was described in the previous section, the model results of the no current case resulted in more accurate asymmetry profiles. The model skill score is negative, which implies that the new SWASH model produces poorer results. The wave height was modelled more accurate with the new SWASH model, as the skill score was positive.

As the statistical properties of the measurements are not known, it is rather difficult to compare measurements and model results at these highly fluctuating parts of the domain. In general, the question is whether the model shows good agreements with data due to the seemingly chaotic nature of model results. As these wiggles are quite substantial and experimental data seems to highly vary over short distances, conclusions on the comparisons between model results and measurements could be biased.

6.4 Conclusion

From this chapter, the following conclusions are drawn:

- The trend of the model results of the experimental data by Ma et al. (2017) was modelled fairly accurate. The trend of the skewness, asymmetry and wave height profiles over the domain closely matched that of the measurements.
- The wave height was overestimated in the deshoaling zone and right part of the domain. This suggests that the model underestimated the breaking of waves on top of the submerged breakwater.
- Comparisons between a current and no current case showed that due to the presence of the current, model results were more accurate compared to experimental data. This was apparent in the wave height evolution over the domain. Model skill scores for the skewness and wave height were positive. Surprisingly, the skill score for the asymmetry was negative, thus better results were obtained without currents.
- Wiggles with substantial sizes were present in the model results. Consequently, conclusions regarding differences in magnitude were difficult to make. Furthermore, the wiggles introduce a certain bias in the model performance.

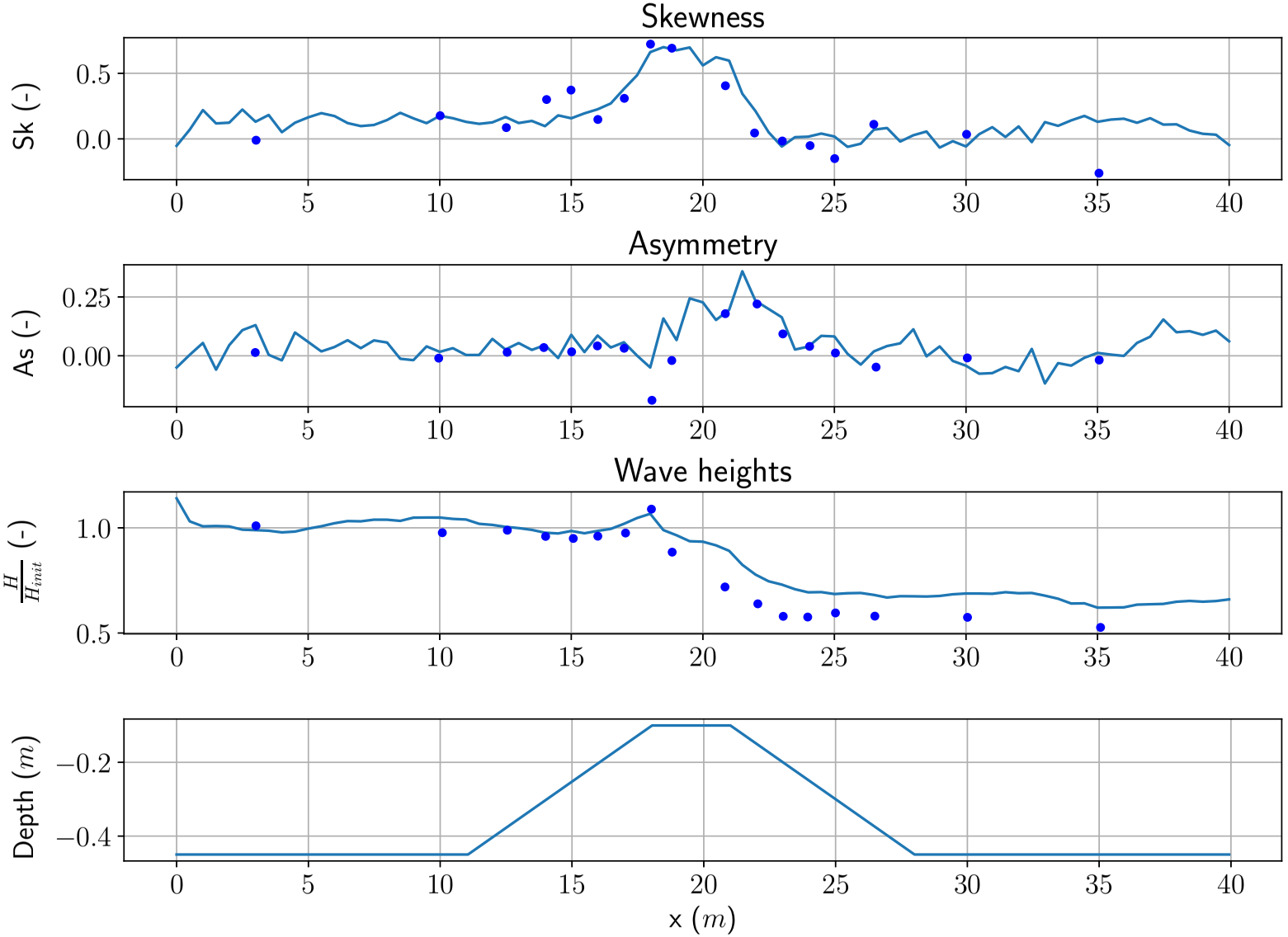

Fig. 6.3.: Skewness, asymmetry and wave height profiles over the domain based on model results are compared with measurements by Ma et al. (2017).

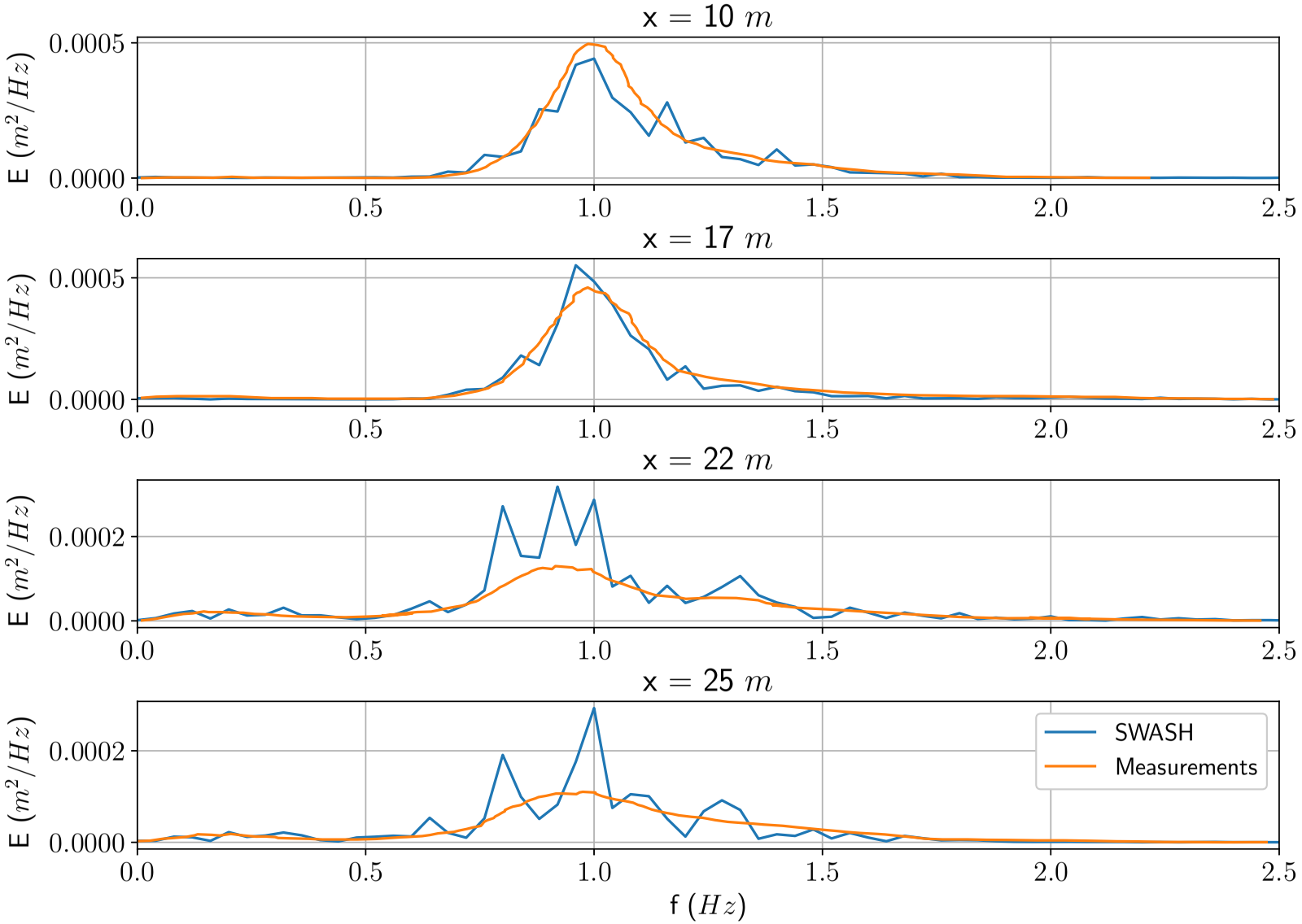

Fig. 6.4.: Wave spectra at four locations are compared with measurements by Ma et al. (2017).

7 Discussion

7.1 Accuracy of numerical schemes for combined wave-current flow

As explained in Chapter 3, initial model results of a uniform bathymetry with default SWASH settings demonstrated a significant decrease (increase) of the wave height in the presence of opposing (following) currents. A simplified test model revealed the two main causes of these effects. The first was the discretization of the water depth with the upwind scheme. For current- and wave-only simulations, this discretization in SWASH is accurate and robust. However, the upwind scheme for the discretization of the water depth does not work in the case of combined wave-current flow. The second case was the discretization of the horizontal advection in the horizontal momentum equation. In the default SWASH settings, a BDF scheme is used, which is a higher order upwind scheme. Results showed that for both opposing and following currents, this scheme led to a decrease of the wave height over the domain. However, these two causes are not independent from each other, as both suggest that central difference schemes should be used for combined wave-current flow. Moreover, energy conservation seems to be part of it.

Theoretically, it can be proven that for energy conservation, a numerical scheme should have a skew symmetric matrix. For simplicity, we assume the following convection equation:

$$\frac{\partial c}{\partial t} + u\frac{\partial c}{\partial x} = 0, \tag{7.1}$$

where c is an undefined disturbance and u is the velocity of c. Using the central difference scheme for the spatial discretization, we can rewrite the result in the following form:

$$\frac{\partial \vec{c}}{\partial t} = A\vec{c}, \tag{7.2}$$

where A is a discretization matrix. A is a real skew symmetric matrix, thus the property $A = -A^T$ holds. As a result, the nonzero eigenvalues of this matrix are all imaginary, meaning that the system is undamped and thus energy is conserved. Therefore, kinetic energy conservation can usually be achieved by using a discrete approximation for the skew-symmetric form of the advection term. For incompressible flows, this amounts to be the application of the central difference scheme in space and the Crank-Nicolson time integration (Morinishi et al., 1998; Verstappen and Veldman, 2003). Conservation of kinetic energy can be an attractive property as it assures an unconditionally stable discretization. Discretizations with improved conservation properties by mimicking certain physical or mathematical properties (e.g. skew-symmetry of the advection operator) are called mimetic discretizations. Mimetic schemes were implemented in SWASH and test simulations provided satisfying results. However, for certain numerical settings, the model results became unstable or showed a decrease or increase of the wave height over the domain. The time step was identified as one of the important settings for stability. Even for cases where the CFL criterion was met, results were unstable. One cause is the fact that the SWASH model suffers from time splitting errors. As a result, energy conservation is not guaranteed, and hence, wave heights can increase or decrease.

Energy losses or gains in combined wave-current flow simulations can be avoided with the central difference scheme. Correspondingly, this scheme should be used for the discretization of the water

depth and advective terms. In this research, this solution was applied to obtain accurate model output. Note that the applied scheme for time integration is leapfrog, which is not mimetic. Consequently, time steps were significantly small. However, the wave height evolution remained stable and thus, energy conservation was valid.

It remains unknown why the application of the mimetic discretizations is a prerequisite. Furthermore, it is unclear how these discretizations are physically related to combined wave-current flows. To the author's best knowledge, the described effects due to the use of an upwind scheme are not reported in previous research. This indicates that models, such as SWASH, inherently possess this issue. In this research, the pragmatic solution is innovative, but not the best answer due to several issues. For instance, in SWASH, the upwind scheme allows the use of an easy drying and flooding algorithm. Moreover, the time step will be significantly larger than for the central difference scheme, resulting in less computational effort. Consequently, a solution for this issue should be pursued.

7.2 Influence of numerical schemes on model results

The importance of the discretization of the water depth and the horizontal advection in the horizontal momentum was a relatively new founding during this study. All the cases in this study were previously modelled with default SWASH settings, which led to the increase and decrease of the wave height as described in Chapter B.

In comparison to the old model, i.e. the WCS method with default SWASH settings for numerical schemes, the new model is capable of modelling the wave height more accurately. However, it is not exactly clear whether the vertical flow structure is modelled sufficiently (see Chapter 5). Results with the old model were more accurate (see Section G.1). Although the results of both models are similar at the wave maker boundary, significant differences are found at the measuring position of Klopman (1994). Generally, the old model produces better results of the vertical structure of the flow.

However, no significant differences in model results of the experiment by Ma et al. (2017) were found for the different SWASH models. In the old model (see Section G.2), the wave height was modelled fairly accurate. The trend of the model results is approximately the same for the new model (see Figure 6.3). The differences in skewness and asymmetry are less visible due to the presence of wiggles. The skill scores were approximately the same for all three parameters, which suggests that both old and new model produced comparable skewness, asymmetry and wave height profiles in terms of accuracy. This does not necessarily mean that the results are the exact same.

In general, the model results imply that the use of numerical schemes might have considerable influence on the model results of combined wave-current flow. It remains an open question whether the gain in modelling accuracy of the wave height is worth more than the decrease in modelling accuracy of the vertical structure of the flow. However, as SWASH is capable of modelling either one, it is obvious that there is a possible chance that SWASH can produce accurate results.

7.3 Modelling approach between current-only, wave-only and combined wave-current flow

The modelling of combined wave-current flow was simplified in this research with the implementation of the WCS method. In general, a different view should be used when modelling combined wave-current flow in comparison to current- and wave-only flows. One important aspect is the spatial discretization, especially the horizontal discretization. Models that only simulate waves do not account for the change in wave length that a wave undergoes in combined wave-current flow. In the case of following currents, the number of gridcells per wave length increases. Inversely, the number of gridcells per wave length decreases in the case of opposing currents. It is important that this effect is taken into account, as proper representation of the wave characteristics is important. For this purpose,

a general framework was presented for modelling combined wave-current flow in the newly extended SWASH model.

It remains difficult to determine what proper rules of thumb are for modelling combined wave-current flow. The spatial discretization is limited, as a relatively high number of gridcells per wave length leads to unstable results. Furthermore, time steps are already low, thus computational time might be significant for simulations of small scale processes. For instance, wave blocking is an interesting phenomenon that can be studied with the new SWASH model. However, due to the restrictions in the grid size and time step, it remains doubtful whether results of the appropriate scale can be obtained.

In general, reliable and high resolution experimental data is scarce, especially for combined wave-current flow. What is more hindering, is the fact that in the present modelling approach, most experiments were approximated as 2DV. However, Dingemans et al. (1996) and Groeneweg and Battjes (2003) suggest that 3D effects are important for the velocity profiles in combined wave-current flow. Consequently, the mismatch in model results and measurements is most likely a combination of hee negligence of the aforementioned 3D effects and a general modelling issue in SWASH.

8 Conclusion and recommendations

8.1 Conclusion

The main goal of this research was to assess whether SWASH is capable of modelling combined wave-current flow for uniform and non-uniform bathymetries in 2DV for opposing and following currents. Based on the findings in this research, it can be concluded that SWASH is to some extent suited for modelling combined wave-current flow.

The bathymetry is important, as it determines to a large extent how the wave is affected by the flow. For uniform bathymetries, the wave has a different wave length compared to still water. For non-uniform bathymetries, the wave length changes. This is mainly determined by the extent of the domain over which the difference in bathymetry is present. Moreover, the velocity of the current is important for both bathymetry types. For instance, if the velocity of an opposing current is too high, blocking of the waves might take place. Therefore, bathymetry and the velocity of the current determine how the waveform changes.

A new method, the WCS method, was implemented to facilitate modelling combined wave-current flow. Furthermore, new implementations in numerical schemes were executed for accurate modelling of combined wave-current flow. The model results indicated that the wave height evolution is fairly accurate for uniform and non-uniform bathymetries. The wave heights in the case of opposing currents demonstrate correct magnitudes, whereas wave heights in the presence of following currents are in general underestimated. For both currents, the imposed wave height was approximately constant over the domain.

Validation results of the uniform bathymetry case showed that SWASH is not capable of modelling the vertical shear in the upper part of the water column. Mildly accurate results were obtained at the wave maker boundary, but results became worse when the combined flow propagated through the domain. However, the shape of the vertical shear is subtly present. This is promising, as an improved model might give useful insights into the theoretical explanation of the vertical shear (Groeneweg and Battjes, 2003). Furthermore, validation results of the non-uniform bathymetry case showed that SWASH is fairly accurate in modelling the changes in the waveform. This means that SWASH might be used as a tool to better understand the physical processes in chaotic environments, such as wave blocking in combined wave current flow (Chawla and Kirby, 1999, 2002).

However, some uncertainties remain in the model results. It is still not fully clear why the use of mimetic discretizations is necessary for modelling combined wave-current flow and how it is physically linked. The use of upwind schemes for the discretization of the water depth and horizontal advection in the horizontal momentum equation leads to significantly poorer model results. Moreover, it is not understood yet why the results of the vertical flow structure in combined wave-current flow is substantially different for varying number of layers. This suggests that effects at the bottom are not modelled correctly or modelling of turbulence is not correct for the entire water column. These are some of the issues that need to be solved before SWASH becomes fully robust in modelling combined wave-current flow.

8.2 Recommendations

Recommendations for future research topics are summarized here. A distinction is made between the numerical schemes, the WCS method and the general SWASH model:

8.2.1 Numerical schemes

- The use of upwind schemes for modelling combined wave-current flow is not working in the present implementation. Although model results were stable, the accuracy was low. No previous research is reported on this. It is advised to perform an analysis to determine the cause of this behaviour.
- It was found that the use of the central difference scheme significantly improves the accuracy of modelled results. Interestingly, the model results still suggest the presence of a minimal increase or decrease of the wave height. It is recommended to analyse the SWASH source code to locate areas in the code where conflicts might arise between wave-only and combined wave-current flow, i.e. upwind schemes are used.
- Although the use of the central difference scheme for certain discretizations proved to be a useful and pragmatic solution, doubts remain regarding the modelling results of the vertical structure of the flow. To minimize errors, a systematic analysis of the effects on the vertical structure of the flow should be made to determine the cause of this behaviour.

8.2.2 WCS method

The WCS method proved to be a useful implementation in the present SWASH model. However, there are some areas for improvement.

- The WCS method is implemented for waves according to linear wave theory. However, for experiments with non-linear waves, such as Klopman (1994), the WCS method could not be used. Due to this restriction, only linear waves could be imposed in this research for combined wave-current flow. It is recommended to extend the WCS method to also include the modelling of non-linear waves.
- If the WCS method is suitable for modelling of non-equidistant layers, modelling wave boundary layers and waves with relatively large kd values is possible.
- Frictional effects in the presence of currents were modelled poorly in the new model. It is recommended to find solutions for this issue, as present research in combined wave-current flow is mostly focused on unravelling more about the wave-current boundary layer (Davies, 2018).
- Since the WCS method is developed for a one-dimensional horizontal domain, three-dimensional effects are neglected. Previous research has demonstrated the importance of the lateral boundaries in these types of flows (Dingemans et al., 1996), thus a proper follow-up would be to extend the WCS method to 3D domains. An effort was made but more research is needed, see Appendix D.4.

8.2.3 SWASH

- The $k-\epsilon$ model was improved during this research, however, many doubts remain. When the amount of vertical layers was increased, generated viscosity profiles with the turbulence model were inaccurate. As there is no initial turbulent kinetic energy profile at the inlet boundary, currents are significantly altered at the start of the domain. It is recommended to analyse model results and improve the present $k-\epsilon$ model in SWASH.
- The present sponge layer technique in SWASH is not suitable for combined wave-current flow. It is recommended to develop a new method that can take into account the water level gradient that results from combined wave-current flow simulations. One option would be to determine a mean water level over the width of the sponge layer. This line can subsequently be used as the

values to which surface elevations and velocities should be dampened to. Another option is to consider sponge layer techniques from previous research (e.g. Zhang et al., 2014).

- SWASH is not capable of modelling non-linear waves. This forces users to generate their own time-series and potential errors can be made. It is, therefore, recommended to implement the option to impose non-linear waves in SWASH. Automation leads to less mistakes by the user. Furthermore, the WCS method can be extended to also allow the imposition of non-linear waves in combined wave-current flow.

Bibliography

Bakker, W. T. & van Doorn, T. (1978). Near-bottom velocities in waves with a current. In *Coastal Engineering 1978* (pp. 1394–1413).

Beji, S. & Battjes, J. A. (1993). Experimental investigation of wave propagation over a bar. *Coastal Engineering*, *19*(1), 151–162.

Bijker, E. (1967). The increase of bed shear in a current due to wave action. In *Coastal Engineering 1966* (pp. 746–765).

Bijker, E. (1992). Mechanics of sediment transport by the combination of waves and current. *Design and Reliability of Coastal Structures, short course during the 23rd ICCE in Venice*.

Blayo, E. & Debreu, L. (2005). Revisiting open boundary conditions from the point of view of characteristic variables. *Ocean Modelling*, *9*(3), 231–252.

Booij, N., Ris, R. & Holthuijsen, L. H. (1999). A third-generation wave model for coastal regions: 1. model description and validation. *Journal of Geophysical Research: Oceans*, *104*(C4), 7649–7666.

Bosboom, J., Reniers, A. & Luijendijk, A. (2014). On the perception of morphodynamic model skill. *Coastal Engineering*, *94*, 112–125.

Briggs, M. J. & Smith, J. M. (1990). The Effect of Wave Directionality on Nearshore Waves. In *Coastal engineering 1990* (pp. 267–280).

Briggs, M. J., Demirbilek, Z. & Green, D. R. (1997). Wave-current interaction in inlets. In *Coastal Engineering 1996* (pp. 1219–1232).

Caruana, R. & Niculescu-Mizil, A. (2006). An Empirical Comparison of Supervised Learning Algorithms. In *Proceedings of the 23rd international conference on machine learning* (pp. 161–168). ICML '06. Pittsburgh, Pennsylvania, USA: ACM.

Chapman, S. J. (2003). *Fortran 90/95 for scientists and engineers*. McGraw-Hill, Inc.

Chawla, A. & Kirby, J. T. (1999). Experimental study of wave breaking and blocking on opposing currents. In *Coastal Engineering 1998* (pp. 759–772).

Chawla, A. & Kirby, J. T. (2002). Monochromatic and random wave breaking at blocking points. *Journal of Geophysical Research: Oceans*, *107*(C7).

Chen, Q., Madsen, P. A., Schäffer, H. A. & Basco, D. R. (1998). Wave-current interaction based on an enhanced Boussinesq approach. *Coastal Engineering*, *33*(1), 11–39.

Chen, Q., Kirby, J. T., Dalrymple, R. A., Shi, F. & Thornton, E. B. (2003). Boussinesq modeling of longshore currents. *Journal of Geophysical Research: Oceans*, *108*(C11).

Christoffersen, J. B. & Jonsson, I. G. (1985). Bed friction and dissipation in a combined current and wave motion. *Ocean Engineering*, *12*(5), 387–423.

Craik, A. D. D. & Leibovich, S. (1976). A rational model for Langmuir circulations. *Journal of Fluid Mechanics*, *73*(3), 401–426.

Davies, A. (2018). A model of the vertical structure of the wave and current bottom boundary layer. In *Modeling marine systems* (pp. 263–297). CRC Press.

de Wit, F. (2016). *Tide-induced currents in a phase-resolving wave model* (Master's thesis, Delft University of Technology).

de Wit, F., Tissier, M., Reniers, A., Aagaard, T., Deigaard, R. & Fuhrman, D. (2017). Including tidal currents in a wave-resolving model.

Dean, R. G. (1990). Freak Waves: A Possible Explanation. In A. Tørum & O. T. Gudmestad (Eds.), *Water Wave Kinematics* (pp. 609–612).

Dingemans, M., van Kester, J., Radder, A. & Uittenbogaard, R. (1996). The Effect of the CL-Vortex Force in 3D Wave-Current Interaction. In *Coastal engineering 1996* (pp. 4821–4832).

Dobrochinski, J. P. (2014). *A combination of swash and harberth to compute wave forces on moored ships* (Master's thesis, Delft University of Technology).

Dodet, G., Bertin, X., Bruneau, N., Fortunato, A. B., Nahon, A. & Roland, A. (2013). Wave-current interactions in a wave-dominated tidal inlet. *Journal of Geophysical Research: Oceans*, *118*(3), 1587–1605.

Dong, G., Chen, H. & Ma, Y. (2014). Parameterization of nonlinear shallow water waves over sloping bottoms. *Coastal Engineering*, *94*, 23–32.

Drost, E. J., Lowe, R. J., Ivey, G. N. & Jones, N. L. (2018). Wave-current interactions in the continental shelf bottom boundary layer of the australian north west shelf during tropical cyclone conditions. *Continental Shelf Research*, *165*, 78–92.

Edwards, T. S. (2007). Effects of aliasing on numerical integration. *Mechanical Systems and Signal Processing*, *21*(1), 165–176.

Elgar, S. (1987). Relationships involving third moments and bispectra of a harmonic process. *IEEE transactions on acoustics, speech, and signal processing*, *35*(12), 1725–1726.

Elias, E., Cleveringa, J., Buijsman, M., Roelvink, J. & Stive, M. (2006). Field and model data analysis of sand transport patterns in Texel Tidal inlet (the Netherlands). *Coastal Engineering*, *53*(3), 505–529.

Euvé, L.-P., Michel, F., Parentani, R. & Rousseaux, G. (2015). Wave blocking and partial transmission in subcritical flows over an obstacle. *Physical Review D*, *91*(2), 024020.

Falnes, J. (2007). A review of wave-energy extraction. *Marine Structures*, *20*(4), 185–201.

Fenton, J. (1985). A fifth-order Stokes theory for steady waves. *Journal of Waterway, Port, Coastal, and Ocean Engineering*, *111*(2), 216–234.

Fenton, J. (1988). The numerical solution of steady water wave problems. *Computers & Geosciences*, *14*(3), 357–368.

Fenton, J. & McKee, W. (1990). On calculating the lengths of water waves. *Coastal Engineering*, *14*(6), 499–513.

Fernando, P. C., Guo, J. & Lin, P. (2011). Wave-current interaction at an angle 1: Experiment. *Journal of Hydraulic Research*, *49*(4), 424–436.

Grant, W. D. & Madsen, O. S. (1979). Combined wave and current interaction with a rough bottom. *Journal of Geophysical Research: Oceans*, *84*(C4), 1797–1808.

Groeneweg, J. (1999). *Wave-current interactions in a generalized Lagrangian mean formulation* (Doctoral dissertation, TU Delft, Delft University of Technology).

Groeneweg, J. & Battjes, J. A. (2003). Three-dimensional wave effects on a steady current. *Journal of Fluid Mechanics*, *478*, 325–343.

Guillas, S., Glover, N. & Malki-Epshtein, L. (2014). Bayesian calibration of the constants of the k-lol turbulence model for a CFD model of street canyon flow. *Computer Methods in Applied Mechanics and Engineering*, *279*, 536–553.

Hansen, W. (1956). Theorie zur Errechnung des Wasserstandes und der Strömungen in Randmeeren nebst Anwendungen1. *Tellus*, *8*(3), 287–300.

Hasselmann, K., Barnett, T., Bouws, E., Carlson, H., Cartwright, D., Enke, K., ... Kruseman, P. et al. (1973). Measurements of wind-wave growth and swell decay during the Joint North Sea Wave Project (JONSWAP). *Ergänzungsheft 8-12*.

Hedges, T. (1987). Combinations of waves and currents: An introduction. *Proc Inst Civ Eng*, *82*, 567–585.

Hjelmervik, K. B. & Trulsen, K. (2009). Freak wave statistics on collinear currents. *Journal of Fluid Mechanics*, *637*, 267–284.

Holloway, J. L. (1958). Smoothing and Filtering of Time Series and Space Fields. In H. Landsberg & J. van Mieghem (Eds.), (Vol. 4, pp. 351–389). Advances in Geophysics.

Hughes, S. A. (1984). *The TMA shallow-water spectrum description and applications*. Coastal Engineering Research Center Vicksburg MS.

Jonsson, I. G., Skougaard, C. & Wang, J. D. (1970). Interaction between waves and currents. In *Coastal Engineering 1970* (pp. 489–507).

Kemp, P. & Simons, R. (1982). The interaction between waves and a turbulent current: Waves propagating with the current. *Journal of Fluid Mechanics*, *116*, 227–250.

Kemp, P. & Simons, R. (1983). The interaction of waves and a turbulent current: Waves propagating against the current. *Journal of Fluid Mechanics*, *130*, 73–89.

Klopman, G. (1992). Vertical structure of the flow due to waves and currents. *Progress Rep. No. H840. 30, Part I, Delft Hydraulics*.

Klopman, G. (1994). Vertical structure of the flow due to waves and currents. *Progress Rep. No. H840. 30, Part II, Delft Hydraulics, prepared for Rijkwaterstaat, Tidal WaterDivision and Commission of the European Communities*.

Klopman, G. & van Leeuwen, P. (1990). An Efficient Method for the Reproduction of Non-Linear Random Waves. In *Coastal Engineering 1990*.

Lai, R. J., Long, S. R. & Huang, N. E. (1989). Laboratory studies of wave-current interaction: Kinematics of the strong interaction. *Journal of Geophysical Research: Oceans*, *94*(C11), 16201–16214.

Larsen, B. E. & Fuhrman, D. R. (2018). On the over-production of turbulence beneath surface waves in Reynolds-averaged Navier–Stokes models. *Journal of Fluid Mechanics*, *853*, 419–460.

Launder, B. & Spalding, D. (1974). The numerical computation of turbulent flows. *Computer Methods in Applied Mechanics and Engineering*, *3*(2), 269–289.

Lavrenov, I. & Porubov, A. (2006). Three reasons for freak wave generation in the non-uniform current. *European Journal of Mechanics - B/Fluids*, *25*(5), 574–585. Rogue waves.

Li, C. W. & Yan, K. (2007). Numerical investigation of wave-current-vegetation interaction. *Journal of Hydraulic Engineering*, *133*(7), 794–803.

Li, Y. & Lin, M. (2010). Hydrodynamic coefficients induced by waves and currents for submerged circular cylinder. *Procedia Engineering*, *4*, 253–261. ISAB-2010.

Longuet-Higgins, M. S. & Stewart, R. W. (1960). Changes in the form of short gravity waves on long waves and tidal currents. *Journal of Fluid Mechanics*, *8*(4), 565–583.

Longuet-Higgins, M. S. & Stewart, R. W. (1961). The changes in amplitude of short gravity waves on steady non-uniform currents. *Journal of Fluid Mechanics*, *10*(4), 529–549.

Lu, Y., Li, S., Zuo, L., Liu, H. & Roelvink, J. (2015). Advances in sediment transport under combined action of waves and currents. *International Journal of Sediment Research*, *30*(4), 351–360.

Ma, X., Ma, Y., Gao, Y. & Dong, G. (2017). Numerical analysis of the nonlinear parameterization of waves in currents over a submerged sill with a non-hydrostatic model. *Journal of Ocean University of China*, *16*(4), 689–696.

Mayer, S., Garapon, A. & Sørensen, L. S. (1998). A fractional step method for unsteady free-surface flow with applications to non-linear wave dynamics. *International Journal for Numerical Methods in Fluids*, *28*(2), 293–315.

Morinishi, Y., Lund, T., Vasilyev, O. & Moin, P. (1998). Fully conservative higher order finite difference schemes for incompressible flow. *Journal of Computational Physics*, *143*(1), 90–124.

Nezu, I. & Rodi, W. (1986). Open-channel flow measurements with a laser Doppler anemometer. *Journal of Hydraulic Engineering*, *112*(5), 335–355.

Nieuwstadt, F. T., Westerweel, J. & Boersma, B. J. (2016). *Turbulence: Introduction to theory and applications of turbulent flows*. Springer.

Peregrine, D. (1976). Interaction of water waves and currents. In *Advances in Applied Mechanics* (Vol. 16, pp. 9–117). Elsevier.

Pierson Jr., W. J. & Moskowitz, L. (1964). A proposed spectral form for fully developed wind seas based on the similarity theory of SA Kitaigorodskii. *Journal of Geophysical Research*, *69*(24), 5181–5190.

Reniers, A., MacMahan, J., Thornton, E. & Stanton, T. (2006). Modelling infragravity motions on a rip-channel beach. *Coastal Engineering*, *53*(2), 209–222. Coastal Hydrodynamics and Morphodynamics.

Richards, P. & Norris, S. (2011). Appropriate boundary conditions for computational wind engineering models revisited. *Journal of Wind Engineering and Industrial Aerodynamics*, *99*(4), 257–266.

Rienecker, M. & Fenton, J. (1981). A Fourier approximation method for steady water waves. *Journal of Fluid Mechanics*, *104*, 119–137.

Rijnsdorp, D. P., Smit, P. B. & Zijlema, M. (2014). Non-hydrostatic modelling of infragravity waves under laboratory conditions. *Coastal Engineering*, *85*, 30–42.

Romero, L., Lenain, L. & Melville, W. K. (2017). Observations of surface wave–current interaction. *Journal of Physical Oceanography*, *47*(3), 615–632.

Ruessink, B., Miles, J., Feddersen, F., Guza, R. & Elgar, S. (2001). Modeling the alongshore current on barred beaches. *Journal of Geophysical Research: Oceans*, *106*(C10), 22451–22463.

Schützhold, R. & Unruh, W. G. (2002). Gravity wave analogues of black holes. *Physical Review D*, *66*(4), 044019.

Shyu, J.-H. & Phillips, O. (1990). The blockage of gravity and capillary waves by longer waves and currents. *Journal of Fluid Mechanics*, *217*, 115–141.

Smith, J. M. & Vincent, C. L. (1992). Shoaling and Decay of Two Wave Trains on Beach. *Journal of Waterway, Port, Coastal, and Ocean Engineering*, *118*(5), 517–533.

Soulsby, R., Hamm, L., Klopman, G., Myrhaug, D., Simons, R. & Thomas, G. (1993). Wave-current interaction within and outside the bottom boundary layer. *Coastal Engineering*, *21*(1-3), 41–69.

Stelling, G. & Duinmeijer, S. P. A. (2003). A staggered conservative scheme for every froude number in rapidly varied shallow water flows. *International Journal for Numerical Methods in Fluids*, *43*(12), 1329–1354.

Stelling, G. & Zijlema, M. (2003). An accurate and efficient finite-difference algorithm for non-hydrostatic free-surface flow with application to wave propagation. *International Journal for Numerical Methods in Fluids*, *43*(1), 1–23.

Stiassnie, M. & Dagan, G. (1979). Partial reflexion of water waves by non-uniform adverse currents. *Journal of Fluid Mechanics*, *92*(1), 119–129.

Stokes, G. G. (1847). On the theory of oscillatory waves. *Trans. Camb. Phil. Soc. 8*, 441–445.

Sutherland, J., Peet, A. & Soulsby, R. (2004). Evaluating the performance of morphological models. *Coastal Engineering*, *51*(8), 917–939. Coastal Morphodynamic Modeling.

Sutskever, I., Vinyals, O. & Le, Q. V. (2014). Sequence to Sequence Learning with Neural Networks. In Z. Ghahramani, M. Welling, C. Cortes, N. D. Lawrence & K. Q. Weinberger (Eds.), *Advances in neural information processing systems 27* (pp. 3104–3112). Curran Associates, Inc.

The SWASH team. (2018). *SWASH user manual*. Version 5.01. Delft University of Technology.

Trulsen, K. & Mei, C. (1993). Double reflection of capillary/gravity waves by a non-uniform current: A boundary-layer theory. *Journal of Fluid Mechanics*, *251*, 239–271.

Umeyama, M. (2005). Reynolds Stresses and Velocity Distributions in a Wave-Current Coexisting Environment. *Journal of Waterway, Port, Coastal, and Ocean Engineering*, *131*(5), 203–212.

Ursell, F. (1953). The long-wave paradox in the theory of gravity waves. In *Mathematical Proceedings of the Cambridge Philosophical Society* (Vol. 49, *4*, pp. 685–694). Cambridge University Press.

van der Boog, C. (2015). *Ripple Predictor in SWASH* (Additional Thesis, Delft University of Technology).

van Rijn, L. C. & Havinga, F. J. (1995). Transport of fine sands by currents and waves. II. *Journal of Waterway, Port, Coastal, and Ocean Engineering*, *121*(2), 123–133.

van Rijn, L. C., Nieuwjaar, M. W. C., van der Kaay, T., Nap, E. & van Kampen, A. (1993). Transport of fine sands by currents and waves. *Journal of Waterway, Port, Coastal, and Ocean Engineering*, *119*(2), 123–143.

Verstappen, R. & Veldman, A. (2003). Symmetry-preserving discretization of turbulent flow. *Journal of Computational Physics*, *187*(1), 343–368.

Wang, J., Ma, Q. & Yan, S. (2018). A fully nonlinear numerical method for modeling wave–current interactions. *Journal of Computational Physics*, *369*, 173–190.

Wolf, J. & Prandle, D. (1999). Some observations of wave-current interaction. *Coastal Engineering*, *37*(3-4), 471–485.

Wu, C. H. & Yao, A. (2004). Laboratory measurements of limiting freak waves on currents. *Journal of Geophysical Research: Oceans*, *109*(C12).

Yan, S., Ma, Q. & Adcock, T. (2010). Investigations of freak waves on uniform current. In *Proceeding of 25th international workshop on water waves and floating bodies, harbin*.

Yu, J. & Slinn, D. N. (2003). Effects of wave-current interaction on rip currents. *Journal of Geophysical Research: Oceans*, *108*(C3).

Yu, Y. Y. (1952). Breaking of waves by an opposing current. *Eos, Transactions American Geophysical Union*, *33*(1), 39–41.

Zhang, Y., Kennedy, A. B., Panda, N., Dawson, C. & Westerink, J. J. (2014). Generating–absorbing sponge layers for phase-resolving wave models. *Coastal Engineering*, *84*, 1–9.

Zijlema, M. & Stelling, G. (2005). Further experiences with computing non-hydrostatic free-surface flows involving water waves. *International Journal for Numerical Methods in Fluids*, *48*(2), 169–197.

Zijlema, M. & Stelling, G. (2008). Efficient computation of surf zone waves using the nonlinear shallow water equations with non-hydrostatic pressure. *Coastal Engineering*, *55*(10), 780–790.

Zijlema, M., Stelling, G. & Smit, P. (2011). SWASH: An operational public domain code for simulating wave fields and rapidly varied flows in coastal waters. *Coastal Engineering*, *58*(10), 992–1012.

List of Symbols

∇	Divergence operator	$-$
$_a$	Absolute (or non-moving) frame of reference	$-$
a	Wave amplitude	m
As	Asymmetry	$-$
b	Growth rate of relaxation	$-$
B_j	Coefficients in Rienecker and Fenton (1981) approximation	$-$
c	Phase velocity	m/s
C_1	Constant $k-\epsilon$ model	$-$
C_2	Constant $k-\epsilon$ model	$-$
c_f	Friction coefficient	$-$
c_g	Group velocity	m/s
$c_{g,a}$	Absolute group velocity	m/s
$c_{g,r}$	Relative group velocity	m/s
c_r	Relative phase velocity	m/s
C_μ	Constant $k-\epsilon$ model	$-$
d	Water depth	m
E	Wave energy	J/m^2
f	Wave frequency	Hz
F	Froude number	$-$
g	Gravitational acceleration	m/s^2
H	Wave height	m
H_s	Significant wave height	m
K	Amount of vertical layers	$-$
k	Turbulent kinetic energy	J/kg
k	Wave number	$1/m$
k_s	Nikuradse roughness height	m
L_D	Length of domain	m
mct	Number of time steps in (peak) wave period	$-$
mxc	Amount of grids used in x-direction	m
n	Factor group velocity	$-$
N	Wave action	Js/m^2
N_F	Amount of Fourier modes in Rienecker and Fenton (1981) approximation	$-$
p_0	Shear production	$1/kg/s$
p_h	Hydrostatic pressure	Pa
p_{nh}	Non-hydrostatic pressure	Pa
p_{tide}	Tidal pressure	Pa
p_Ω	Shear production potential flow	$1/kg/s$
q	Specific discharge	m^2/s
$_r$	Relative (or moving) frame of reference	$-$
S	Source term	J/m^2
S_{ij}	Strain rate tensor	$-$

Sk	Skewness	$-$
S_x	Radiation stress in the x-direction	J/m^2
t	Time	s
T	Wave period	s
T_{cycle}	Cycle period for spectrum	s
T_{mov}	Period for moving average	s
T_p	Peak wave period	s
U	Current velocity	m/s
u_*	Shear velocity	m/s
u	Velocity in x-direction	m/s
$\overrightarrow{u}$	Velocity vector in 3D	m/s
u_{orb}	Horizontal orbital velocity	m/s
$\overline{u}_{st}$	Stokes drift	m/s
w	Velocity in z-direction	m/s
x	Horizontal coordinate	m
z	Vertical coordinate	m
z_0	Integration constant	$-$
Δt	Time step	s
Δx	Grid size in x-direction	m
Δz	Grid size in z-direction	m
Ω_{ij}	Rotation rate tensor	$-$
α_{WCS}	Scaling constant WCS method	$-$
β	Relative distance in sponge layer	$-$
γ	Weighing function	$-$
ζ	Free surface elevation	m
η	Water level	m
κ	Von Kármán constant	$-$
λ_2	Damping coefficient	$-$
ν^h	Horizontal eddy viscosity	m^2/s
ν^v	Vertical eddy viscosity	m^2/s
ρ	Density	kg/m^3
σ	Relative wave angular frequency	rad/s
σ_k	Constant $k-\epsilon$ model	$-$
σ_ϵ	Constant $k-\epsilon$ model	$-$
τ_b	Bottom shear stress	Pa
ω	Absolute wave angular frequency	rad/s
ϵ	Rate of dissipation of turbulence energy	m^2/s^3

List of Abbreviations

1D	1 Dimensional
2D	2 Dimensional
2DH	2 Dimensional Horizontal
2DV	2 Dimensional Vertical
3D	3 Dimensional
BDF	Backward Differentiation Formula
CFL	Courant-Friedrichs-Lewy
JONSWAP	JOint North Sea WAve Project
LDV	Laser Doppler velocimetry
MUSCL	Monotonic Upwind Scheme for Conservation Laws
PM	Pierson-Moskowitz
RANS	Reynolds-averaged Navier-Stokes
RHS	Right Hand Side
RMSE	Root Mean Square Error
SWASH	Simulating WAves till SHore
TMA	Texel Marsen Arsloe
WCS	Wave in Current Scaling

List of Figures

List of Tables

SWASH source code manual

A

This chapter will provide an overview of the SWASH model source code and basic instructions regarding programming within the SWASH model. At the time of this report, SWASH 5.01A is the most recent version. Files and scripts used in the SWASH model are made clear by emphasis (e.g. *Swash.ftn90*). This simple and short manual is mainly created for students and researchers interested in understanding and modifying SWASH source code.

A.1 Implementation SWASH

SWASH is written in Fortran and freely available for download. Users can make the choice between either SWASH binaries (only for Microsoft Windows) or the SWASH source code which needs to be compiled with a Fortran compiler. With the use of the compiled executable and input files, numerical simulations can be made. For more information about the input commands, reference is made to the user manual. For more information about the compiling of the SWASH model Fortran scripts and setting up the right environment for either serial or parallel runs, reference is made to the implementation manual [1]. This manual will provide more insight about the scripts used to compile the SWASH model, since information about usage and installation is already extensive. There is, however, an overview of the compiling process available in Section A.3.8.

The advantage of SWASH being open source is that modifications in the source code can be made to include processes that have not been accounted for in the model. Although SWASH is being improved frequently, there are still limitations to the model, such as the main topic of this thesis. However, before adjusting the source code, it is advisable to understand the structure of the model itself.

An overview of the SWASH scripts and their mutual dependance is provided in Figure A.2. This flowchart only shows main program and pre/post-processing routines, thus graphs for other processes, such as compiling, will be provided if necessary.

A.2 Fortran 90

An overview of compiling and using basic commands in Fortran will be provided in this section. In case of desire for more information, the user is advised to search for more extensive (online) tutorials (e.g. Chapman, 2003).

[1] SWASH download files, user and implementation manuals can be found on http://swash.sourceforge.net/

Fig. A.1.: Colours used to distinguish Fortran units in this manual.

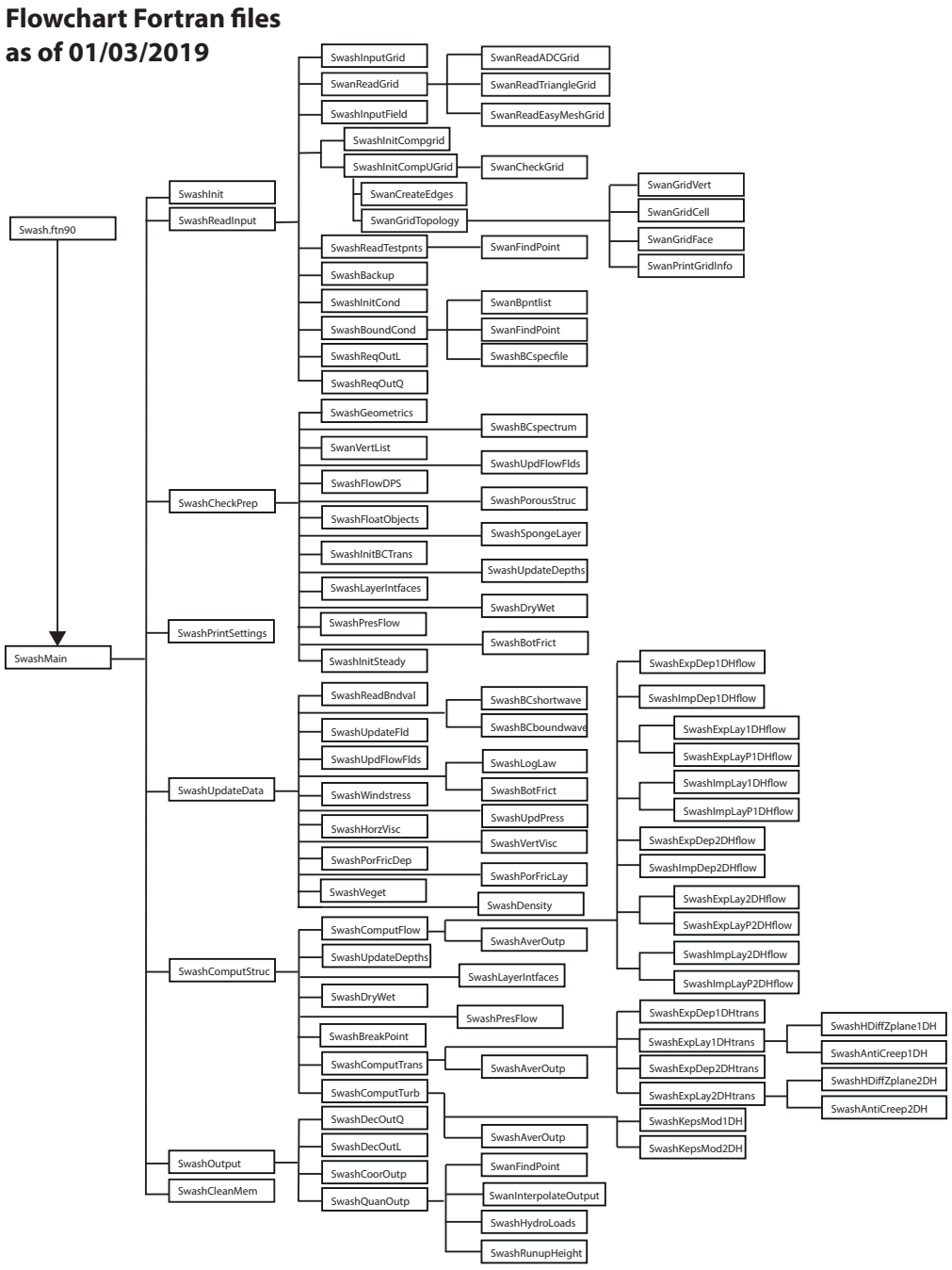

Fig. A.2.: Flowchart of the Fortran scripts used in the SWASH model. Modified version of van der Boog (2015).

A.2.1 General information Fortran

Fortran (**FOR**mula **TRAN**slation) is a high-level programming language created by the technology company IBM. Its purpose is mainly served in the scientific community. From 1957 and onwards, Fortran has provided the tools for numerical and scientific computations. Many versions of Fortran exist and SWASH is written in Fortran 90. This is important since the functionality of older or newer versions may be deprecated/not exist in Fortran 90.

The reason why Fortran is still heavily used is due to its high performance. Compared to programming languages such as Python or MATLAB, the computational time is significantly less for Fortran. This is due to the Fortran source code being compiled, whereas the code in Python or MATLAB is interpreted. Especially for array computations, the Fortran compiler performs fast. A disadvantage is that Fortran requires programming in a less user-friendly environment (compiling and running executable) and tasks other than computations (e.g. graphs) might reduce its advantage in computational time. It is advised to use Fortran output together with Python or MATLAB for visualisations.

For more information regarding programming in Fortran, reference is made to the SWAN programming manual[2], of which the rules are also applicable to SWASH, and Chapman (2003).

A.2.2 Fortran setup

Programming with Fortran starts with the use of the environment in which the scripts are written. Fortran can be written in many editors. Examples are Notepad++, Microsoft Visual Studio, Code::Blocks or VIM. The choice depends on the preferences of the user, but it is advised for beginners to use editors with themes in which the code is coloured in order to show dependencies.

A Fortran script needs to be compiled for usage. Compiling results in an executable that can be used to output results. An example will be given in the following section. In order to compile, the user needs a Fortran compiler. There are several compilers available, of which the Intel Compiler (free for non-commercial, personal use) and G95 compilers are highly recommended. More information can be found in the SWASH implementation manual.

A.2.3 Fortran basics

Programming the SWASH model needs to be done in a logical and clear manner since scripts and codes will be used and understood by multiple users. Fortran provides the fundamental architecture in order to achieve this. In Fortran, the main unit in programming is the so called *program*. Therefore, each programming work in Fortran is done first by declaring *program*. Important to remember is that such declarations also need to be ended, thus a typical Fortran script will start with the declaration of *program* and at the end of the script, *program* will be ended with *end program*.

In case of numerical models such as SWASH, writing all code in one script is not only very difficult but also prone to mistakes and non-efficient programming. Fortran provides more units next to *program*, such as *function* or *subroutine*, in order to divide the code in blocks. When it is e.g. desired to calculate the abc-formula multiple times in the main script, a *function* can be written externally (independent of the main script) and used multiple times without repeating the entire code in the main script.

A.3 SWASH source code

Following the layout provided in Figure A.2 and SWASH implementation manual, in this section the Fortran scripts used in the SWASH model will be explained with respect to their function. The interplay between subroutines and the main program is highlighted and the use of functions is shown. For more information about other variables, reference is made to the scripts themselves. For general purposes, a section on the compiling process of SWASH is provided.

[2] http://swanmodel.sourceforge.net/

A.3.1 General modules

The main functions used for computations and programming purposes are stored in the general SWASH modules. There are three general modules: *ocpmod.ftn90*, *SwashModule1.ftn90* and *SwashModule2.ftn90*.

ocpmod.ftn90

In this general module, four modules are stored, namely *OCPCOMM1*, *OCPCOMM2*, *OCPCOMM3* and *OCPCOMM4*. These modules are used by the Ocean Pack Service Routines and SWAN, and they are directly used in SWASH. They contain common variables that are used in multiple other scripts in SWASH. An example is *OCPCOMM3* which defines the mesh size and number of grid points in the computational domain for output. This module is as a result used in *SwashCoorOutp.ftn90*.

SwashModule1.ftn90

This module contains again common variables that are widely used in the SWASH related scripts. There are five modules, namely *SwashCommdata1*, *SwashCommdata2*, *SwashCommdata3*, *SwashCommdata4* and *SwashTimecomm*. These modules define variables such as the units of some of the physical parameters as well as the physical parameters themselves, the input grid sizes and time related parameters.

SwashModule2.ftn90

SwashModule2.ftn90 contains with respect to *SwashModule1.ftn90* variables that are allocatable. In Fortran, variables need to be defined explicitly. There is no requirement with respect to the size of the variables if the data is static. However, for dynamic arrays that have different sizes depending on the use of the program, Fortran allows the use of the allocatable argument. With this functionality, dynamic arrays only need to be defined in their rank. When these arrays need to be used in a script, they are allocated with their respective size and after usage, deallocated to preserve memory size. This is a very powerful tool because e.g. in SWASH, the numerical simulation depends on the grid size and this could of course be different for multiple simulations. Thus with the use of the allocatable argument, dynamics arrays can be created linked to the input of the user.

In the *SwashModule2.ftn90* module, arrays regarding output and computations are defined, e.g. an array *kgrpnt* is created that serves as an index table with the addresses of each grid point, non-active (equal to 1) and active (larger than 1).

A.3.2 Modules for flow, solvers and MPI

SwashFlowdata.ftn90

One of the core modules in the SWASH model is *SwashFlowdata.ftn90*. This module contains data for flow computations. Users that want to modify the source code need to study this module in depth since definitions regarding the computational grid, velocity and water level points and boundary conditions are mentioned.

SwashSolvedata.ftn90

Another core module is *SwashSolvedata.ftn90*. In this module, data for solving the systems of equations is defined.

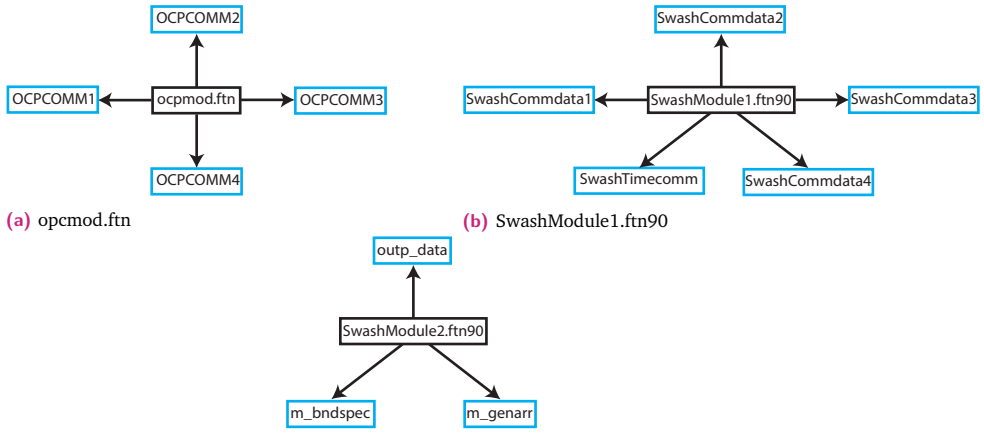

(a) opcmod.ftn

(b) SwashModule1.ftn90

(c) SwashModule1.ftn90

Fig. A.3.: Overview of modules in the general modules scripts.

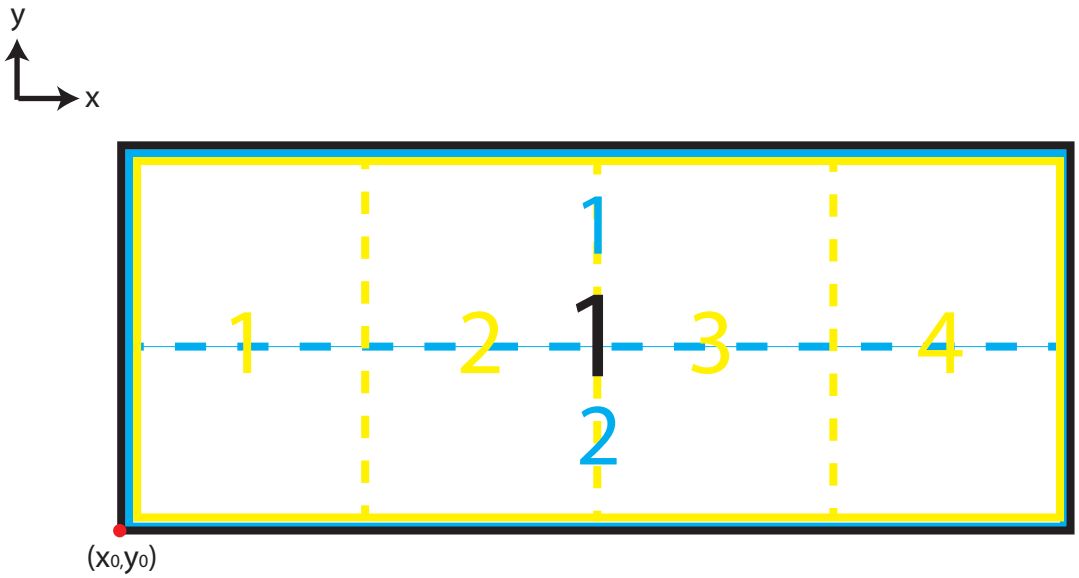

Fig. A.4.: 2DH domain divided in 1, 2 and 4 subdomains with distinct colors black, blue and yellow respectively. To make it clear, the boundaries of the domains are overlapping; the domains are the same size.

m_parall.ftn

In this module, the data regarding MPI runs is defined. One of the main features of SWASH is the possibility of performing parallel runs in order to reduce computational time. This is also known as a MPI run. A MPI run is a computation that is carried out parallel with processors of the computer used for different domains. This reduces the computational significantly. If e.g. a computation is performed on a 2DH domain, a computer with four processors could reduce the computation to four subdomains taking place simultaneously. An example is given in Figure A.4. Let us assume that for a serial run (simulation with one processor), the computation will take 24 hours (black domain). For a MPI run with 2 processors, the computational time would be reduced to 12 hours (blue subdomains). For a MPI run with 4 processors, the computational time would be 6 hours (yellow subdomains) and so forth. To ensure a MPI run SWASH needs *machinefile*, a file that contains the nodes in the user's parallel environment. Whether a split is made in the x- or y-axis is up to the user: this choice is specified in *swashinit*, which is created after running the SWASH executable for the first time (see implementation manual for more information).

swanparll.ftn

This module builds upon *m_parall.ftn* and provides 30 functions, as used in SWAN, to initiate MPI runs with SWASH. For detailed information, direct reference is made to *swanparll.ftn*.

A.3.3 Other routines

In this section, the routines other than the previous and main SWASH routines are mentioned. Table A.1 gives an overview of each file and corresponding Fortran units.

ocpmix.ftn

This file contains miscellaneous routines in the form of functions and subroutines.

ocpcre.ftn

Command reading routines are stored in this file.

ocpids.ftn

Installation routines are defined. E.g., the choices made in *swashinit* are processed within this file.

swanser.ftn

Service routines from SWAN reused in SWASH are defined in this file.

SwashServices.ftn90

Just like the previous file, this scripts stores the SWASH service routines.

A.3.4 Main program

Swash.ftn90 *Swash.ftn90* is the main script of the SWASH model (as in, *program swash* is defined in this script). In this script, the SWASH model is initialised by identifying if there will be a MPI run. Whatever the result may be, a call is made to subroutine *SwashMain*.

SwashMain.ftn90 *SwashMain.ftn90* is the master script of the SWASH model. Initialisation, pre- and post-processing and computations are performed with this script as the main hub. As described in the script itself, first a call is made to subroutine *SwashInit* in order to read and process user commands. Afterwards, *SwashCheckPrep* is called upon in order to check inputs and prepare computations. Then *SwashUpdateData* and *SwashCompute* are called for a number of time steps. Ultimately, *SwashOutput* is used to produce output. In this order, the following sections will provide information for the relevant scripts.

A.3.5 Pre-processing routines

SWASH initialisation

SwashInit.ftn90 SWASH is initialised by *SwashInit.ftn90*. Several variables and arrays used in computations are given a definition, e.g. gravitational acceleration is equal to $9.813 m/s^2$. This script also makes use of the *OCPINI* subroutine from *ocpids.ftn* to create the *swashinit* initialisation file.

Unit \ Script	swanparll.ftn		ocpmix.ftn	ocpcre.ftn	ocpids.ftn	swanser.ftn		SwashServices.ftn90	
Fortran Units	SWBLADM	SWORB	BUGFIX	EQCSTR	DTSTTI	ANGDEG	SINBTG	disprel	periodic
	SWBROADC	SWORB	COPYCH	GETKAR	DTTIST	ANGRAD	SINCMP	fluxlim	periodici
	SWBROADCD	SWPARTIT	DTINTI	IGNORE	OCDTIM	BOUNPT	SINUPT	jonswap	sigmacoor
	SWCOLBLK	SWRECVFLD	DTRETI	INCSTR	OCPINI	CHGBAS	SPRCON		
	SWCOLLECT	SWRECVNB	DTTIME	INCTIM		CVCHEK	SIRAY	SwashSolvers.ftn90	
	SWCOLOUT	SWRECVNBD	DTTIWR	INDBLE	swanout2.ftn	CVMESH	SVALQI	ave	pcg
	SWCOLTAB	SWREDUCE	EQDBLE	INKEYW	SBLKPT	DEGCNV	SVARTP	avm	pcg2
	SWDECOMP	SWREDUCI	EQREAL	ININTG	SWBLKP	EVALF	SWCOPI	avmp	sip
	SWEXCHG	SWREDUCR	FOR	ININTV	SWBLOK	GAMMAF	SWCOPR	bicgstab	tridiag
	SWEXCHGI	SWREDUCD	INAR2D	INITVD	SWRMAT	GAMMLN	SWIPOL	dac	tridiag2
	SWEXCHGD	SWSENDFLD	LSPLIT	INREAL	SWTABP	INTSTR	SWI2B	dac2	
	SWEXITMPI	SWSENDNB	MSGERR	KEYWIS		NEWTON	SWNMPS	ilu	
	SWGATHER	SWSENDNBD	REPARM	LEESEL		NEWT1D	SWPRTI	ilud	
	SWGATHERD	SWSTRIP	STPNOW	NWLINE		NUMSTR	SWR2B	iluds	
	SWINITMPI	SWSYNC	STRACE	PUTKAR		READXY	SWTSTA	ivl	
			TABHED	RDINIT		REFIXY	SWTSTO	ivu	
				UPCASE		TXPBLA	SwanInter-	newton1D	
				WRNKEY			polatePoint	newton2D	
								SwanCompdata.ftn90	
								SwanCompdata	
								SwanGridobjects.ftn90	
								SwanGridobjects	
								SwanGriddata.ftn90	
								SwanGriddata	
								SwanPointinMesh.ftn90	
								SwanPointinMesh	
								SwanThreadBounds.ftn90	
								SwanThreadBounds	

Tab. A.1.: Fortran units listed per script in alphabetical order.

SWASH input

SwashReadInput.ftn90 The next step performed in *SwashMain.ftn90* is the reading of user input. This is done according to the standard *swash.edt* file, found in the SWASH user manual. This file forms the basis for user input and according to keywords specified in this file, *SwashReadInput.ftn90* reads and processes the input. Complementary scripts are used in this script e.g. to import the input grid specified by the user. These scripts are not necessarily used in every SWASH run since they are linked to their own keyword. Nonetheless, other scripts used in *SwashReadInput.ftn90* are (in order of source code, line number included between parenthesis) *SwashInputGrid.ftn90* (1822), *SwanReadGrid.ftn90* (1886), *SwashInputField.ftn90* (1891), *SwashInitCompGrid.ftn90* (1899, 1907), *SwashInitCompUgrid.ftn90* (1916), *SwanCreateEdges.ftn90* (1918), *SwanGridTopology.ftn90* (1920), *SwashReadTestpnts.ftn90* (1978), *SwashBackup.ftn90* (1996), *SwashInitCond.ftn90* (2005), *SwashBoundCond.ftn90* (2019), *SwashReqOutL.ftn90* (2055) and *SwashReqOutQ.ftn90* (2061).

SWASH input check

SwashCheckPrep.ftn90 After input is imported, SWASH switches to *SwashCheckPrep.ftn90*. This script checks inconsistencies in the settings and makes preparations before the computation is started. When necessary, changes are made in order to ensure a stable run. The complimentary scripts used are *SwashGeometrics.ftn90* (793), *SwashBCspectrum.ftn90* (1198), *SwanVertlist.ftn90* (1361), *SwashUpdFlowFlds.ftn90* (2063), *SwashFlowDP.ftn90* (2232), *SwashPorousStruc.ftn90* (2237), *SwashFloatObjects.ftn90* (2242), *SwashSpongeLayer.ftn90* (2564), *SwashInitBCtrans.ftn90* (2589), *SwashUpdateDepths.ftn90* (3878), *SwashLayerIntfaces.ftn90* (3889), *SwashDryWet.ftn90* (3895), *SwashPresFlow.ftn90* (3902), *SwashBotFrict.ftn90* (3909) and *SwashInitSteady.ftn90* (3915).

SWASH settings

SwashPrintSettings.ftn90 If the user has already used SWASH, he/she knows that checking the .prt file is important in case of errors in the simulation. In the script *SwashPrintSettings.ftn90*, the settings as observed in a typical .prt file are printed.

SWASH data update

SwashUpdateData.ftn90 When the input is checked, the data to be processed in the computational routines needs to be updated. *SwashUpdateData.ftn90* updates the data for the flow and input fields and the boundary conditions. Boundary conditions are read with *SwashReadBndval.ftn90* (264) and flow fields are updated with *SwashUpdateFld.ftn90* (multiple, starting at 1481). Other used scripts are *SwashUpdFlowFlds.ftn90* (1515), *SwashLogLaw.ftn90* (1523), *SwashBotFrict.ftn90* (1525), *SwashWindStress.ftn90* (1534), *SwashUpdPress.ftn90* (1544), *SwashHorzVisc.ftn90* (1553/1555), *SwashVertVisc.ftn90* (1564), *SwashPorFricDep.ftn90* (1571), *SwashPorFricLay.ftn90* (1573), *SwashVeget.ftn90* (1579) and *SwashDensity.ftn90* (1584).

A.3.6 Computational routines

SWASH flow computation

SwashComputStruc.ftn90 If the pre-processing routines are over, SWASH switches over to the computational routines. *SwashComputStruc.ftn90* is the main script for the computational routines. The first call is made to *SwashComputFlow.ftn90* (69) to solve the shallow water equations. This is done either in depth-averaged 1D/2D mode or in the multi-layered mode. A subgrid approach is also available in SWASH, in which the vertical structure of the wave-induced flow field is solved at a finer scale

than e.g. the hydrostatic pressure. After output is averaged, the depths in the computational domain are updated with *SwashUpdateDepths.ftn90* (77/79). For multi-layered mode, the layer interfaces are updated with *SwashLayerIntfaces.ftn90* (87). Other updates are made with *SwashDryWet.ftn90* (93), *SwashPresFlow.ftn90* (100) and *SwashBreakPoint.ftn90* (107)

SWASH transport and turbulence computation

SwashComputTrans.ftn90 Transport of constituents is solved by means of the transport equations. In *SwashComputTrans.ftn90*, the 1D/2D transport equations are solved similar to the shallow water equations, either in depth-averaged mode (*SwashExpDep1DHtrans.ftn90* (77), *SwashExpDep2DHtrans.ftn90* (97)), multi-layered mode (*SwashExpLay1DHtrans.ftn90* (84), *SwashExpLay2DHtrans.ftn90* (104)).

SwashComputTurb.ftn90 Turbulence quantities are solved in *SwashComputTurb.ftn90* by means of solving a 3D turbulence model. For 1D (*SwashKepsMod1DH.ftn90*) and 2D (*SwashKepsMod2DH.ftn90*), the standard $k-\epsilon$ model is solved.

A.3.7 Post-processing routines

SwashOutput.ftn90 When the computations are finished for one time step, the user's desired output needs to be created. SWASH output is created with *SwashOutput.ftn90*. First of all, output quantities and points are decoded in *SwashDecOutQ.ftn90* (135) and *SwashDecOutL.ftn90* (163). Depending on the output points, output coordinates are calculated with *SwashCoorOutp.ftn90* (177). At these coordinates, *SwashQuanOutp.ftn90* (181) calculates the output quantities. If the user modelled the hydronamic loads acting on a floating body, *SwashHydroLoads.ftn90* (189) calculates these loads. If the wave runup height is requested, the output will be generated in *SwashRunupHeight.ftn90* (193).

SwashCleanMem.ftn90 When all simulation steps are processed by SWASH and the requested output has been exported, the memory used by SWASH needs to be cleaned. This is done within the script *SwashCleanMem.ftn90*.

A.3.8 SWASH Compiling

SWASH is compiled with the use of *make*, software that builds large executable applications. To use this tool, *make* makes use of a file called *Makefile*. This file provides the necessary specifications needed for compiling the desired program and such a file is also included in the SWASH files. For example, before compiling SWASH, a machine specific file called *macros.inc* is needed for specifications of the Fortran compiler, whether or not a MPI (explained in following section) compiler is available etc. With the use of *make* and *Makefile*, the command (MS Windows)

```
nmake config
```

leads to the initialization of *platform.pl*, a Perl (programming language) script that creates *macros.inc*. It also becomes clear in this script why it is important to include the Fortran Compiler executable in the System Path Variables: *platform.pl* specifically searches for the compiler executable in the user's Path to specify the compiler in *macros.inc*.

If *macros.inc* is created, the source code is ready to be compiled. However, depending on the user's system and certain preferences, some subroutines of the SWASH source code should be adapted. This takes place with the Perl script *switch.pl*. If every setting is to the user's preference, compiling takes place with *make* after which a serial, OpenMP or MPI SWASH executable is created. An overview of the compiling process has been given in Figure A.5.

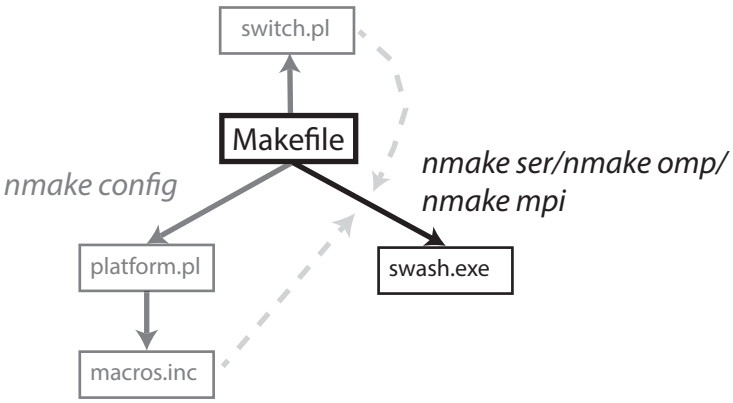

Fig. A.5.: Flowchart of compiling process for SWASH. More information can be found in the scripts (with comments) and the SWASH implementation manual.

B Assessment of effects of numerical schemes on model results

Initial model results of combined wave-current flow showed that the wave height was either increasing or decreasing over the domain. This depended on the direction of the current, with decreasing (increasing) wave heights for opposing (following) currents. A test model was set up to determine what the cause of this problem was. It was found that the discretization of the water depth and advection terms were the main cause of problem. Results are summarized in the following sections.

B.1 Model setup

A simple 1D, multi-layered model was set up with two layers. In order to neglect non-linear effects as much as possible, a monochromatic wave with period $10\ s$ and wave height $0.01\ m$ was imposed. The numerical domain had a water depth of $5\ m$ and the number of grids was 1000. The discharges for the opposing and following currents were -5 and $5\ m^2/s$, resulting in velocities of -1 and $1\ m/s$ respectively. A sponge layer of width $400\ m$ was used at the right end of the domain. Note that the same tests were performed for a 1D depth-averaged model and results (not shown here) were the same as for the multi-layered model.

B.2 Discretization of water depth

The governing equations for the SWASH model were simplified and gradually extended with the omitted terms. The most simplified model was realised by only taking into account local inertia and the spatial gradient in water level for the momentum equation. Non-hydrostatic modelling was enabled to ensure proper modelling of the waves[1]. Thus, the resulting equations as solved by SWASH were:

$$\frac{\partial u}{\partial t} + g\frac{\partial \zeta}{\partial x} = -\frac{1}{\rho}\frac{\partial p_{nh}}{\partial x}, \tag{B.1}$$

$$\frac{\partial w}{\partial t} + g\frac{\partial \zeta}{\partial z} = -\frac{1}{\rho}\frac{\partial p_{nh}}{\partial z} - g, \tag{B.2}$$

$$\frac{\partial \zeta}{\partial t} + \frac{\partial}{\partial x}\int_{-d}^{\zeta} u dz = 0. \tag{B.3}$$

In total, six runs were initialised by combining the options for the current (opposing, following or no current) and discretization of the water depth (upwind or central difference). Initial results showed that the models with the central difference scheme became unstable for the same time steps as used for the upwind scheme runs. Thus, the time step was lowered by factor 25 for stable model runs. More details about the time step are given in Section 4.6. Results with the model are summarized in Figure B.1.

The wave height evolution for the no current cases indicate that the choice of discretization of the water depth does not alter the wave height evolution. For both discretization choices, the wave height stays constant over the domain. However, for both the following and opposing current cases, the wave

[1] Simulations with hydrostatic modelling were also performed and no substantial differences were found with non-hydrostatic modelling

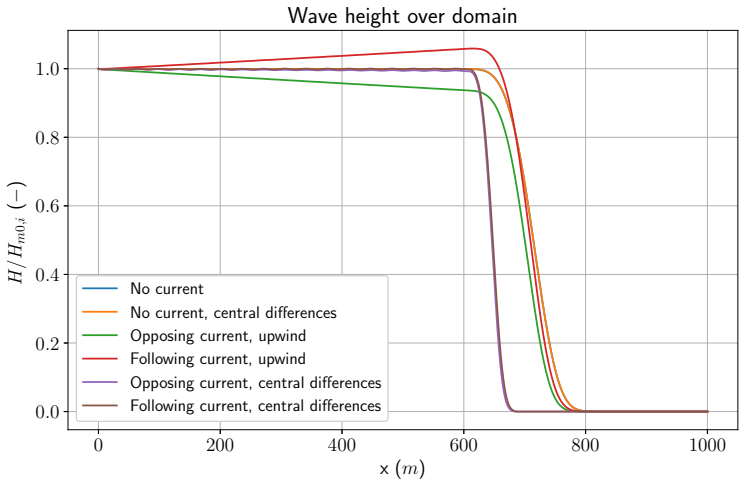

Fig. B.1.: The evolution of the wave height over the domain for a wave with and without the presence of a current. The wave heights are normalised with the wave height at the inlet boundary at the left side of the domain. The wave height evolution for both no current cases are overlapping. The wave heights in the sponge layer are null as the wave is absorbed.

height evolution is constant, increasing or decreasing. The difference in results depends on the applied discretization scheme.

Based on theory (see Chapter 2), a constant wave height should be present for a uniform bathymetry. Numerically, the upwind scheme introduces damping in the numerical solution as it is asymmetric around its point of consideration. For no currents, no significant damping is observed in the results. However, for the opposing current, the damping leads to significant decrease of the wave height over the domain. In the following current case, energy is added to the system, leading to an increase of the wave height. The damping effect of the upwind scheme seems to be enlarged for wave-current simulations in SWASH.

The central difference scheme is symmetric around its point of consideration. For this case, the numerical solution does not show significant damping. However, wiggles can be observed in the results, which are present due to the aforementioned property of the central differences scheme. Use of the central differences scheme leads to wiggles in the numerical solution, but in terms of accuracy, better results are obtained for the wave height. Thus, the central differences scheme should be used for the discretization of the water depth to obtain a constant wave height evolution.

B.3 Discretization of advection in momentum equations

B.3.1 Discretization of horizontal advection in horizontal momentum equation

The simplified model from the previous section was extended by adding the horizontal advection term in the horizontal momentum equation. The resulting momentum equations are now:

$$\frac{\partial u}{\partial t} + g\frac{\partial \zeta}{\partial x} + \frac{\partial uu}{\partial x} = -\frac{1}{\rho}\frac{\partial p_{nh}}{\partial x}, \tag{B.4}$$

$$\frac{\partial w}{\partial t} + g\frac{\partial \zeta}{\partial z} = -\frac{1}{\rho}\frac{\partial p_{nh}}{\partial z} - g. \tag{B.5}$$

SWASH uses the MacCormack predictor-corrector scheme by default for solving the horizontal advection. This scheme first predicts an intermediate value of the velocity. In the corrector step, this intermediate value is corrected for with the use of a second order correction (Zijlema et al., 2011). Two different implementations were used for the horizontal advection term. In the first implementation, the corrector step was removed. In the second implementation, the central difference scheme was

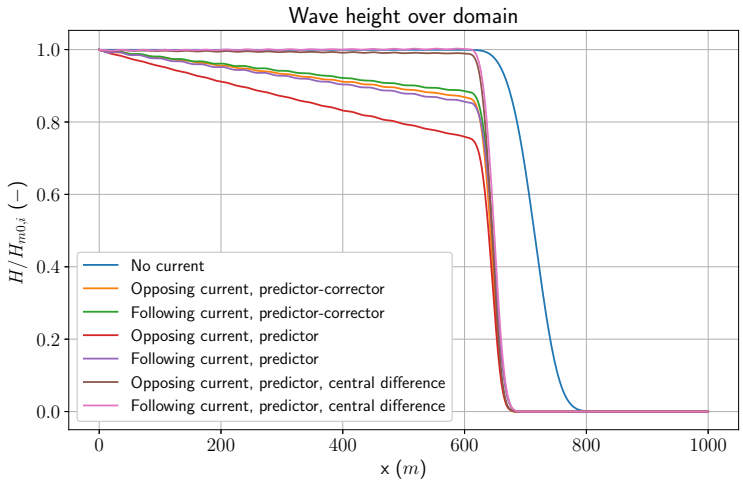

Fig. B.2.: The evolution of the wave height over the domain for a wave with and without the presence of a current. The wave heights are normalised with the wave height at the inlet boundary at the left side of the domain. The wave heights in the sponge layer are null as the wave is absorbed.

used in determining the advective velocity in the predictor step. The corrector step was also removed. Model results are shown in Figure B.2.

The model results with the default options result in a significant decrease of the wave height for opposing and following currents. The difference between wave height at the beginning of the domain and sponge layer is in the order of 10%. When the corrector step is turned off, the wave height decreases more. When the central difference scheme is used in the predictor step, wave heights stay constant over the domain for opposing and following currents. As a result, the present SWASH release is updated with this new formulation for the discretization of the horizontal advection in the horizontal momentum equation.

B.3.2 Discretization of horizontal advection in vertical momentum equation

The simplified model from the previous section was extended by adding the horizontal advection term in the vertical momentum equation. The resulting momentum equations are now:

$$\frac{\partial u}{\partial t} + g\frac{\partial \zeta}{\partial x} + \frac{\partial uu}{\partial x} = -\frac{1}{\rho}\frac{\partial p_{nh}}{\partial x}, \tag{B.6}$$

$$\frac{\partial w}{\partial t} + g\frac{\partial \zeta}{\partial z} + \frac{\partial uw}{\partial x} = -\frac{1}{\rho}\frac{\partial p_{nh}}{\partial z} - g. \tag{B.7}$$

SWASH, by default, uses the second order BDF scheme for the discretization of this term, but there is an option to use the central difference scheme. Results are summarized in Figure B.3. It is clear from these results that this choice of discretization does not have a significant effect on the model results, thus the default scheme can be used.

B.3.3 Discretization of vertical advection in horizontal momentum equation

The simplified model from the previous section was extended by adding the vertical advection term in the horizontal momentum equation. The resulting momentum equations are now:

$$\frac{\partial u}{\partial t} + g\frac{\partial \zeta}{\partial x} + \frac{\partial uu}{\partial x} + \frac{\partial wu}{\partial z} = -\frac{1}{\rho}\frac{\partial p_{nh}}{\partial x}, \tag{B.8}$$

$$\frac{\partial w}{\partial t} + g\frac{\partial \zeta}{\partial z} + \frac{\partial wu}{\partial x} = -\frac{1}{\rho}\frac{\partial p_{nh}}{\partial z} - g. \tag{B.9}$$

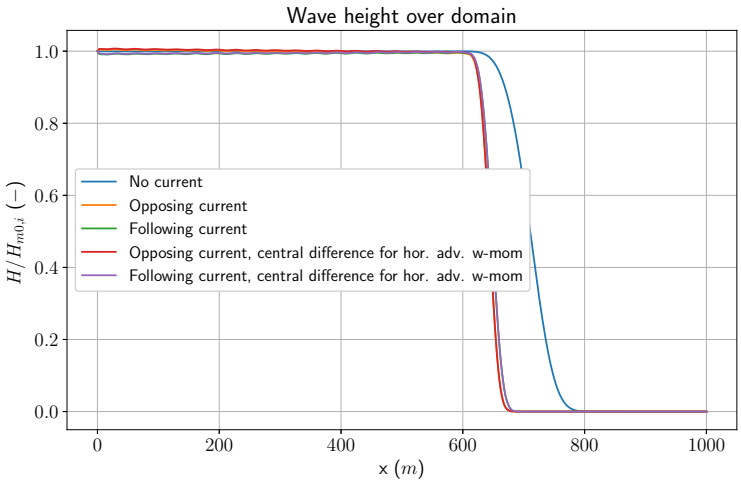

Fig. B.3.: The evolution of the wave height over the domain for a wave with and without the presence of a current. The wave heights are normalised with the wave height at the inlet boundary at the left side of the domain. The wave heights in the sponge layer are null as the wave is absorbed.

SWASH, by default, uses the first order upwind scheme for, but there is an option to use the central difference scheme for the discretization of this term. Results are summarized in Figure B.4. They indicate that the central difference scheme might be the preferred scheme for discretization for opposing currents. The wave height decrease is relatively smaller with the central difference scheme in comparison to the upwind scheme. Therefore, the central difference scheme should be used for the discretization of the vertical advection in the horizontal momentum equation.

B.3.4 Discretization of vertical advection in vertical momentum equation

The simplified model from the previous section was extended by adding the vertical advection term in the horizontal momentum equation. The resulting momentum equations are now:

$$\frac{\partial u}{\partial t} + g\frac{\partial \zeta}{\partial x} + \frac{\partial uu}{\partial x} + \frac{\partial wu}{\partial z} = -\frac{1}{\rho}\frac{\partial p_{nh}}{\partial x}, \tag{B.10}$$

$$\frac{\partial w}{\partial t} + g\frac{\partial \zeta}{\partial z} + \frac{\partial uw}{\partial x} + \frac{\partial ww}{\partial z} = -\frac{1}{\rho}\frac{\partial p_{nh}}{\partial z} - g. \tag{B.11}$$

SWASH, by default, uses the first order upwind scheme for, but there is an option to use the central difference scheme for the discretization of this term. However, the SWASH manual advises not to alter the default scheme. For testing purposes, results were still generated. They are summarized in Figure B.5. There is no substantial difference with the results from the previous section, thus the default scheme can be used.

B.4 Effects of bottom friction on model results

Although the discretization of the bottom friction was not changed, it must be noted that the results are different when bottom friction taken into account. Results of the no, opposing and following currents are summarized in Figure B.6. For no currents, the bottom friction is negligible and, thus the wave height stays constant in the domain. For both opposing and following currents, bottom friction leads to a reduction of the wave height. It is not known whether this is a numerical artefact or increased dissipation due to the presence of a current.

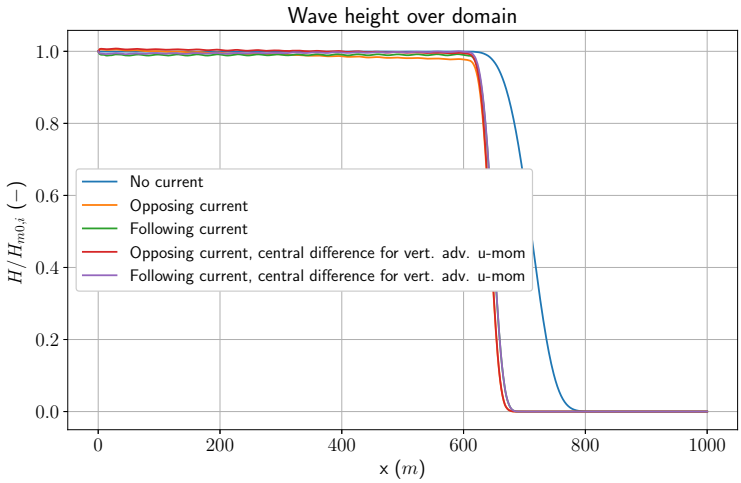

Fig. B.4.: The evolution of the wave height over the domain for a wave with and without the presence of a current. The wave heights are normalised with the wave height at the inlet boundary at the left side of the domain. The wave heights in the sponge layer are null as the wave is absorbed.

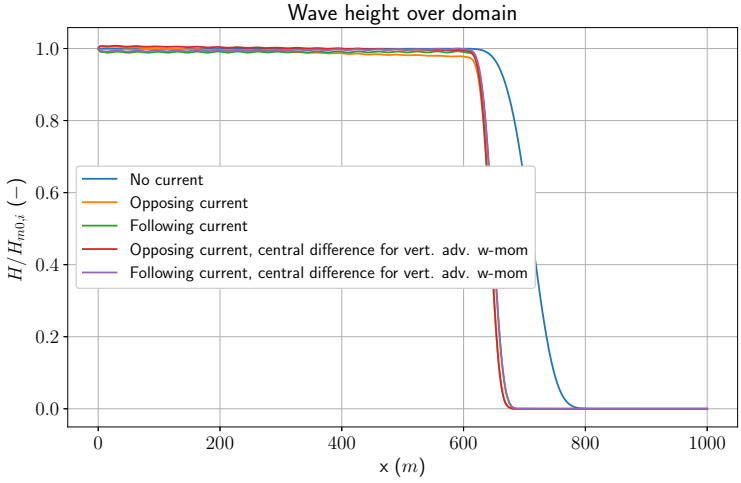

Fig. B.5.: The evolution of the wave height over the domain for a wave with and without the presence of a current. The wave heights are normalised with the wave height at the inlet boundary at the left side of the domain. The wave heights in the sponge layer are null as the wave is absorbed.

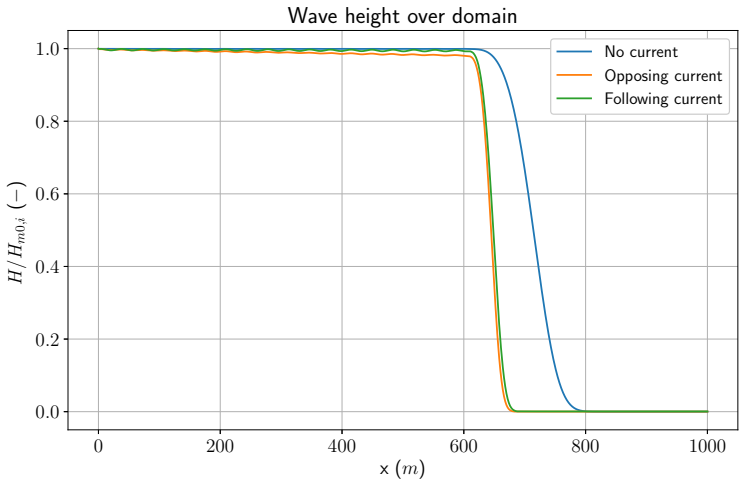

Fig. B.6.: The evolution of the wave height over the domain for a wave with and without the presence of a current. The wave heights are normalised with the wave height at the inlet boundary at the left side of the domain. The wave heights in the sponge layer are null as the wave is absorbed.

C

Generation of non-linear waves

As mentioned in Section 3.1.3, non-linear waves can only be imposed in SWASH with the use of user-generated time series. In this research, non-linear wave theory is used for cases with non-linear waves. Three approximations are used, namely those by Rienecker and Fenton (1981), Fenton (1985) and Fenton (1988).

Rienecker and Fenton (1981) proposed the use of a streaming function to calculate parameters for waves of constant form propagating over a steady fluid. Starting from potential flow, they introduced Fourier series for a stream function $\psi(x,z)$ (1D) such that, after a tedious derivation, the following equation was obtained:

$$u(x,z) = B_0 + k\sum_{j=1}^{N_F} u_j(x,z), \tag{C.1}$$

where B_0 is a coefficient, N_F is the amount of Fourier modes and $u_j(x,z)$ is defined as:

$$u_j(x,z) = jB_j \frac{\cosh(jkz)}{\cosh(jkd)} \cos(jkx). \tag{C.2}$$

The system of equations that had been derived can be solved with Newton's method. The convergence is fast and around five iterations are typically needed.

The method requires the input of the wave height and wave period and allows room for additional input, for instance a mean background current. The numerical implementation shows that the results are in good agreement with a wide variety of waves, either linear of non-linear.

To generalize the method even further, Fenton (1988) proposed a modified version in which the equations were rewritten in terms of the wave number and the calculations of the Jacobian matrix were simplified. This resulted in a method that was applicable for waves in deep and shallow water. This method was also used to generate time series.

The final method used was specifically catered to Stokes waves. Fenton (1985) proposed a method enabling users to generate Stokes waves up to order 5. For all methods, toolboxes in Python and MATLAB are used to generate time series.

Supplementary material for WCS method

D

D.1 Sensitivity analysis moving average

D.1.1 Importance of moving average period

The moving average used for the velocity signal at the grid point next to the numerical wave maker and for the water depth at the numerical wave maker could require some tuning by the user if results are inaccurate. According to the definition of the moving average, Δt and T_{mov} can be used as tuning parameters, but, in general, Δt is fixed for a certain amount of grids according to the CFL criterion (see Equation 3.7). Therefore, the period over which the signal is averaged should be chosen such that errors are the lowest or, if possible, omitted. Convergence in this context is defined as the time needed to reach equilibrium values.

Note that due to the use of a moving average, spin up time can be significantly large if there are no initial values for certain parameters. When the WCS method is used, it is recommended to always use initial fields for the current velocity and water level. With this approach, the equilibrium values are reached relatively sooner and thus computational time is reduced substantially.

D.1.2 Results for different moving average periods

Long and short wave signals are given in Figure D.1. In this example, a long wave signal with amplitude $1\ m$ and period of $4\ hours$ is summed up together with a short wave signal with amplitude $0.5\ m$ and period $8\ s$. A time step of $0.02\ s$ is chosen with a total time equal to the period of the long wave. The results of the moving averages are shown in the three subfigures in Figure D.1. For each subfigure, a different averaging period T_{mov} is chosen. The first subfigure uses a T_{mov} of 1 short wave period, the second subfigure 10 short wave periods and the third subfigure 100 short wave periods.

Results show that there are different ways of either underfitting or overfitting the long wave signal. Underfitting is defined as the presence of a substantial remainder of the short wave signal. If the averaging period is too small, the moving average is still able to differentiate long and short wave signals, but a significantly large oscillating signal remains. Overfitting is defined as significant mismatch between the averaged and long wave signals. If the averaging period is too large, overfitting takes place and the underlying long wave signal is shifted substantially in time.

D.1.3 Results for common model setup

The long wave, from the previous example, is not entirely representative for our modelling purposes. The previous example is given to just illustrate the results of applying moving averages on time series. For our cases, the velocity due to the current will have a different signal pattern compared to the previous example.

During steady-state conditions, the velocity of the current is not changing in time. For our cases, results are shown in Figure D.2a. The water level will, due to the water level gradient initiated by the current, increase or decrease depending on the direction of the current. This is visualised in the first $100\ s$. Values are in the order of magnitude for a test run with combined wave-current flow.

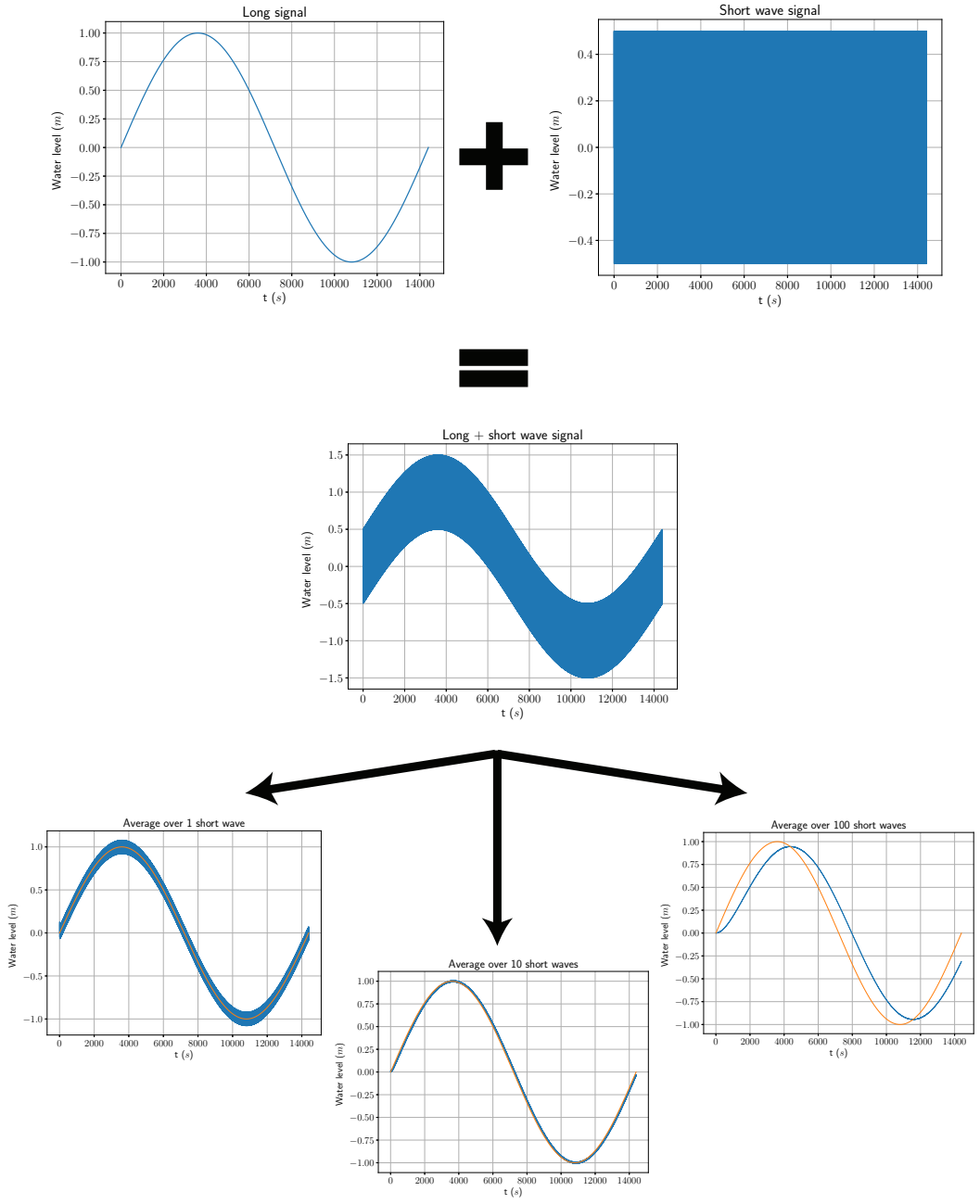

Fig. D.1.: Moving average example of a long and short wave signal averaged out over multiple time frames. The orange lines in the three subplots below represent the long wave signal. The blue lines represent the moving average signal.

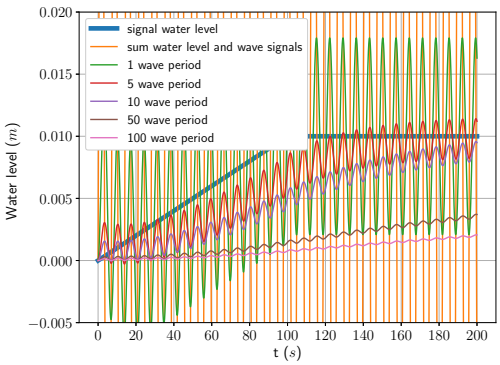

(a) The blue line represents the water level signal, while the yellow line is the summation of both water level and short wave signals. The other lines show the moving average as a function of time.

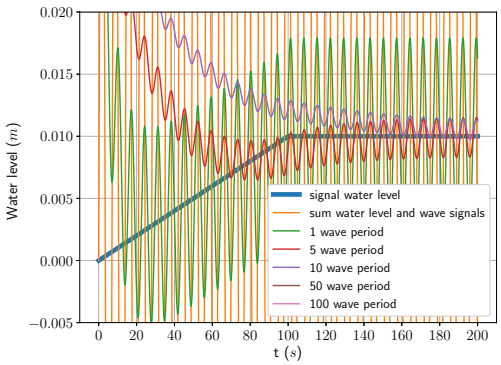

(b) This example includes an initial difference between moving average and the wave signal. The blue line represents the water level signal, while the yellow line is the summation of both water level and short wave signals. The other lines show the moving average as a function of time.

Fig. D.2.: Examples of moving averages of arbitrary values. These moving averages represent a typical case of combined wave-current flow.

After spin up, an equilibrium water level gradient, thus water level, will be present in the domain. The results suggest that, after spin up, every moving average period will lead to the long wave signal for $t \to \infty$. Therefore, independent of the choice of the wave averaging period, an equilibrium will always be found. However, the spin up time should also be considered, as it increases for larger moving averaging periods. There is a trade-off between accuracy and computational time: although small noises remain for small wave averaging periods, one has to assess the gain in computational efforts against smaller errors in accuracy.

The initial estimate for the moving average period is important as it reduces spin up substantially. The effects of a large difference between initial estimate and moving average period are shown in Figure D.2b. Results show that this initial difference is dampened out quickly for smaller wave averaging periods, while the opposite holds for longer periods.

For moving average periods of 50 and 100 wave periods, the convergence is remarkably slow, such that results are not even visible in Figure D.2b. The difference between the initial and equilibrium values is thus of absolute importance. Further results (not shown here) indicate that the larger this difference is, the faster convergence takes place. For instance, an initial estimate of $0.03\ m$ converges much faster than in the case of an initial estimate of $0\ m$.

D.2 SWASH commands for WCS method

New SWASH commands are introduced in the implementation of the WCS method in SWASH. As these new commands are not reported in the user manual, they will be shortly discussed in this section. For more information about SWASH commands in general, reference is made to the SWASH user manual (The SWASH team, 2018).

It is important to always use a velocity boundary condition and a discharge boundary condition with the WCS method. Based on the derivation as provided in Sections 3.2.3 and 3.2.4, the user must at all times use the velocity boundary at the left end of the numerical domain (West) and the discharge boundary at the right end (East). Due to a bug in the source code, the combination of a velocity and discharge boundary leads to empty values for the discharge boundary. This was fixed in the newest patch, but no sufficient time was left to modify the source code. Therefore, the discharge should be defined twice: in the discharge boundary condition and in a variable called 'DISCH(ARGE)'. An example is given below:

```
BOU SIDE E BTYPE DISCH LOG CON -10.0

SET DISCHARGE -10.0
```

In this example, a value of $-10.0\ m^2/s$ is prescribed at the discharge boundary condition. The value used in the WCS method is the value defined by the 'SET DISCHARGE' command, which in this case is also $-10.0\ m^2/s$. If different values are used, the results are not correct.

The amount of moving average periods can be set with the command:

```
SET MOVAVEPER 5.0
```

In this example, the moving average period equals five wave cycles. In general, the moving average period is initially equal to 10 averaging periods, as this was found to be optimal in Section 3.2.5.

Waves can be imposed in the same way as the present SWASH release. To simulate a current-only situation, a zero amplitude Fourier series can be used at the velocity boundary.

D.3 Comparison present SWASH release and WCS method

As an early benchmark test, combined wave-current flow was tested with the present SWASH release. Simulations were supplied with user-generated time series at the numerical wave maker. These time series included both the velocities of the wave as well as the current. Corrections were included for both of them. The drawback of this is that an extra step is required (by means of an additional script) to simulate combined wave-current flow in SWASH.

To show the capacity of the WCS method, the same model is used for comparison. The model input is of no importance as this example focusses more on the simplicity of adding waves and currents with the WCS method. Results of both model versions are shown in Figure D.3. The wave heights are almost completely equal and wave blocking, as observed in the results with the present SWASH release, is also found back with the use of the WTC method.

The input files are given in Sections D.3.1 and D.3.2. The present SWASH release needs a substantial amount of pre-processing steps, whereas the WCS method requires only the input value for the discharge at the discharge boundary condition.

D.3.1 Input file of present SWASH release

```
$*************HEADING************************************
$
PROJ 'T71wcu03' 'T71'
$
$  Case 2: wave against a current over a submerged bar
$         H = 0.02 m, T = 1.2 s, Uc = -0.17 m/s
$
$ -|-------------------------------------------------------|--
$  | This SWASH input file is part of the bench mark tests for|
$  | SWASH. More information about this test can be found in |
$  | an accompanied document.                              |
$ -|-------------------------------------------------------|--
$
$************MODEL INPUT*********************************
$
MODE DYN ONED
$
CGRID 0. 0. 0. 60. 0. 3000 0
$
VERT 3
$
```

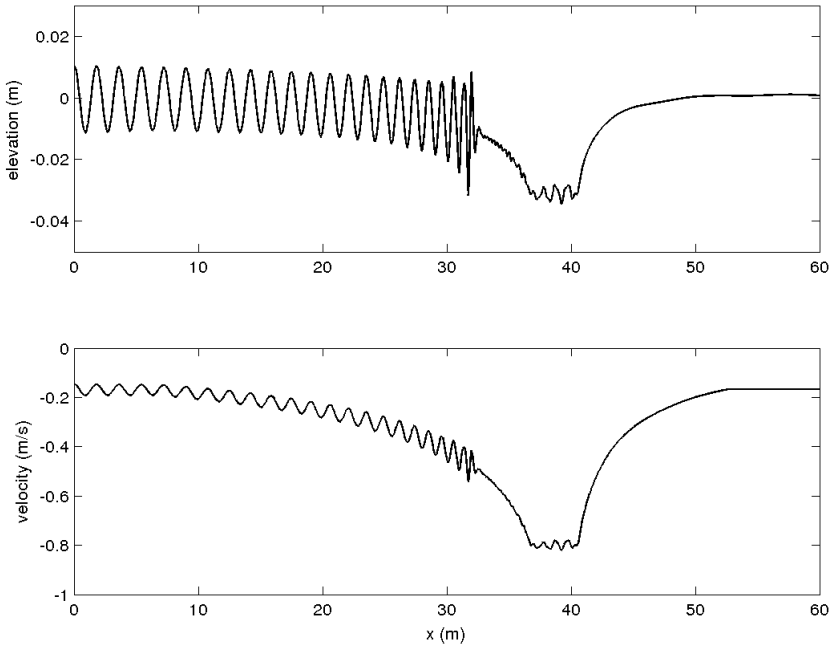

(a) Example with the present SWASH release.

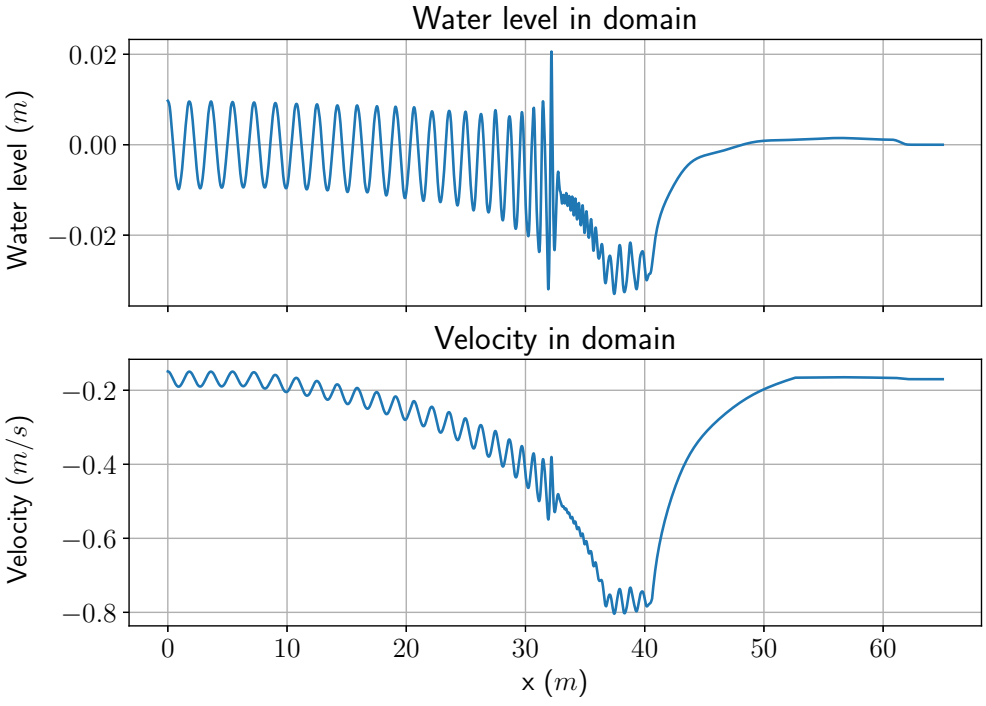

(b) Same numerical model settings but with the WCS method.

Fig. D.3.: Comparison between present SWASH release and WCS method.

```
INPGRID BOTTOM 0. 0. 0. 3000 0 0.02 1.
READINP BOTTOM 1. 't71wavcu.bot' 1 0 FREE
$
INIT VX = -0.17
$
BOU SIDE W BTYPE VEL LAY 1 SMOO 1.2 SEC CON SERIES 't71wcu03_01.bnd'
BOU SIDE W BTYPE VEL LAY 2 SMOO 1.2 SEC CON SERIES 't71wcu03_02.bnd'
BOU SIDE W BTYPE VEL LAY 3 SMOO 1.2 SEC CON SERIES 't71wcu03_03.bnd'
BOU SIDE E BTYPE RADIATION
$
NONHYDrostatic BOX PREC ILU
BREAK
SET BACKVISC 0.0001
$
DISCRET UPW MOM
DISCRET UPW WMOM
$
TIMEI METH EXPL 0.2 0.5
$
$************ OUTPUT REQUESTS ************************
$
TABLE 'COMPGRID' NOHEAD 't71wcu03.tbl' DIST WATL VEL
$
TEST 1,0
COMPUTE 000000.000 0.002 SEC 000300.000
STOP
```

D.3.2 Input file of WTC method

```
PROJECT 'test' '01'

MODE DYN ONED

CGRID 0. 0. 0. 65. 0. 3250 0

VERT 3

INPGRID BOTTOM 0. 0. 0. 3250 0 0.02 1.
READINP BOTTOM 1. 't71wavcu_ext.bot' 1 0 FREE

BOU SIDE W BTYPE VEL HYP CON REG 0.02 1.2
BOU SIDE E BTYPE DISCH CON -0.136

SET DISCHARGE -0.136

SPON E 5

INIT VX = -0.17

NONHYDrostatic BOX PREC ILU
BREAK
SET BACKVISC 0.0001

DISCRET UPW MOM
DISCRET UPW WMOM

TIMEI METH EXPL 0.2 0.5

TABLE 'COMPGRID' NOHEAD 'watlevgrad_dom.tbl' XP WATLEV VEL
TABLE 'COMPGRID' NOHEAD 'watlevgrad_multtim_dom.tbl' XP WATLEV VEL OUT 000000.000 1 SEC

COMPUTE 000000.000 0.002 SEC 000300.000
```

```
STOP
```

D.4 Extension of WCS method to 3D domain

In this research, only 2DV modelling is used. However, an extension of the WCS method to allow 3D modelling might be needed for future research. In this section, a preliminary analysis of the results for a 3D domain is given.

D.4.1 Approach in WCS method for 3D domain

In SWASH, boundary conditions are repeated along the entire side in a 2D domain. This means that the same procedure is applied at every boundary point. Therefore, the WCS method as described for 2DV domains is still applicable. However, the outflow of the current at the boundaries is difficult to define, because waves and currents are now vectors, i.e. they have a magnitude and direction.

The wave-current angle at the boundaries is used for mass conservation. For simplification, it is assumed that the Northern and Southern boundaries are closed. Therefore, the vectorial component of the current velocity in West/East direction will be scaled with the WCS method, as outflow is only possible along this axis of the domain.

D.4.2 Model setup and results

A 2D test model was set up. The numerical domain had a size of $500x500\ m$. The water depth was $10\ m$ and two layers were used. A monochromatic wave with period $7\ s$ and height $0.2\ m$ was imposed. Results with the extension of the WCS method are shown in Figure D.4.

The 3D results show that the wave was uniform in the y-domain. The wave was propagating in the x-domain and absorbed by a sponge layer. The velocities indicate the presence of a current. This was also observed along a transect in the y-domain. The wave height does not seem to be exactly matching the imposed values, which suggest that the iterative solver in the WCS method needs to be improved for 3D modelling. However, the results show that 3D modelling is possible with the WCS method.

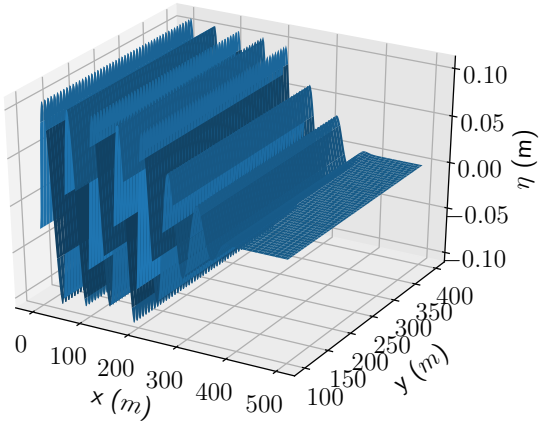

(a) A 3D plot of the water level.

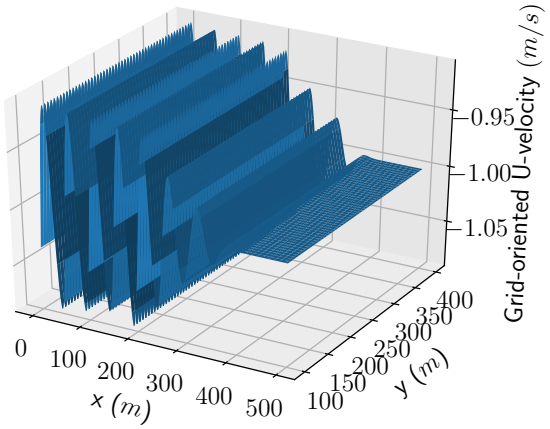

(b) A 3D plot of the grid-oriented U-velocity.

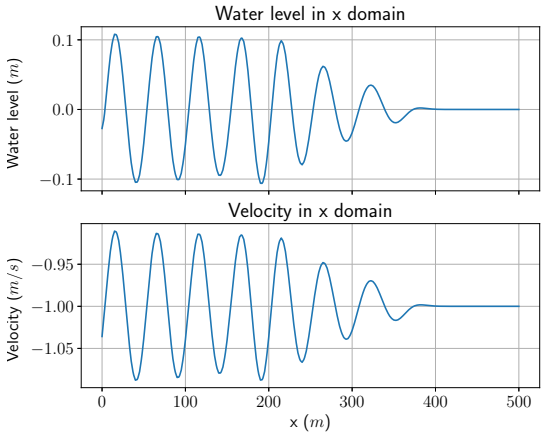

(c) Water level and velocity profiles on a transect at $y = 250\ m$.

Fig. D.4.: Model results of the extended WCS method in 3D.

E

Derivation and analysis of analytical solution for non-uniform bathymetry

E.1 Derivation of analytical solution

In Chapter 4, a numerical model was set up for a basic case with a non-uniform bathymetry. We can derive the analytical solution for the basic case based on conservation of wave action (see Section 2.1). With the use of Equation 2.7, we can obtain the analytical result of the wave height. For convenience, the equation is repeated here:

$$\frac{\rho g H^2}{8\sigma}(U + nc_r) = \text{constant}.$$

It is important to note that frictional effects are ignored. These are usually added as a source term in the wave action balance. However, for simplicity, these effects are ignored.

The integrated wave action balance can be discretized and solved with a numerical implementation. The discretization is obtained by applying a forward moving scheme, similar to the explicit Euler scheme. The discretized equation is:

$$\frac{\rho g H_{i+1}}{8\sigma_{i+1}}(U_{i+1} + n_{i+1}c_{r,i+1}) - \frac{\rho g H_i}{8\sigma_i}(U_i + n_i c_{r,i}) = 0, \tag{E.1}$$

where i and $i+1$ are subsequent grid points in the discretized domain. Rewriting the equation allows us to solve for the wave height at the next grid point:

$$H_{i+1} = \frac{H_i \sigma_{i+1}}{\sigma_i} \frac{(U_i + n_i c_{r,i})}{(U_{i+1} + n_{i+1} c_{r,i+1})}. \tag{E.2}$$

Equation E.2 represent a boundary value problem, for which a boundary condition is needed to obtain the solution. Therefore, we need some additional information. The discharge has an absolute magnitude of $5\ m^2/s$. Since the water depths in the domain are known, we can calculate the velocities at each location. Thus, the absolute velocity has a magnitude between $0.5\ m/s$ and $1.0\ m/s$.

Furthermore, we know the wave parameters at the inlet boundary, as we impose the wave. Therefore, the wave parameters are the boundary conditions we use to solve the integrated wave action balance. More specifically, the wave period and wave height are used. We also can calculate the relative wave frequency σ, group and phase velocity factor n and the phase velocity c_r at every location in the domain. With these pieces of information, the wave action balance can be solved.

E.2 Analysis of analytical solution

The analytical solution for the non-uniform bathymetry case in Section 4.2. is shown in Figure E.1. The relative frequency, σ, increased (decreased) in the shoaling area in the presence of opposing (following) currents. In the deshoaling area, σ decreased (increased) in the presence of opposing (following) currents. This is in accordance with theory (see Section 2.6).

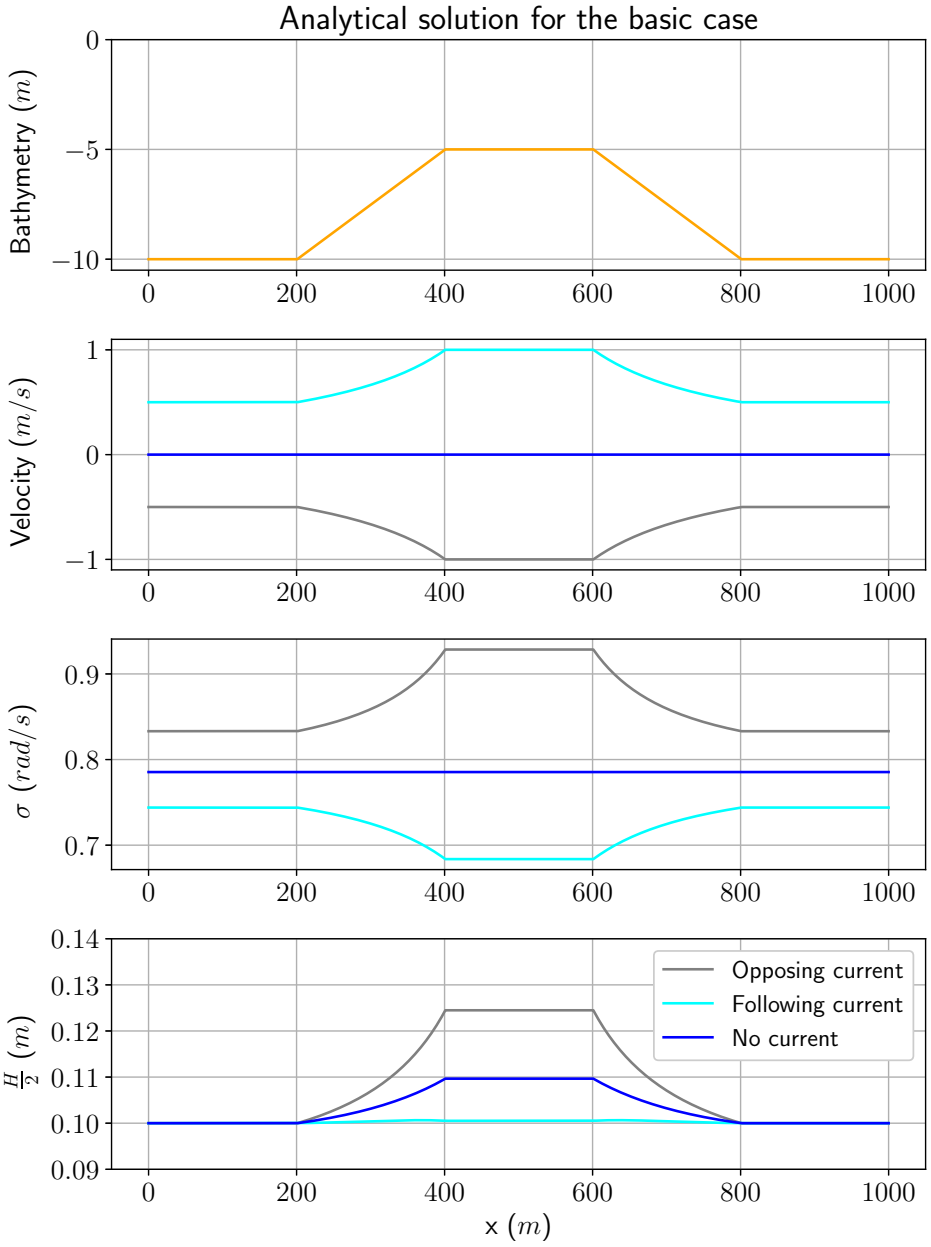

Fig. E.1.: The analytical solution to the wave action balance for the basic case.

For the no current case, the wave amplitude was only affected by depth-induced shoaling. In the shoaling area, the wave amplitude was increased by a factor of $\sqrt{\frac{c_{g\,deep}}{c_{g\,shallow}}} \approx 1.12$. On top of the submerged breakwater, the wave amplitude stayed constant. In the deshoaling area, the wave amplitude decreased with the same factor, resulting in same wave amplitude as at the inlet boundary.

In the case of an opposing current, the increase in velocity led to an extra increase of the amplitude. As the wave was compressed by the current, energy bunching took place, resulting in an increase of wave amplitude. Together with the shoaling effects of the water depth, the wave amplitude was amplified significantly more than in the no current case. After passage through the deshoaling area, the wave height returned to its initial value.

The wave amplitude almost stayed constant in the case of a following current. As the wave length was increasing in the shoaling area, the energy of the wave was spread over a larger surface area, resulting in a decrease of the wave amplitude. In general, depth-induced shoaling in case of decreasing depths leads to an increase of the wave amplitude. Thus, both events effectively cancelled each other out. There was still a small increase of wave amplitude, indicating that the shoaling effects by the water depth were more dominant than the lengthening of the wave by the following current.

In all cases, wave amplitude were changing in the shoaling and deshoaling areas. The wave did not lose any energy, as the wave amplitude returned to its initial value after the deshoaling area. This was observed for all cases. This is as expected, since the governing equation is energy conservative.

F

Analysis of model results of current- and wave-only cases by Klopman (1994)

In this chapter, model results of the current- and wave-only experiments by Klopman (1994) are analysed. More details about the experiments can be found in Section 3.3.1. Note that point and position are used interchangeably.

F.1 Model setup of current- and wave-only cases

In this section, the model setup of the current- and wave-only cases is given. Note that the framework, as defined in Chapter 4, was not used, as it is mainly created for simulations of combined wave-current flow.

F.1.1 Numerical domain

The flume, as used by Klopman (1994), had a total length of $46\ m$. However, the length of the area of interest is equal to $34.2\ m$, since the flow-circulation circuit and its openings can be ignored in the numerical model (see Figure 3.4).

The boundaries in the SWASH model should be about two wave lengths distant from the area of interest (The SWASH team, 2018). Therefore, two sections with a length of $5\ m$ were added to the beginning and end of the numerical domain. Furthermore, an additional $10\ m$ of domain was added at both ends. This was done to ensure sufficient space for the flow to develop. Thus, the total numerical domain length was $65\ m$. Output was generated at the original measuring position of Klopman (1994), which in the new frame of reference was $32.5\ m$ from either end of the domain.

A sketch of the setup of the numerical model is given in Figure F.1. The currents, as imposed by Klopman (1994), always propagated from left to right in the wave-current flume. However, model results of opposing and following currents were produced. This was to assess whether SWASH is capable of producing the same results for a different orientation. For the wave-only case, Klopman (1994) used a wave propagating from right to left. For the simulations with damping of the current or wave, a sponge layer with length $8.0\ m$ was placed at the outflow boundary.

F.1.2 Spatial discretization

The number of grids of the current- and wave-only case were 90 and 1300 respectively. For the wave-only case, this resulted in approximately 53 gridcells per wave length, which is sufficient to capture the wave characteristics. For the vertical discretization, 10 layers were used.

F.1.3 Boundary conditions

There are some small differences between the boundary conditions of the present SWASH release and the new version with the WCS method. These differences are highlighted below.

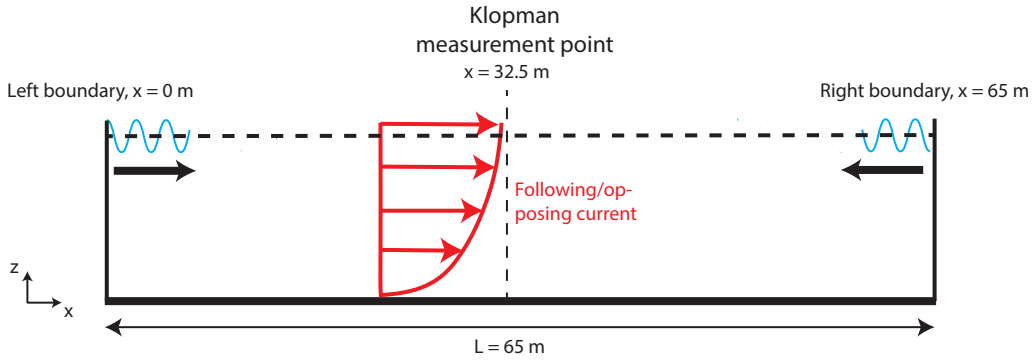

Fig. F.1.: Numerical model setup of Klopman (1994) experiment. The black arrows show the direction of wave propagation. The red arrows show the (logarithmic) velocity profile of the current, which always propagates from left to right. At the middle, the output point is placed to compare model results with measurements.

Wave

The waves imposed by Klopman (1994) were non-linear. To model these waves, time series were generated with the methods mentioned in Section C. A simulation with linear waves was also made, since the Ursell number limit for linear wave theory is not exceeded significantly. A monochromatic wave period $1.44\ s$ and height $0.12\ m$ was assumed. These are, in fact, the characteristics of the carrier wave as imposed by Klopman (1994).

Current

A comparison between measurements and initial SWASH results suggested that the imposed discharge in the model was incorrect. A logarithmic fit with the measurements was made with Equation 3.39. Note that the differences and, thus, matching velocity profiles between the core, logarithmic wall and viscous (sub)layers were assumed to be reduced to just the logarithmic velocity profile. Results, shown in Figure F.2, suggested that the total discharge was equal to approximately $76\ l/s$. This is different from the discharge of $80\ l/s$ as reported by Klopman (1994). It was mentioned by Klopman (1994) that due to the apparent cross-talk and Bragg-cell frequency shift problems with the LDV flow meter, flow velocities were underestimated by 7%. This is approximately the difference in discharges, but this was not confirmed. To conclude, a discharge of $76\ l/s$ was used in the model. The initial velocity was therefore equal to $0.152\ m/s$. Spin up time was decreased by imposing an initial velocity field based on the imposed discharge.

Based on the description given in Section 3.3.1, the velocity profile of the current was approximated as logarithmic. Since there is no data available at other sections in the Klopman (1994) experiment, it is not known whether the flow profile is actually uniform or logarithmic at the start of the experimental domain. This assumption was, thus, made in the model settings.

Present SWASH release

For the present SWASH release, a discharge boundary was used at the upstream end of the domain (left end in Figure F.1). At the downstream end, a water level boundary was used. In the current-only

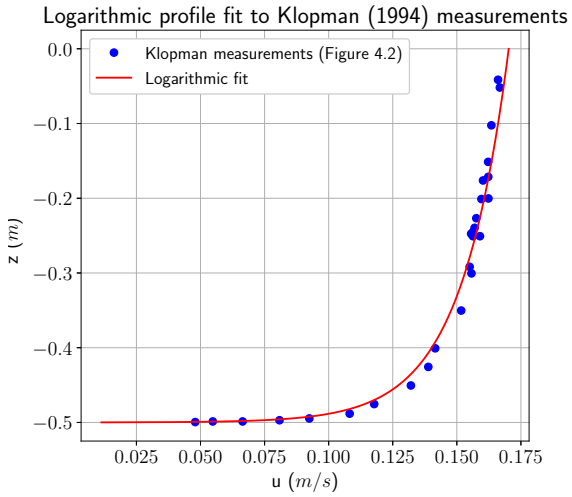

Fig. F.2.: Logarithmic profile fit of experimental data measured by Klopman (1994).

case, a water level gradient will develop. Therefore, the value at the water level boundary was chosen, such that the water level at the halfway point would equal $0\ m$.

WCS method

For the WCS method, it is prescribed to always use hyperbolic velocities and discharge boundaries. For both following and opposing currents, logarithmic profiles were used. Additional settings (e.g. moving average period) were kept the same as described in Section 3.2.

F.1.4 General model settings

Vertical mixing was taken into account by applying the standard $k-\epsilon$ model. Bottom friction was modelled with the law of the wall, using a Nikuradse roughness height of $1.2\ mm$ (see Section 3.3.1). The total simulation time was $20\ min$ with $5\ min$ spin up time.

F.2 Model results of current-only case without sponge layer

In this section, the model results of the current-only case are analysed. Flow velocity profiles at various moments in time at the measuring point were generated for opposing and following currents. The spatial evolution of the flow velocity profile was also obtained. Results of the following current are shown in Figure F.3. These results were obtained with the present SWASH release. Note that the velocities in the spatial domain plot are outputted at $t = 20\ min$, while the measurements by Klopman (1994) are time-averaged. In general, the flow velocity profiles show a good fit with the experimental data. The profiles are overlapping in time, which means that model output is stationary in time.

F.2.1 Generation of turbulent viscosities

There remains a difference in the order of several mm/s between model results and measurements. The lower half of the velocity profile, as measured by Klopman (1994), is slightly underestimated by the model, while the upper half is slightly overestimated. This indicates that the calculation of viscosity profile could be further optimized. The time-averaged viscosity profile of the last 10 minutes of simulation time is shown in Figure F.4.

Groeneweg (1999) used the experiments by Klopman (1994) to validate his numerical model. Compared to the numerical model results by Groeneweg (1999), the eddy viscosity produced by SWASH is

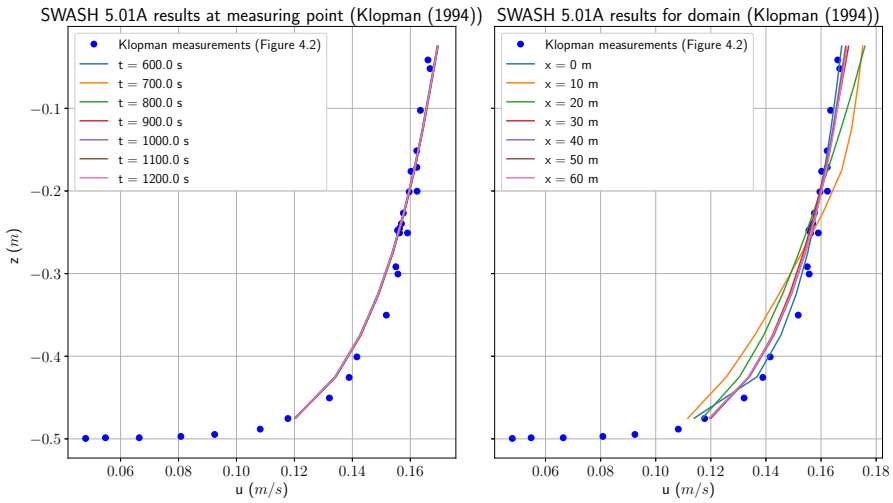

Fig. F.3.: Data from Klopman (1994) measurements (Figure 4.2, original report) compared with SWASH results in time and space. In the left figure, SWASH results in time are shown. Not all lines are visible since they are overlapping. The flow velocity profile development in space at $t = 20\ min$ is shown in the right figure.

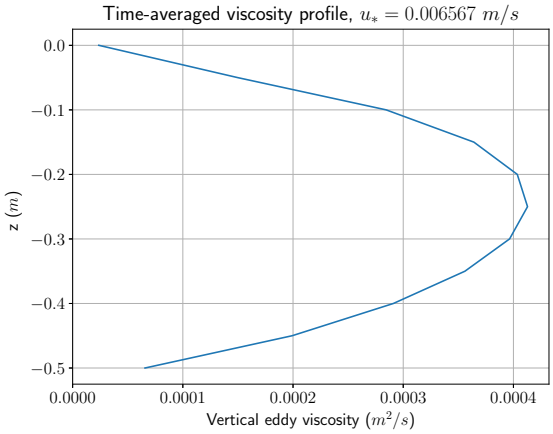

Fig. F.4.: The time-averaged vertical eddy viscosity profile at the measuring point of Klopman (1994).

larger. However, the model results of Groeneweg (1999) were in good agreement with measurements. This means that the viscosity is still slightly underestimated by SWASH. The bottom shear stress in the model by Groeneweg (1999) was $5.4 \cdot 10^{-2}\ N/m^2$. By using the simple equation, $\tau_b = \rho {u_*}^2$, SWASH yields a bottom shear stress of $4.3 \cdot 10^{-2}\ N/m^2$. This is slightly less than the value found by Groeneweg (1999) and could indicate why the viscosity profile is underestimated. Note that due to the use of 10 vertical layers, the distance between the layers at and near the bottom is about $3\ cm$. Therefore, developments near the bottom are not completely taken into account. This might be the difference in bottom shear stresses, but this was not further tested.

To generate other conditions of turbulence, different roughness heights were used in the model. However, results (see Figure F.5) suggested that the fit decreased for larger roughness heights. The last option considered was the optimization of the $k - \epsilon$ model. The model constants (Table 3.1) could be adjusted for larger viscosity values. However, this was ultimately avoided, as the interdependence between model constants can lead to further errors (Guillas et al., 2014; Richards and Norris, 2011).

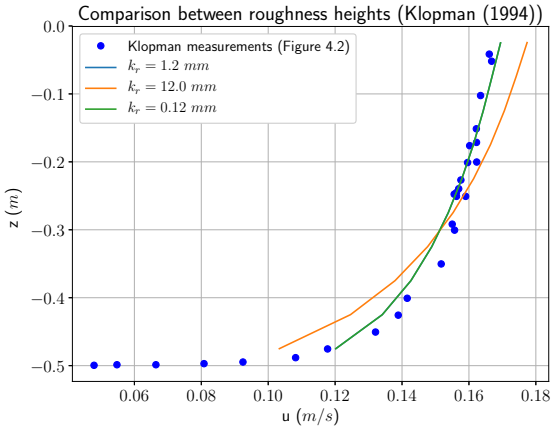

Fig. F.5.: Data from Klopman measurements (Figure 4.2, original report) compared with results of the present SWASH release for a following current. The Nikuradse roughness height was varied to assess the changes in velocity profiles. Results are outputted at measuring point of Klopman (1994) at $t = 20\ min$. The blue and green lines are overlapping as results exactly match.

F.2.2 Incomplete configuration of turbulence modelling in SWASH

The results from Figure F.3 show substantial differences between flow velocity profiles for $0\ m < x < 30\ m$. The velocity profile at the inlet boundary completely matched the measurement data. This makes sense, as a logarithmic profile was imposed. However, as the flow started propagating through the domain, the flow velocity profiles were altered significantly. At the measurement position of Klopman (1994) and forward, the flow velocity profile become uniform in space. Tests with longer numerical domains were made to confirm this. After the flow velocity profile becomes uniform in space, the fit with measurement data is good.

The altering of the flow velocity profile for $0\ m < x < 30\ m$ is rather unexpected, since the flow velocity profile starts logarithmic. For the experiments by Klopman (1994), a safe assumption is that the vertical structure of the flow was not logarithmic at the inlet boundary. The flow was disturbed, since it was imposed through a box filled with marbles. For a disturbed flow, the adaptation length of the velocity profile is around $10 - 30$ times the water depth. For this experiment, this resulted in a range of $5\ m - 15\ m$. Thus, a fully logarithmic flow velocity profile at the inlet boundary, should already lead to spatial uniformity. This was, however, not the case. It was found that this inconsistency in results was linked to the modelling of turbulence. SWASH does not use an initial turbulent kinetic energy profile at the inlet boundary. Therefore, turbulent mixing near this boundary is not modelled correctly. As the flow propagates through the domain, turbulent kinetic energy accumulates and correct orders of magnitudes are found. Results of the following current case are shown in Figure F.6 at $t = 20\ min$. It is clear that the turbulent kinetic energy profile at the inlet boundary was approximately equal to 0. A future update of SWASH will include the use of an initial turbulent kinetic energy profile. For this research, this issue was already solved indirectly with the addition of a buffer zone to the numerical domain. This allowed sufficient space for the generation of turbulent kinetic energy.

F.2.3 Comparison present SWASH release and WCS method

The previous results were obtained with the present SWASH release. The WCS method was also used for generating the same flow. The essential difference, explained in more detail in Section 3.2, is that the outflow boundary scales the velocity at the previous grid point (relative to flow direction). This results in a dynamic behaviour of the water level profile over the domain and time series at the outflow boundary. The same oscillating behaviour was observed in the model results of the present SWASH release, but it was less evident due to the use of a constant water level.

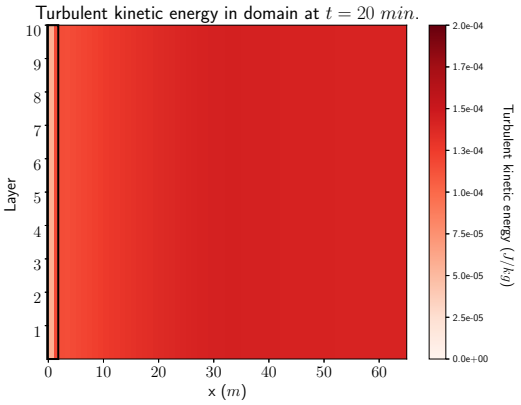

Fig. F.6.: Turbulent kinetic energy profile in the domain at $t = 20\ min$. The black box emphasises the turbulent kinetic energy at the inlet boundary.

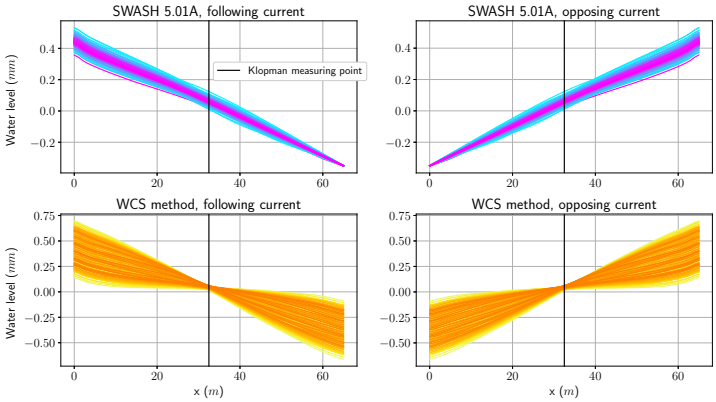

Fig. F.7.: Water level profiles of the model runs with SWASH 5.01A and WCS method. The profiles are plotted every 5 seconds, between $t = 10\ min$ and $t = 20\ min$. Note that the vertical scale is in mm while the horizontal scale is in m.

The water level profiles resulting from both methods are shown in Figure F.7. Results of both methods are symmetric for opposing and following currents. However, the spread in water levels is significantly larger of the model results with the WCS method. As a result, flow velocity profiles were oscillating repeatedly in time. This is shown in Figure F.8. Although the differences are relatively small, it is obvious that the velocity profiles are not stationary in time.

To conclude, time-averaged flow velocity profiles were found to be the same between the present SWASH release and newly developed model with the WCS method. All model results were interpolated on a spatial grid in the vertical. As SWASH produces output at the layer interfaces that fluctuate in time, it is not possible to take the time-average of all output at one layer. By doing so, a residual flow would be taken into account, as the output is essentially created within a semi-Lagrangian frame of reference. After interpolation, velocities were time-averaged from $t = 10\ min$ to $t = 20\ min$. Results are shown in Figure 5.1. The results of both methods, for either a following or opposing current, matched exactly.

F.3 Model results of current-only case with sponge layer

In this section, the model results of the current-only case with sponge layer are analysed. It was already shown in Section 4.7 that the use of a sponge layer might have considerable influence on the results. The model results in Section F.2 show that the same results are obtained for a following and opposing

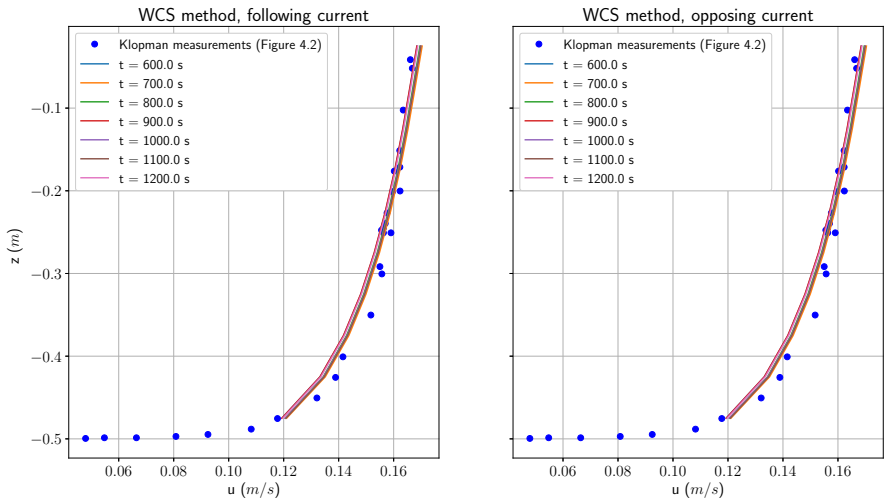

Fig. F.8.: Data from Klopman measurements (Figure 4.2, original report) compared with results of the WCS method for a following and opposing current. Results are outputted at measuring point of Klopman (1994).

current, with the present SWASH release and the WCS method. In the model runs from this section, the sponge layer was placed at the right end of the domain in all model simulations. This provided two unique cases: the first case is a model in which the sponge layer is not affecting the flow velocity profile at the inlet. This was the case for a following current. The second case provided information in which the sponge layer directly influences the flow at the inlet point. This holds for cases with opposing currents.

F.3.1 Evolution of model results in time and space

Results of the following current, obtained with the present SWASH release, are discussed in this section. Figure F.9 summarizes the results. Flow velocities were decreasing in time: this is shown in detail in the left figure. Note that in comparison to the magnitude of the mean flow, this effect is significantly smaller. In comparison to Figure F.3, the match with the experimental data declined severely. Better fits at other locations in the domain were not found. The effect of the sponge layer can be seen at $x = 60\ m$; the flow velocity is, relative to previous locations, substantially smaller.

F.3.2 Comparison present SWASH release and WCS method

The time-averaged flow velocity profiles, obtained with both methods, are shown in Figure 5.1. Furthermore, time-averaged water level profiles and the time evolution of the volume in the domain are shown in Figure F.10. The time-averaged flow velocity profiles showed significant differences between both methods and directions of the current. The difference between the results of both methods is due to the water level profiles. In general, the water level profiles generated with the present SWASH release showed large gradients near the sponge layer in comparison to the WCS method. These relatively large gradients were present due to the use of a constant water level. As a result, reflection might occur in the combined wave-current flow simulations with the present SWASH release, since gradients were in the order of 10% in comparison with the imposed wave height by Klopman (1994).

The decrease and increase of the volume of water in the domain was analysed for both methods. For the following current, a volume increase was observed with the present SWASH release. However, a volume decrease was observed with the WCS method. For the opposing current, the volume stayed constant with the present SWASH release, whereas results with the WCS method showed a volume

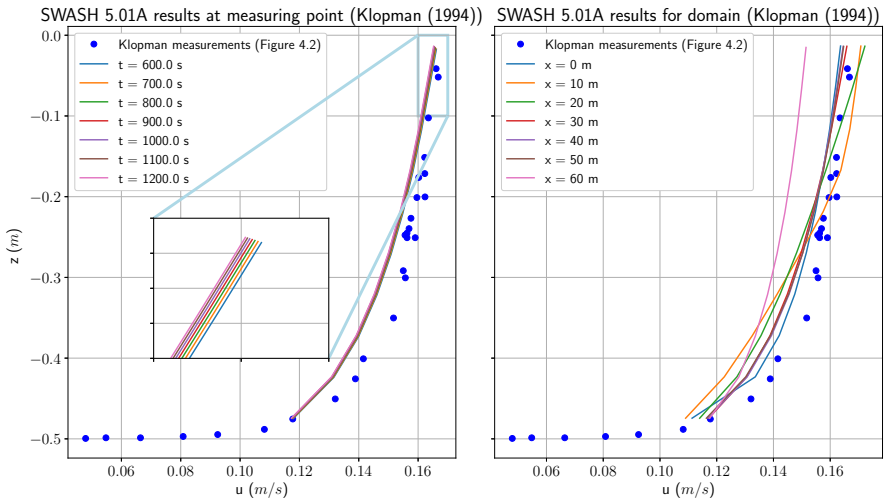

Fig. F.9.: Data from Klopman (1994) measurements (Figure 4.2, original report) compared with SWASH results in time and space. A sponge layer of length $8.0\ m$ was placed at the right end of the numerical domain. In the left figure, SWASH results in time are shown. The box shows a zoomed-in section of the flow for $0.16 < x < 0.17$ and $-0.1 < z < 0$. The flow velocity profile development in space at $t = 20\ min$ is shown in the right figure.

increase. In comparison to all cases, results suggest that the present SWASH release generally produces the lowest volume change for following or opposing currents. This might suggest that the present sponge layer technique in SWASH works better when water levels are prescribed at the end of the sponge layer.

F.4 Model results of wave-only case

In this section, the model results of the wave-only case are analysed. The measurements by Klopman (1994) of the wave-only experiment showed the Eulerian piecewise compensation flow for the Stokes drift (see Section 3.1.3). The theoretical Stokes drift profile is shown in Figure F.11. Time-averaged velocity profiles were obtained by interpolating the model output on a fixed grid in the vertical and, subsequently, time-averaging over the last 50 waves.

F.4.1 Comparison of results between time series and default SWASH input

The results of the simulations with generated time series and default SWASH input are shown in Figure 5.3. In general, a good fit was obtained between results of all cases and the experimental data. The time-averaged profiles of the non-linear waves, generated with the methods by Rienecker and Fenton (1981) and Fenton (1988), led to the best fits. It was expected that these methods led to the same result, since both methods are computationally the same, with the latter being more computational friendly. The wave generated with the default SWASH input, i.e. with linear wave theory, led to satisfying results. However, the time-averaged profile was overestimated in comparison to the results with time series.

The clear outlier was the result of the non-linear wave approximated with the method by Fenton (1985). The time-averaged profile did have a similar shape as the mean Eulerian flow, but the magnitude was significantly underestimated. A possible cause was found by comparing velocities per computational layers between the all time series. The method by Fenton (1985) overestimates the velocities of the non-linear wave in comparison to the other methods. It was found that the method by Fenton (1985) was highly sensitive to the input of the wave length. When this value was changed in the order of a

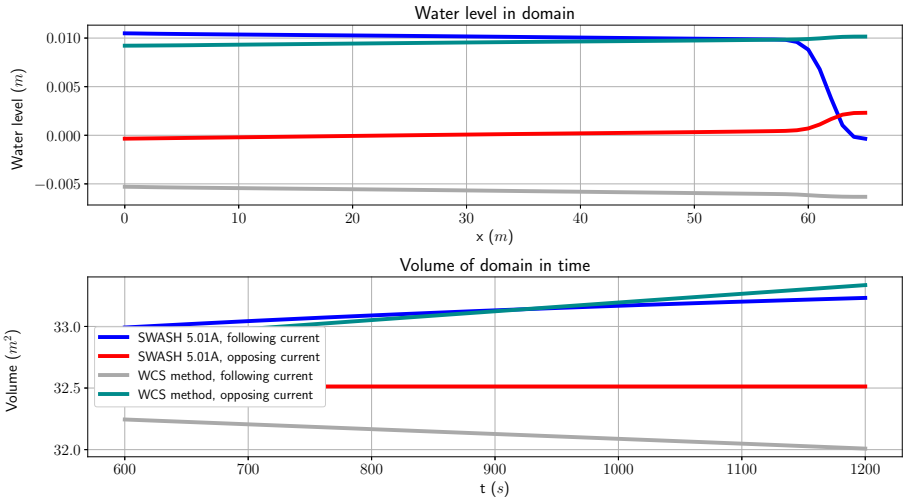

Fig. F.10.: Time-averaged water level profiles and volume of the domain in time for the two methods and four cases.

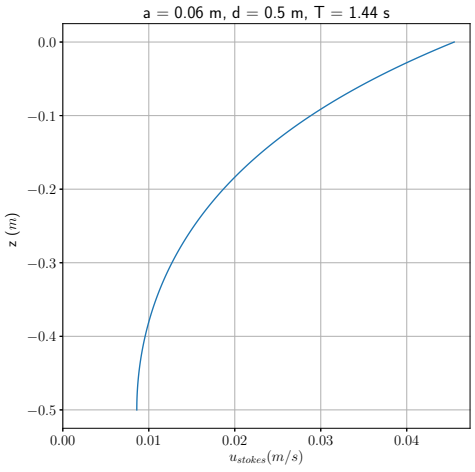

Fig. F.11.: The theoretically expected Stokes drift profile of the experiment by Klopman (1994).

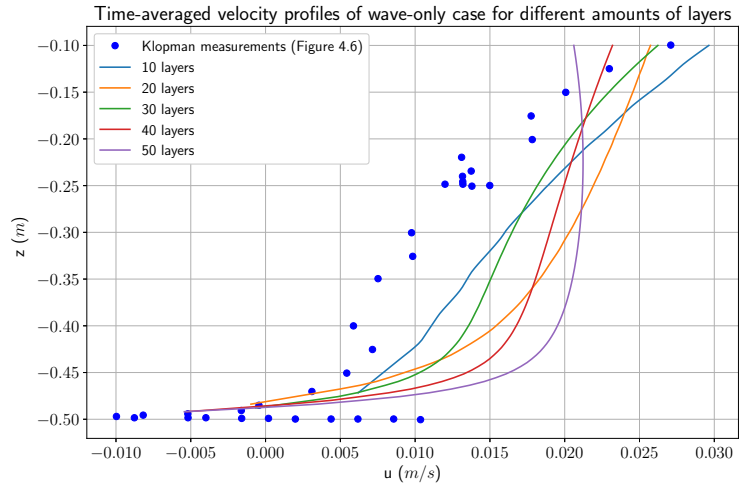

Fig. F.12.: The time-averaged velocity profiles of different amounts of layers.

few %'s, velocities were approximately equal to the values found with the methods by Rienecker and Fenton (1981) and Fenton (1988).

F.4.2 Comparison of results of different numbers of layers

The initial goal of a larger number of layers was to include the wave boundary layer ($-0.5\ m < z < -0.45\ m$). However, this led, at maximum, to vertical grid sizes in the order of $1\ cm$, which was still insufficient to allow proper modelling of the boundary layer. As the computational time increased substantially, no further attempts were made to include the wave boundary layer. One possible option was to specify layers as a relative percentage of the entire water depth, i.e. layers with different thickness, to obtain a higher density of layers near the bottom. However, this was not feasible for simulations with combined wave-current flow, as the WCS method is specifically derived for equidistant layers (see Section 3.2.2).

Time-averaged velocity profiles of different numbers of layers are shown in Figure F.12. The linear wave, i.e. default SWASH input, was used at the boundary. Rather unexpected results were obtained, as the time-averaged velocity profiles started to substantially differentiate from measurement data for an increasing number of layers. Furthermore, the profiles for the cases with more than 30 layers were not in line with theory, as the shape of the Stokes drift profile was significantly violated in the upper part of the water depth. However, it is not known what the cause of this behaviour is. One attempt was to generate output of the friction coefficients, as calculated by SWASH, for a different number of layers. However, values were matching, thus indicating that SWASH computes the bottom friction correctly no matter the number of layers.

G

Model results of Chapters 5 and 6 with default SWASH settings

The following results were obtained with an older SWASH model. The difference with the present model lies in the used numerical schemes. The older SWASH model used default settings. The BDF scheme was used for the horizontal advection in the horizontal momentum equation. Furthermore, the upwind scheme was used for the discretization of the water depth.

G.1 Model results of experiment by Klopman (1994)

The results of time-averaged velocity profiles indicate that the choice of numerical schemes significantly influenced the accuracy and vertical flow structure. Results at the measuring position of Klopman (1994) and wave maker boundary are shown in Figures G.1 and G.2.

G.2 Model results of experiment by Ma et al. (2017)

The results of skewness, asymmetry and wave height profiles indicate that the choice of numerical schemes does not have a significant influence. Results with the SWASH model with default settings for the numerical schemes is shown in Figure G.3.

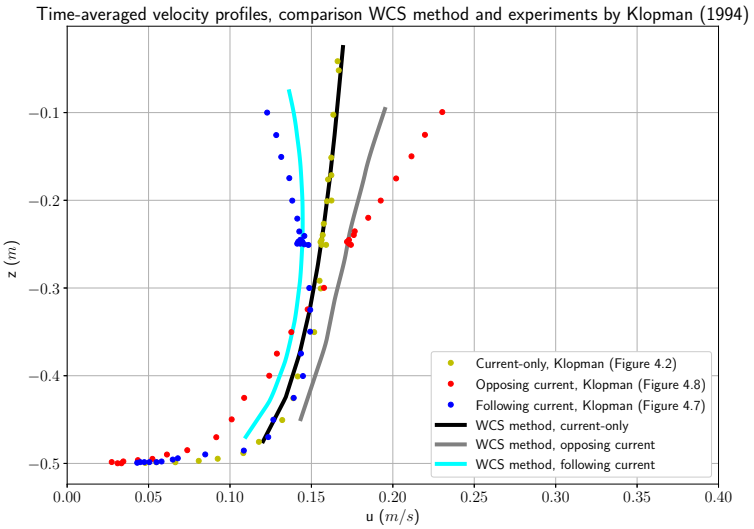

Fig. G.1.: The time-averaged horizontal velocity profiles for the current-only, opposing current and following current cases. Model results at the measuring position of Klopman (1994) are compared with experimental data. Results were obtained with an older SWASH model, that made use of the default settings for the numerical schemes.

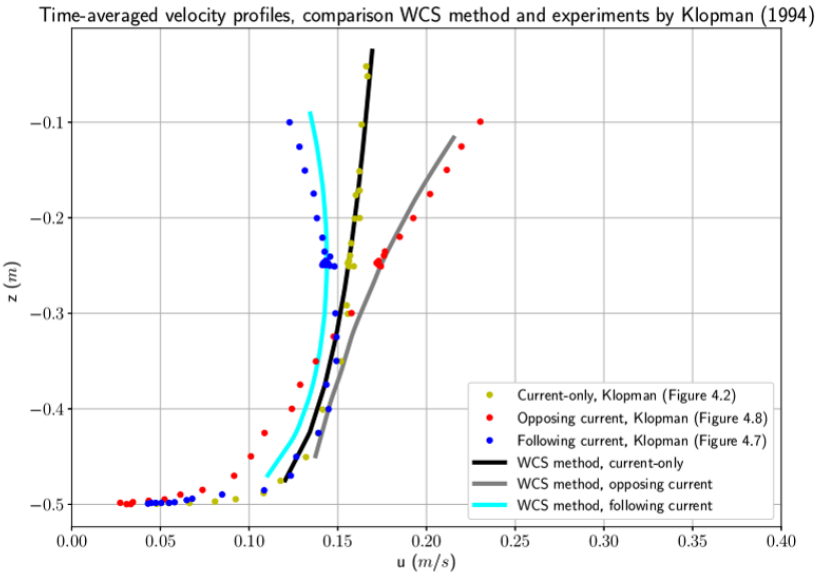

Fig. G.2.: The time-averaged horizontal velocity profiles for the current-only, opposing current and following current cases. Model results at the wave maker boundary are compared with experimental data. Results were obtained with an older SWASH model, that made use of the default settings for the numerical schemes.

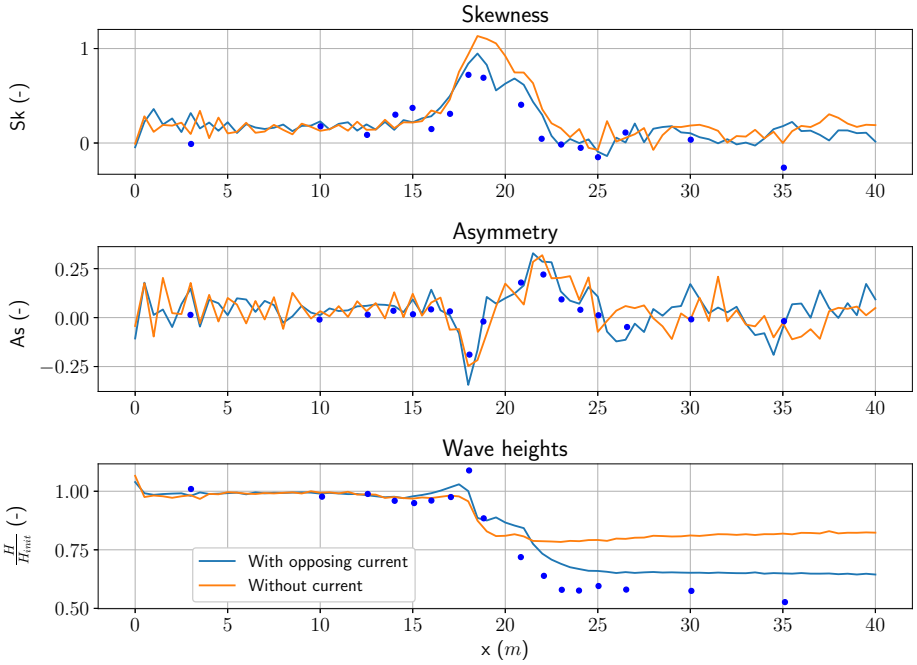

Fig. G.3.: Skewness, asymmetry and wave height profiles over the domain based on model results are compared with measurements by Ma et al. (2017). Model results with and without a current are shown.

Colophon

This thesis was typeset with LaTeX 2$_\varepsilon$. It uses the *Clean Thesis* style developed by Ricardo Langner. More information can be found at http://cleanthesis.der-ric.de/.

Declaration

Delft, May, 2019

Tolga Cömert